Inflammatory pain regulation through TRPV1 ion channel and phosphoinositide signaling

Anastasiia Stratiievska

A dissertation

submitted in partial fulfillment of the

requirement for the degree of

Doctor of Philosophy

University of Washington

2019

Reading Committee:

Sharona E. Gordon

Bertil Hille

William N. Zagotta

Program Authorized to Offer Degree:

Physiology and Biophysics

University of Washington

Abstract

Inflammatory pain regulation through TRPV1 ion channel and phosphoinositide signaling

Anastasiia Stratiievska

Chair of the Supervisory Committee

Sharona E. Gordon

Department of Physiology and Biophysics

Inflammatory pain is one of the biggest challenges facing contemporary society. The TRPV1 ion channel is a major player in inflammatory pain. During inflammation TRPV1 is regulated by both modulation of gating and changes in channel number on the plasma membrane. Phosphoinositides are a class of membrane lipids which are directly involved in regulation of channel activity and signaling. PIP_2 is a phosphoinositide which affects gating of TRPV1 but whether it activates or inhibits was controversial. We showed that under physiological conditions PIP_2 activates TRPV1, while in non-physiological conditions, PIP_2 inhibits TRPV1, which resolves the controversy in the literature.

The phospholipid PIP_3 is a product of a lipid kinase called PI3K, which is also involved in inflammatory pain. During inflammation, increased PI3K activity leads to increased PIP_3, which leads to fusion of vesicles containing TRPV1 with the plasma membrane. This mechanism underlies increased sensitivity to pain during inflammation. We identified a novel mechanism for reciprocal regulation between PI3K and TRPV1 during inflammation, which results in potentiation of PI3K activity. A soluble fragment of TRPV1 called the ARD was sufficient to reproduce this effect. To move this work further, we are optimizing a novel opto-PI3K system to achieve better spatial and temporal control of PI3K activity. This will be significant for advancing our understanding of the mechanism of inflammatory pain and opening possibilities for developing new treatments.

Table of contents

List of Figures

List of Tables

Acknowledgements

I am grateful to Elena A. Lukyanetz (Bogomolets Institute of Physiology NASU, Kyiv, Ukraine) for support during transition to a PhD program. Heartfelt thanks to Sharona E. Gordon (University of Washington, Seattle, WA) for trusting in me every step of the way. My sincere thanks go to Bertil Hille and Lea Miller (University of Washington, Seattle, WA) for help navigating the new environment of University of Washington and tuning my CV. I would like to express my gratitude to the committee for helpful comments and support along the way. I'm grateful to William N. Zagotta (University of Washington, Seattle, WA) for helpful discussions and comments. This research would not be possible without the tremendous help from Mika Munari (University of Washington, Seattle, WA). Big appreciation is due to Eric N. Senning (The University of Texas at Austin, Austin, Texas) for patience in teaching me imaging and electrophysiology. I acknowledge the great contribution of the co-authors Marcus D. Collins, Carmen A. Ufret-Vincenty, Francoise Haeseleer. Appreciation is due to Mario Rosasco, Leslayann Schesterson, Gucan Dai and Gilbert Martinez for helpful comments and discussions. I greatly appreciate the help from undergraduate students Ruian Yang, Alex Pazevic and Sara G. Nelson and a visiting scientist Lígia Araujo Naves (Federal University of Minas Gerais, Brazil). I acknowledge the contribution of collaborators Stephen Smith and Jonathan Lautz (Seattle Childrens research institute, Seattle, WA). Sincere thanks to Doug Tisher (University of California, San Francisco, CA) and Jared Toettcher (Princeton University, Princeton, NJ) for help with troubleshooting the PhyB system.

I am grateful to my husband Oleksandr Stratiievskyi for incredible patience, support and love. Heartfelt thanks to my parents Iryna and Oleg Pylypiuk, and my brother Stanislav. My sincere thanks go to my dear friends Gaby Bergollo, Alina Kremnova, Elena Zhukovetz, Diana Golovei, Nata Ivanova, Mariana Burlak, Nadia Slusarenko and Tatiana Chernysh.

This research would not have been possible without funding from NIGMS of NIH R01GM100718 and R01GM125351; NEI of NIH R01EY017564 and P30EY001730; NCRR of NIH S10RR025429; NIDDK P30DK017047, T32EY007031, T32HL00782 and T32HL007312; NIMH of NIH R01MH113545; NIBIB of NIH T32EB001650; NIH S10RR025429; and a Royalty Research Fund Award from the University of Washington.

Dedication

I dedicated my work to my late Grandfather Yaroslav Semenovich Pylypiuk, who was a PhD candidate in analytical chemistry. He taught me to apply the critical thinking and scientific approach to the world. I strive to teach everyone else the same.

Also, to you (most likely a successor graduate student), curious enough to read this: I salute your endeavors!

1 Introduction

Cell membranes are asymmetrical lipid bilayers embedding multiple classes of proteins involved in signal transduction from extracellular environment to the intracellular compartments. The classes of surface proteins involved in signal transduction include ion channel receptors, G-protein coupled receptors (GPCRs) and receptor tyrosine kinases (RTKs) (refer to section 1.4 for more info) (Uings and Farrow, 2000).

Ion channel receptors are pore forming transmembrane proteins that change permeability of the pore to ions in response to a variety of physical or chemical stimuli (Alexander SPH, 2011). For example, Transient Receptor Vanilloid family member 1 (TRPV1) ion channel is a multi-modal receptor expressed in sensory neurons that can be activated by heat, protons and capsaicin (a pungent compound from chili peppers) (Caterina et al., 1997). Excitatory stimuli, such as heat, lead to an influx of cations, such as Na^+ and Ca^{2+}, through the channel pore, and depolarization of the membrane potential of the neuron and action potential firing (Caterina et al., 1997). Sensory neurons that express receptors to painful stimuli are called nociceptors (Messlinger, 1997). Located in the Dorsal Root Ganglion (DRG), these neurons translate such stimuli into action potentials that are transmitted along the membrane of an axon (an elongation of the neuron which extends from cell body) to the dorsal horn of the spinal cord. Interneurons then carry the electrical signals to the brain, where they are interpreted as painful (Willis and Coggeshall, 1978).

Resting membrane potential is defined by a set of unique characteristics of a plasma membrane of a cell. Membrane potential is established by a balance of charged carriers – ions. The resting membrane potential of nociceptors is around -55 to -80 mV (Du et al., 2014).Lipid bilayers are very poorly permeable to ions (for example, permeability coefficient of a red blood cell membrane is ~10^{-4} cm/s (Prankerd, 1965)) and its general purpose is to isolate the inside of the cells from the outside. Ion channels embedded in the lipid bilayer are selectively permeable to ions. Sodium (Na^+) ions are prevalent on the outside of the cells, while potassium (K^+) ions are enriched on the inside. This balance is finely tuned by the activity of two-pore domain (K2P) "leak" K^+ channels (Li and Toyoda, 2015) and the Na^+/K^+-ATPase exchanger (Skou, 1957, Clausen et al., 2017). Two-pore domain (K2P) "leak" K^+ channel are a family of K^+ channels that are permeable to K^+ at rest (Li and Toyoda, 2015). Electrical consequences of “leak” channels activity were described by classic work of Hodgkin A.L. and Huxley A.F. in 1952 (Hodgkin et al., 1952, Hodgkin and

Huxley, 1952a, Hodgkin and Huxley, 1952b, Hodgkin and Huxley, 1952c), long before the existence of ion channels was discovered. Na^+/K^+-ATPase exchanger is a transporter that exchanges 3 Na^+ ions outwardly and hydrolyzes 1 ATP molecule for 2 K^+ ions inwardly, thus, in total, removing one positive charge from the intracellular space (Skou, 1957, Clausen et al., 2017).

Besides leading to depolarization upon the increase in Ca^{2+} cytoplasmic concentrations, Ca^{2+} ions act as second messenger regulating a variety of the intracellular signaling processes, including lipid homeostasis, ion channel activity, gene expression, protein phosphorylation, energy production in mitochondria and much more (Clapham, 1995). In one instance, Ca^{2+} influx leads to activation of a Phospholipase C (PLC) and degradation of a signaling phospholipid phosphatidylinositol 4,5-bisphosphate ($PI(4,5)P_2$, commonly called PIP_2) into two classical signaling molecules inositol 1,4,5-trisphosphate (IP_3) and diacylglycerol (DAG)(Xu et al., 2003). In resting cells, PIP_2 is localized to the inner leaflet of the plasma membrane at concentrations (1% of all phospholipids), that are relatively high compared to other phosphoinositides (Suh and Hille, 2008). Multiple ion channels were reported to be regulated by PIP_2, for example, TRPV1, KCNQ, Kv, Kir, etc (Suh and Hille, 2008) (more on regulation of TRPV1 by PIP_2 - in chapter 2). In addition, increase in concentration of a related signaling lipid PIP_3 at the plasma membrane leads to activation of many downstream signaling pathways including cell survival, and motility via exocytosis (more about this in chapter 3) (Insall and Weiner, 2001).

Taken together, phosphoinositides and their signaling are tightly involved in a regulation of ion channel functions. Here we will focus on the regulation of TRPV1 ion channel by phosphoinositides PIP_2 and PIP_3.

1.1 Techniques used to study ion channels and lipids

There are two commonly used approaches to study ion channels in physiological conditions of a living cell: patch-clamp electrophysiology and fluorescence imaging. Each approach offers advantages and suffers from disadvantages. The best experimental designs maximize advantages of the approach for the particular questions needed to be answered while minimizing the disadvantages.

1.1.1 Patch clamp electrophysiology

Patch-clamp electrophysiology is a family of methods pioneered by Neher E. and Sakmann B. (Sakmann and Neher, 1984, Hamill et al., 1981) that is used to record electrical activity of the cell. In brief, electrical potential across the membrane of a cell is recorded as the difference between the ground electrode immersed in the bath solution and the micro electrode which is tightly attached to the cell membrane via a high resistance giga-Ohm seal (Fig. 1.1). Current or voltage across the membrane may then be "clamped" – fixed with the feedback circuit of an amplifier by offsetting the voltage or current at the micro electrode. In Voltage-clamp voltage across the membrane is monitored and controlled. This allows to record current with fixed membrane potential across the membrane. During such recording, receptor agonists may be applied and their effects on current through the open channels may be recorded. Additionally, typical measurements include IV curve which is a plot of a current at different membrane potentials. Overall, disadvantage of this approach is low through put, because only one cell may be recorded at a time.

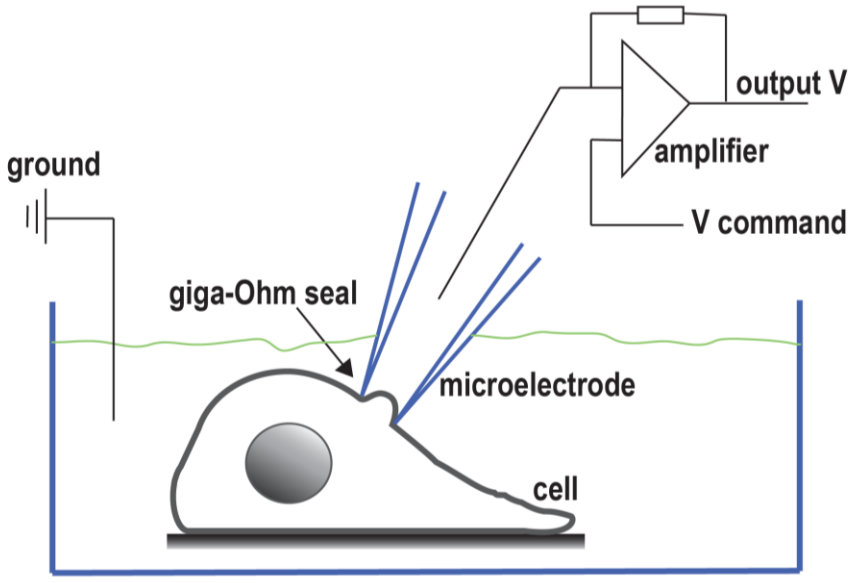

Fig. 1.1 Cartoon representing patch clamp electrophysiology experiment

There are several configurations of voltage-clamp recordings, see Fig. 1.2 (Hamill et al., 1981, Sakmann and Neher, 1984). The micro electrode may be attached to the cell in cell-attached configuration – when the membrane under the electrode is intact (Fig. 1.2A). In perforated patch configuration, the cell membrane under the micro electrode may be perforated using large pore-forming antibiotics such as amphotericin B (Fig. 1.2B). Alternatively, the cell membrane under the electrode may be destroyed by suction and the whole cell cytoplasm may be exposed to the micro electrode (whole-cell configuration Fig. 1.2C). Perforated patch and whole-cell configurations allow for “clamping” of the entire plasma membrane with most of the intracellular components intact. This provides the advantages of the more physiological intracellular environment, but this environment cannot be precisely controlled. These disadvantages are addressed in the cell-detached configurations that are achieved by pulling the micro electrode away from the cell-attached (for inside-out) or whole cell (for outside-out) configurations (see Fig. 1.2D and E respectively). Inside-out and outside out configurations provide precise control over solutions on both sides of the membrane but lack other intracellular components which may be a serious downside for ion channels highly dependent on cytoplasmic factors.

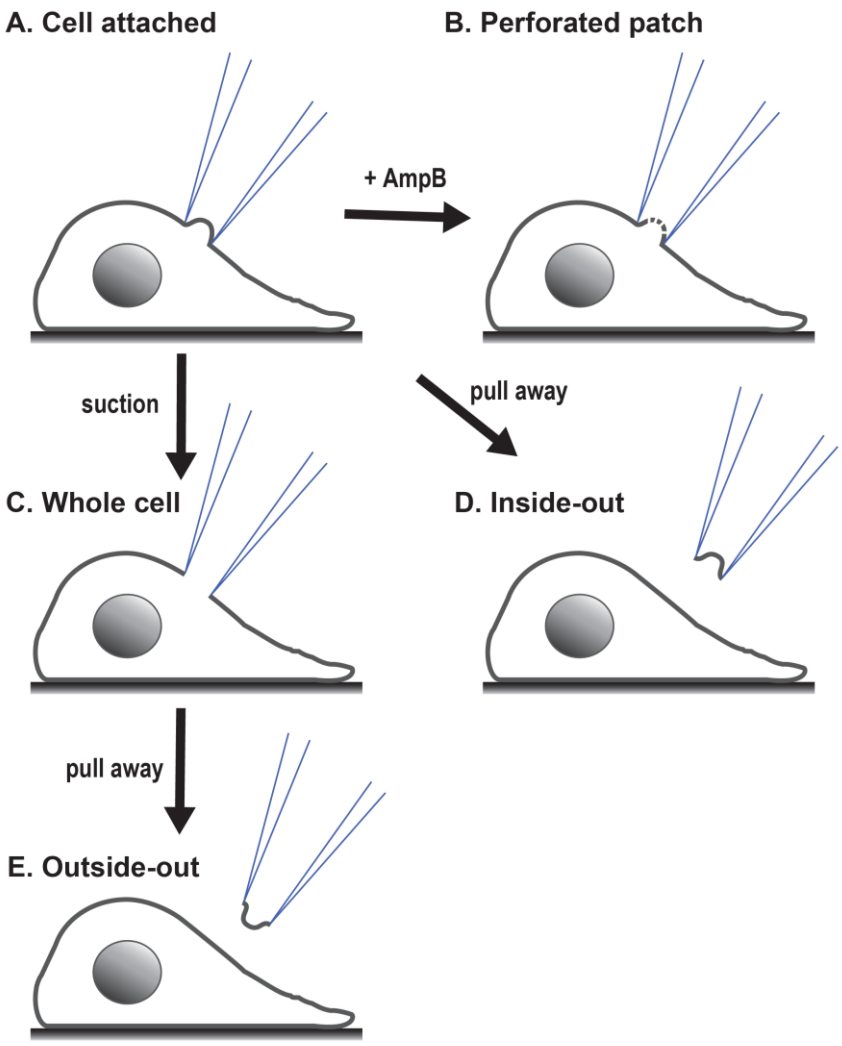

Fig. 1.2 Voltage clamp configurations.
A) Cell attached; B) with addition of Amphotericin B perforated patch is achieved; C) Whole cell; by pulling micro electrode away inside-out (D) or outside out are achieved

In the current clamp configuration, the current across the membrane is monitored and controlled, while voltage is recorded (Wickenden, 2014). During this kind of recording, action potentials of an excitable cell may be recorded. The experimenter may modulate electrical activity of the cell by apply ion channels agonists, as well as by injecting current, and thus mimicking opening of the ion channels.

1.1.2 Fluorescence microscopy

Microscopy is a technique that uses light and a set of magnifying lenses to achieve images of objects smaller than human eye can see. Fluorescence microscopy takes advantage of fluorescence phenomena when fluorophore molecules absorb a photon of light and emit a photon with a lower energy- a longer wavelength of light (Sanderson et al., 2014). Absorption of a photon with a higher energy is called excitation of the fluorophore and emission of a lower energy photon – emission. Fluorescent proteins (FPs) are a group of visible wavelength fluorophores which were first purified from *Aequorea victoria* jellyfish (Inouye et al., 1985, D and Nicol, 1955). Fluorescent proteins are commonly fused to other proteins and used as a tool to visualize proteins when expressed in live cells (Tsien, 1980). All this combined allows for high throughput experiments because multiple cells may be imaged at once. Another advantage is that cell physiology is not perturbed by a microelectrode. The disadvantage of this method comes from the fact that FP-fusion proteins have to be exogenously expressed and may not fully represent behavior of endogenous proteins.

Confocal microscopy is a type of a fluorescence microscopy used to image a thin slice of cell volume (Sanderson et al., 2014). This is achieved by using a pinhole placed between the light source and a specimen. This allows for higher spatial resolution as a smaller volume is illuminated and therefore light scattering is reduced. In order to achieve this, pinhole or a light source must be moved around to collect the image from the whole field of view. This leads to the disadvantage of slow image acquisition for scanning confocal microscope where the whole area is scanned sequentially. This issue is addressed in spinning disk confocal microscope where a disk with multiple pinholes is spinning at high speed and therefore, the whole area is illuminated faster.

Total internal reflection fluorescence (TIRF) microscopy is a type of a fluorescence microscopy where only a thin layer (~300 nm) of fluorophores directly adjacent to the plasma membrane is excited (Mattheyses and Axelrod, 2006). Total internal reflection is achieved by a specific angle where almost all the laser light is reflected from the bottom of the glass coverslip where cells are plated, and only a small portion of light called the evanescent field reaches the sample (Fig. 1.3). This allows for selective excitation of fluorophores adjacent to the plasma membrane of the cells as well as high signal-to-noise ratio (see

more in sections 3.6.1 and 3.6.2). The drawback of this approach is that only adherent cultured cells may be used. The most common application of TIRF microscopy is in studies of protein-of-interest membrane translocation. For example, Fig. 1.3 shows an adherent cell expressing a cytoplasmic fluorophore (Fig. 1.3, circles) which is only excited when near the plasma membrane of the cell (Fig. 1.3, green circles). If a stimulus leads to translocation of the fluorophore to the plasma membrane (Fig. 1.3, right), the increase of near-membrane fluorescence is detected.

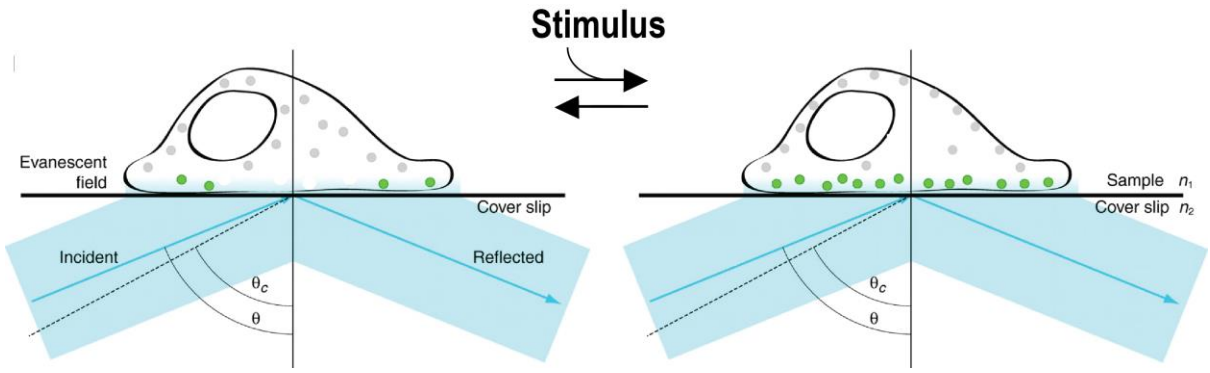

Fig. 1.3 Cartoon representation for TIRF microscopy. (modified from (Mattheyses et al., 2010).

Calcium imaging is a specific case of fluorescence microscopy which takes advantage of fluorophores with different excitation/emission properties dependent on calcium concentration. Two such categories of fluorophores are calcium chelator-based dyes and genetically encoded GCaMPs (Nakai et al., 2001). Calcium chelator dyes must be “loaded” in the cytoplasm of a cell, where they bind calcium ions with specific affinity. The disadvantages of this is that chelation of calcium by the dye may result in disruption of calcium homeostasis. GCaMPs are green fluorescent protein (GFP) genetically modified fused to calmodulin, and M13 (a peptide sequence from myosin light chain kinase) (Nakai et al., 2001). GCaMPs have the advantage over the calcium dyes because they rely on cell protein expression, and any effects on calcium homeostasis may be compensated by adjustments in expression levels.

All of the experimental methodologies described above rely on cell culture for preparation of cell samples. Primary tissues, such as Dorsal Root Ganglia can be dissociated into single cells and placed in supplement-enriched media inside of the incubator at 37°C and 5% CO_2 atmosphere. Cultured neurons are commonly used to study electrical activity in response to various stimuli by electrophysiology or calcium

imaging. The main disadvantage of primary tissue cultures is that differentiated cells survive for a limited time and divide a limited number of times. Alternatively, immortalized cell lines are commonly used for their ability to divide an infinite number of times in culture. Cell lines are often used to study exogenously expressed proteins of interest which are carried into the cell in a form of plasmid DNA using transfection reagents. The main disadvantage or immortalized cell lines is that they are often polyploid and are prone to accumulating mutations if maintained in culture for prolonged periods.

1.2 TRPV1 ion channel

Sensitivity to a specific noxious stimulus is defined by types of ion channel receptors expressed on the surface of the neuron. Here we will focus on select members of the TRP channel superfamily. TRPV1 is the most intensively studied member of the TRP channels superfamily (13123 entries on Pubmed to date). It is most widely expressed in small-diameter sensory neurons of DRG involved in pain sensation(Davis et al., 2000). TRPV1 is a non-selective cation channel that can be activated by a variety of noxious stimuli including heat (>42°C), protons (EC50 pH 5.8), and chemicals, for instance, a spicy compound from chili pepper – capsaicin(Caterina et al., 1999). TRPV1 forms a homotetrameric channel with six transmembrane domains and cytoplasmic C- and N- termini (Yao et al., 2011). TRPV1 N-terminus contains an Ankyrin repeats domain (ARD) - a domain consisting of 6 repeats homologous to ankyrin – which is important for interaction with intracellular regulators of TRPV1 (Lishko et al., 2007) (more on this in sections 1.2.1 and 1.2.2). TRPV1 transmembrane domain structure is homologous to voltage gated potassium channels (Kv) (Caterina et al., 1999). However, in contrast to Kv channels, the voltage-dependence of TRPs is very weak (Caterina et al., 1997). A recent explosion of high resolution CryoEM (Liao et al., 2013, Gao et al., 2016, Huynh et al., 2016a, Zubcevic et al., 2016b, Zubcevic et al., 2016a, Deng et al., 2018, Saotome et al., 2016) 3D structures of TRPV channels revealed a great amount of detail with atomic precision for structures the like agonist binding pocket, two gates in the channel pore and the interaction between C-terminus and the N-terminus proposed to stabilize the tetrameric channel.

1.2.1 Regulation of TRPV1

Two common ways for regulation of ion channels are modulation of ion channel activity and changes in the number of channels in the PM. Modulation of TRPV1 activity involves interaction with a variety of intracellular factors, such as PIP_2, Ca^{2+}, and kinases, etc. Just c-terminal to the S6 transmembrane segment of many TRP channels is a region called the TRP helix that is loosely conserved in almost all TRP channels, except TRPA1 and distantly related TRPMLs and TRPPs. This region is important for PIP_2 binding (Ufret-Vincenty et al., 2011) and channel tetramerization (Liao et al., 2013, Erler et al., 2004). There are two Calcium-calmodulin (Ca^{2+}/CaM) binding sites one for each C-(Rosenbaum et al., 2004) and N-termini(Lau et al., 2012, Numazaki et al., 2003), but whether they are functionally important is controversial. TRPV1 can be phosphorylated by PKA and/or PKC or de-phosphorylated by calcineurin on a number of sites within N- and C-termini that modulate channel activity and sensitivity (Novakova-Tousova et al., 2007, Docherty et al., 1996, Mohapatra and Nau, 2005, Bhave et al., 2003, Bhave et al., 2002, Mohapatra and Nau, 2003, Stein et al., 2006). PKC and PKA were proposed to be one of the mechanisms that acutely upregulate TRPV1 activity in response to inflammatory mediators, such as bradykinin (Mathivanan et al., 2016, Gonzalez et al., 2012). It was shown that TRPV1 C-terminus is directly interacting with the tubulin of microtubules in vitro and in living cells using FRET (Goswami, 2012, Goswami et al., 2007). This interaction could be the key component of the scaffold for multiple protein interactions that can affect both single channel activity and trafficking.

Ion channel trafficking is another major mechanism for regulation of their activity. For example, it was established that TRPV1 is a major player in inflammatory thermal sensitization, which is carried out in part by increase of TRPV1 channel number on plasma membrane (Stein et al., 2006, Bonnington and McNaughton, 2003). An increase in the number of TRPV1 ion channels leads to bigger depolarization of the neuronal membrane, and therefore higher sensitivity to the normal non-painful stimuli. One approach to abolishing hypersensitivity to non-painful stimuli is to decrease the number of channels at the plasma membrane by intervention with membrane trafficking. Such an approach commonly utilizes botulinum toxin which interferes with exocytosis and leads to a decrease in number of channels (Camprubi-Robles et al., 2009). Class I PI3Kinase is a key player in upregulation of TRPV1 channels in response to inflammation

(Stein et al., 2006, Bonnington and McNaughton, 2003). Refer to section 1.4 and (Stratiievska et al., 2018) for further details.

1.2.2 Ankyrin repeat domain

Ankyrin repeat domain (ARD) consist of a short ~33 aa sequence motif repeats (Sedgwick and Smerdon, 1999) which are packed with the helix-loop-helix topology (Lishko et al., 2007, Michaely et al., 2002) and, in different proteins, may be repeated from two to thirty four times (Mosavi et al., 2004). Fig. 1.4 shows X-ray structure of the 13-24 ARD of human ankyrin-r and linker (PDB ID:1N11). Ankyrin repeats stack on each other to form a tightly packed spring-like structure with hydrophobic core and very large solvent-accessible surface (Sedgwick and Smerdon, 1999). Helix sequences are more conserved than loops. Loops (sometimes referred as fingers) vary in length and form a large surface suitable for electrostatic interactions, for this reason, they are responsible for the diversity of functions that ARD-containing proteins exhibit (Mosavi et al., 2004).

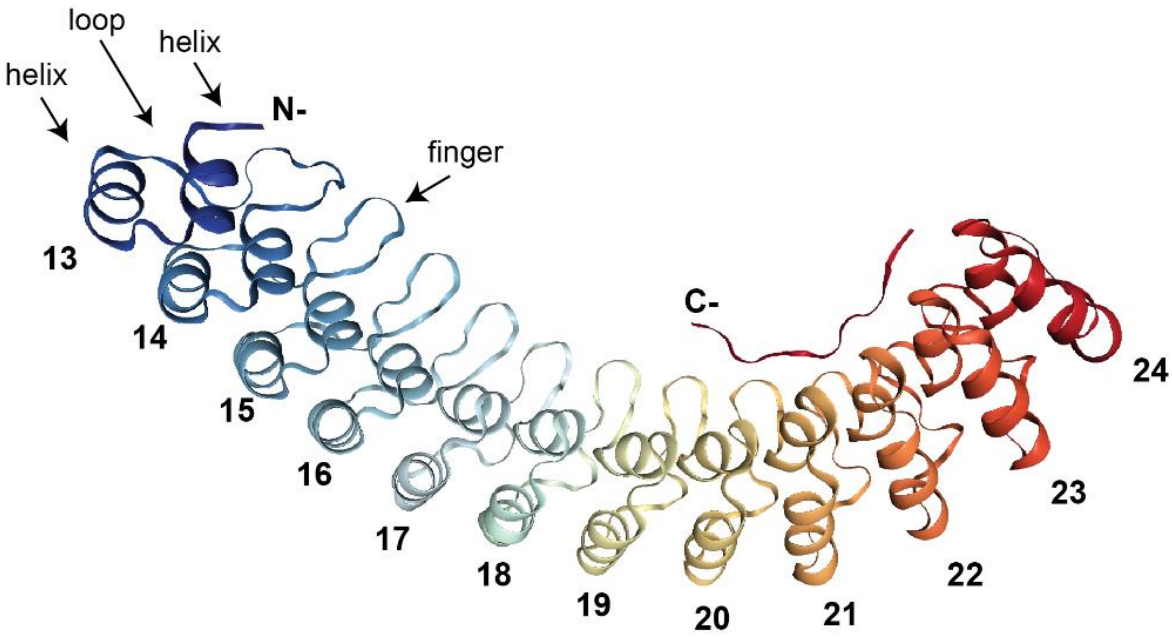

Fig. 1.4 X-ray structure of the 13-24 ARD of human ankyrin-r and linker (PDB ID:1N11).
There are 12 helix-loop-helix motifs (repeats), each repeat is colored individually. Fingers are loops between conserved repeats.

ARD is one of the most abundant domain families in the human genome (Lander et al., 2001) (*Homo sapiens* 916 proteins (EMBL-EBI, 2019)). ARDs are found in a wide variety of proteins across most forms of life and they are involved in diverse physiological processes. ARDs are found in several families of transcription factors (most famous Notch (Lubman et al., 2004) and NFkB) and regulatory proteins (for example cyclin-dependent kinase inhibitors).

N-terminus of TRPV1 and all other members of TRPV family contains six Ankyrin repeat domains (ARD) (Lishko et al., 2007) which is proposed to be responsible for many protein-protein interactions (Fig. 1.5). ARDs of TRPV channels are often referred to as palm-like structure with loops corresponding to "fingers" (Fig. 1.5). TRPV2 and TRPV4 have highly similar sequence to TRPV1, contain ARD as well. Cryo-EM structures of TRPV1, TRPV2, TRPV4 and TRPV6 are very similar with ARD sticking down from the membrane and splaying out and away from the pore along the inner membrane surface (Gao et al., 2016, Shigematsu et al., 2010, Huynh et al., 2016a, Huynh et al., 2016b). Another TRP channel TRPA1 contains >16 ARDs which unlike TRPVs do not spray away from the pore but form the cylindrical structure around the coiled-coil region (Paulsen et al., 2015). TRPC channels also contain ARD, and their structure looks similar to TRPA1 with ARD oriented downward surrounding the coiled-coil region (Tang et al., 2018). Until recently, every member of TRPM family was believed to lack ARD, but recent Cryo-EM of TRPM4 revealed two ARD-like domains in the N-terminus (Winkler et al., 2017) even though this was not apparent from the primary sequence.

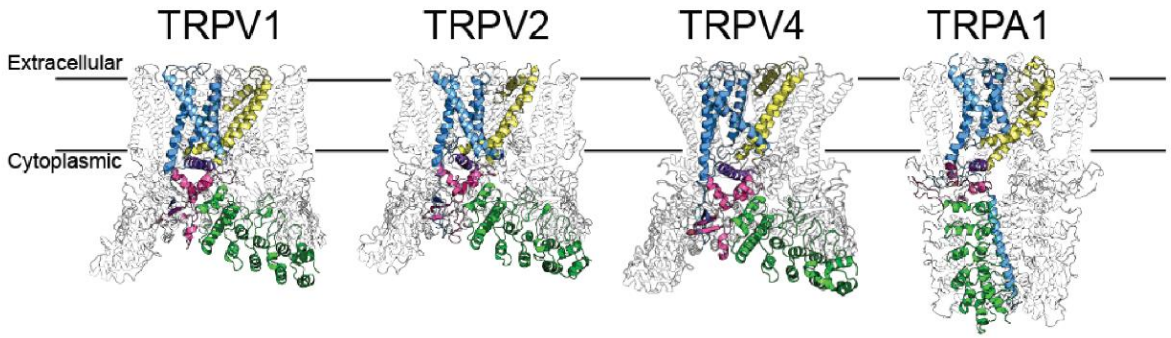

Fig. 1.5 Comparison of TRP channels Cryo-EM structures

One subunit of each channel is colored as follows: ARD – green, TRP helix – purple, Pre-S1 – pink, Pore – yellow, all other parts of the subunit are depicted in blue. The remaining three subunits are outlined in gray for clarity. Cryo-EM structures of rat TRPV1, rat TRPV2, frog TRPV4 and human TRPA1 from PDB IDs 3J5P, 5HI9, 6BBJ, 3J9P, respectively, are shown.

The common feature of TRP ARDs is that they act as a hub for regulators of channel function. For instance, the TRPV1 ARD interact with PKA, PKC, A-kinase adaptor protein 79/150 (AKAP79/150) and calmodulin, (Bhave et al., 2002, Bonnington and McNaughton, 2003, Jeske et al., 2008). Similarly, TRPV4 ARD bind calmodulin, AKAP79/150 and PIP_2 (Strotmann et al., 2003, Mack and Fischer, 2017, Takahashi et al., 2014). Many agonists activate TRPA1 channel by covalently modifying multiple cysteines on the ARDs.

1.3 PI3-Kinase

Phosphatidylinositol 3-kinases (PI3Ks) play key roles in regulating cell growth, cell cycle entry, cell migration and cell survival in response to cell stimulation by growth factors(Latorre et al., 2007) and hormones (Cantley, 2002). PI3K family members are divided into three classes. The best characterized class I PI3Ks (2920 out of 5364 total PI3K Pubmed entries to date) are heterodimers consisting of a catalytic p110 and a regulatory p85 subunits (Fig. 1.6). The catalytic subunit p110 has several functionally distinct domains: N-terminal adaptor-binding domain (ABD, also called p85 binding domain), a Ras-binding domain (RBD), a C2 domain, a helical domain and a catalytic domain. p85 regulatory subunit contains a Src homology 3 (SH3) domain, two proline-rich (PR) regions (PR1 and PR2) separated by a Rho-GAP/BCR-homology (BH) domain, and two Src homology 2 (SH2) domains (nSH2, cSH2) with an intervening inter-

SH2 (iSH) domain(Cheung et al., 2015). p85 regulatory subunit also serves as a “hub” for many protein-protein interactions that fine-tune the PI3K activity. For example, Ca^{2+}/calmodulin binds PI3K on cSH2 domain and enhances its activity (Joyal et al., 1997). In the basal state, the regulatory p85 subunit stabilizes the catalytic p110 subunit via iSH – ABD interaction and inhibits its enzymatic activity via nSH2 – helical

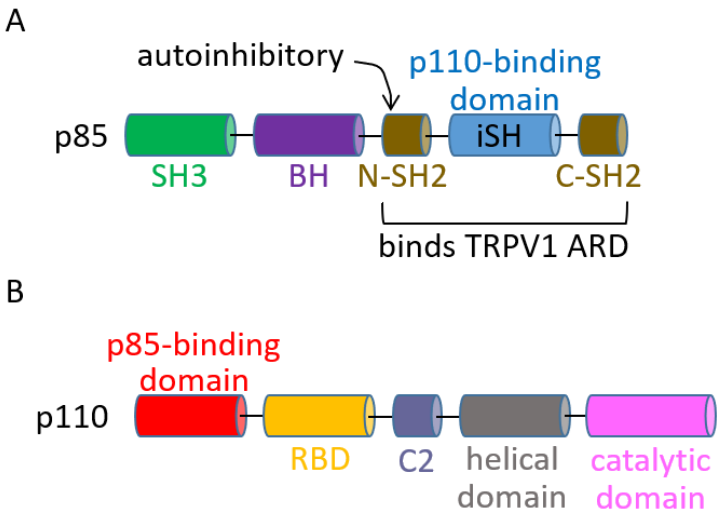

Fig. 1.6 Cartoon representation of the domain architecture of class I PI3K subunits. (A) regulatory subunit of class I PI3K p85. (B) catalytic subunit of class I PI3K p110.

domain interaction (Miled et al., 2007). Upon stimulation by growth factors, SH2 domains of p85 bind to one of the phospho-tyrosine residues on the receptor protein kinases (RTKs) (Dikic et al., 1995). This interaction brings the PI3K heterodimer to the plasma membrane and therefore promotes its activity due to close proximity to the lipid substrate (Cantley, 2002). Activated PI3Ks convert phosphatidylinositol-4,5-bisphosphate (PIP_2) to phosphatidylinositol-3,4,5-triphosphate (PIP_3). PIP_3 then recruits proteins that contain a PIP_3-specific pleckstrin homology domain (PH domain), such as Akt serine/threonine kinase to the cell membrane (James et al., 1996). The active membrane-associated Akt phosphorylate numerous protein targets, that mediate cell motility, actin remodeling, protein expression and membrane trafficking (Burgering and Coffer, 1995, Alessi et al., 1997, Ramaswamy et al., 1999, Aikawa et al., 2000, Haugh et al., 2000).

PI3K-dependent membrane trafficking is an important and conserved mechanism of acute response to growth factors and inflammatory mediators. For example, adipocytes and muscle cells use this

mechanism to regulate the number of GLUT4 glucose transporters on the plasma membrane, and thus glucose uptake in response to insulin (Huang and Czech, 2007). It has been shown that PI3K regulate membrane trafficking of TRPV1 in response to inflammation (Bonnington and McNaughton, 2003, Stein et al., 2006). As mentioned earlier, there is also evidence for direct interaction between PI3K and TRPV1, as it was observed in yeast 2-hybrid experiments and with recombinant PI3K and TRPV1 *in vitro* (Stein et al., 2006). These findings suggest a critical role for PI3K signaling in the induction of TRPV1 sensitization by NGF.

1.4 Inflammatory hyperalgesia

Increased pain caused by inflammation, or inflammatory hyperalgesia, is one of the most overwhelming features of inflammatory conditions (Ji et al., 2014). After tissue injury, locally released inflammatory mediators directly stimulate and sensitize nociceptive fibers of primary afferent neurons that innervate the inflamed tissue (Ren and Dubner, 1999, Donnerer et al., 1992). This includes classic inflammatory mediators (for example, bradykinin, prostaglandins, H^+, ATP and nerve growth factor), pro-inflammatory cytokines and chemokines (Ji et al., 2014).

Nerve growth factor (NGF) plays a crucial role in the development and survival of primary sensory neurons (Patel et al., 2000, Barde et al., 1980). In addition, NGF is also released during inflammation or injury (Donnerer et al., 1992), and causes hyperalgesia that can last from several hours to days (Petty et al., 1994). NGF acts directly on sensory terminals of DRG neurons (peptidergic C-fiber nociceptors (Donnerer et al., 1992)), which express two kinds of NGF receptors. NGF receptors are Receptor tyrosine kinases (RTK). Two kinds of NGF receptors are: the high-affinity Tropomyosin-receptor-kinase A (TrkA) (McMahon et al., 1995), and the low-affinity neurotrophin receptor, p75 (Lee et al., 1992). Upon NGF binding, NGF receptors undergo dimerization and autophosphorylation at several tyrosine residues (Cunningham et al., 1997) Phosphorylation of each tyrosine selectively triggers several intracellular signaling pathways via binding of specific effector proteins (Lemmon and Schlessinger, 2010). .

NGF produces profound hypersensitivity to heat and mechanical stimuli through two temporally distinct mechanisms. At first, a NGF-TrkA/p75 interaction activates downstream signaling pathways, including phospholipase C (PLC), mitogen-activated protein kinase (MAPK), and phosphoinositide 3-kinase

(PI3K) (Zhu and Oxford, 2007). In a matter of tens of minutes, this results in functional potentiation of target proteins at the peripheral nociceptor terminal, notably TRPV1, leading to a rapid change in heat sensitivity (Chuang et al., 2001). PIP_2 is a substrate for PI3K which phosphorylates it at the phospho-inositol ring 3 position to make another signaling lipid PIP_3 (more about this in section 1.3). In addition to these rapid actions, NGF is also retrogradely transported to the nucleus of the nociceptor (Tsui-Pierchala and Ginty, 1999), where it promotes increased expression of pronociceptive proteins, including substance P, TRPV1, and the Nav1.8 voltage-gated sodium channel subunit (Chao, 2003, Ji et al., 2002). These processes underlie the chronic hyperalgesia.

1.4.1 Involvement of TRPV1 in inflammatory hyperalgesia

Studies with the TRPV1 knockout mice determined that they show little, if any, inflammation-induced hyperalgesia (Caterina et al., 2000a, Davis et al., 2000) which points to the major role of TRPV1 in this process. Many studies have demonstrated that hyperalgesia in response to inflammatory mediators is carried out by modulation of TRPV1 activity through two mechanisms. First, PKA (Mohapatra and Nau, 2003, Bhave et al., 2002) or PKC (Bonnington and McNaughton, 2003) phosphorylation For example, bradykinin and prostaglandins released during inflammation or injury can activate PKC or PKA through their corresponding receptors. This leads to TRPV1 and enhanced sensitivity to capsaicin or heat (Bhave et al., 2003, Bhave et al., 2002, Zhu et al., 2009).

The second mechanism modulation of TRPV1 activity is through SNARE-dependent vesicular fusion (Camprubi-Robles et al., 2009) leading to increase in TRPV1 channel number on the plasma membrane of nociceptors. For example, TRPV1 sensitization mediated by NGF, ATP, and IGF-I is accompanied by a higher channel expression in the neuronal plasma membrane without measurable changes in channel gating properties, which was dependent on PI3-Kinase (Stein et al., 2006, Zhang et al., 2005, Bonnington and McNaughton, 2003) and prevented by blockade of regulated exocytosis (Camprubi-Robles et al., 2009) (see Fig. 1.7 for mechanism). A TrkA mutation that decouples NGF binding from activation of PI3K eliminates TRPV1 sensitization (Zhu and Oxford, 2007). Taken together, these findings suggest that there are at least two different mechanisms for TRPV1 sensitization by inflammatory

mediators: by increased channel activity (e.g. via phosphorylation) and increased channel number on the surface of the nociceptors.

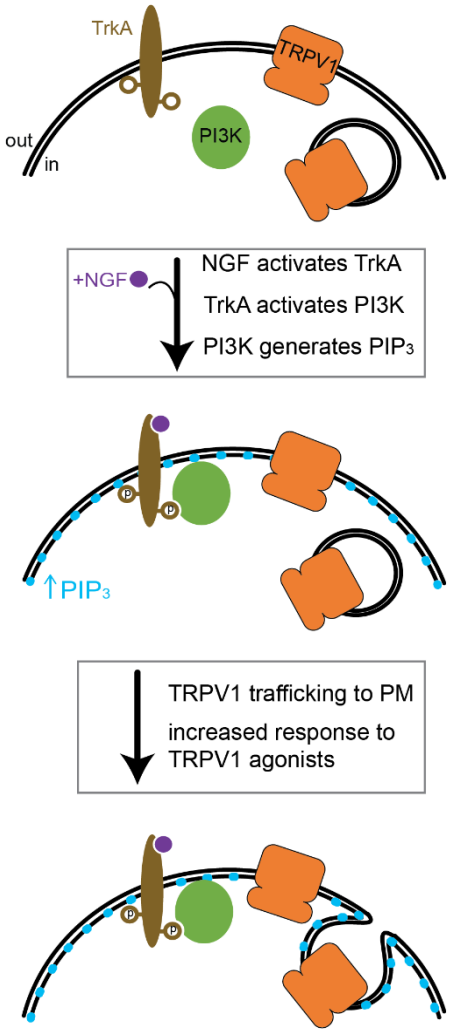

Fig. 1.7 Cartoon depicting signaling pathway leading to TRPV1 sensitization by NGF

A number of lines of evidence support the role of PI3K in TRPV1 sensitization described above. NGF sensitization of TRPV1 responses was absent in DRG neurons isolated from PI3K regulatory subunit p85α knock-out (KO) mice, and upon pharmacological inhibition of PI3K (Stein et al., 2006, Zhu and Oxford, 2007). In addition, the class I PI3K regulatory subunit p85 (more specifically, region of the two SH2 domains of the p85) was shown to interact with N-terminus of TRPV1 both in vitro and in yeast 2-hybrid studies (Stein et al., 2006). Until recently, it was not clear what was a physiological importance of this physical

interaction, and whether it influenced PI3K or TRPV1 activity directly. We have recently shown that physical interaction between PI3K and TRPV1 leads to potentiation of PI3K activity, suggesting a novel reciprocal regulation ((Stratiievska et al., 2018) and chapter 3. We have localized this to the ARD domain of TRPV1, which was sufficient to produce potentiation of PI3K activity.

1.4.2 Other TRPs in inflammatory hyperalgesia

TRPV2 is an ion channel with about 50% sequence similarity to TRPV1. This receptor, unlike TRPV1, has a higher threshold for heat activation (>52°C) and is mechanically sensitive (Caterina et al., 1999). Unlike TRPV1, TRPV2 is expressed by medium to large diameter sensory neurons which relay proprioception. TRPV2-/- mice have high neonatal mortality and are characterized by normal thermal and mechanical nociception (Park et al., 2011). Interestingly, unlike TRPV1, only the C-terminus of TRPV2 has been reported to interact with Calmodulin and this interaction does not affect channel Ca^{2+}-dependent desensitization (Phelps et al., 2010, Mercado et al., 2010). Highly expressed in skeletal and cardiac muscle, TRPV2 translocates to the cell membrane leading to higher intracellular Ca^{2+} in response to insulin-like growth factor-1 (IGF-1) (Iwata et al., 2009). This is the major cause of calcium overload and myocyte cell death, especially implicated in Duchenne muscular dystrophy (Lorin et al., 2015). PI3K is necessary for insertion of TRPV2-containing vesicles into plasma membrane of myocytes (Kanzaki et al., 1999). To summarize, although there is a lack of evidence for TRPV2 involvement in inflammatory hyperalgesia, TRPV2 may be involved in other similar signaling pathways.

It has been demonstrated that another close relative of TRPV1, TRPV4 plays a crucial role in mechanical pain sensation and hyperalgesia (Alessandri-Haber et al., 2006). TRPV4 is also warmth-activated, but unlike TRPV1, TRPV4 is mechanosensitive channel that is also involved in osmosensation. Similarly, to TRPV1, second-messenger pathways of cAMP/PKA and the PKC were proposed to be involved in TRPV4-dependent mechanical hyperalgesia (Alessandri-Haber et al., 2006, Cenac et al., 2010). Like TRPV1, TRPV4 N- and C-terminus have been reported to bind Calmodulin which is important for Ca^{2+}-dependent channel desensitization (Lishko et al., 2007, Phelps et al., 2010, Gonzalez et al., 2012) Importantly, inflammatory mediators such as metabolites of arachidonic acid (Watanabe et al., 2003),

prostaglandin E2 (PGE2) (Gu et al., 2003), and histamine (Cenac et al., 2010) were shown to activate and/or sensitize TRPV4.

TRPA1 is an ion channel sensitive to pungent irritants from mustard and garlic, and is also activated by painfully cold temperatures and mechanical stimuli (Kwan et al., 2006). Like TRPV1, TRPA1 has an ARD (~17 repeats compared to 6), that have different orientation from those of TRPV subfamily channels. TRPA1 has been proposed to function in diverse sensory processes, including thermal (cold) nociception (Karashima et al., 2009) and inflammatory pain (Bautista et al., 2006). TRPA1 is co-expressed with TRPV1 in a population of nociceptive DRG neurons where it is involved in inflammation- and nerve injury-induced cold hyperalgesia. Similarly to TRPV1, inflammatory mediators, such as bradykinin, sensitize TRPA1 in a PLC/PKA dependent manner (Meents et al., 2017, Wang et al., 2008), and NGF – in a p38 MAPK dependent manner to induce cold hyperalgesia (sensitivity to painful cold) (Obata et al., 2005). Like TRPV1, TRPA1 is also regulated by Ca^{2+}/calmodulin and directly interact with it via proximal C-terminal binding site in a Ca^{2+} dependent manner (Hasan et al., 2017).

2 Regulation of TRPV1 Ion Channel by Phosphoinositide (4,5)-Bisphosphate: THE ROLE OF MEMBRANE ASYMMETRY

Eric N. Senning[1], Marcus D. Collins[1], Anastasiia Stratiievska[1], Carmen A. Ufret-Vincenty, and Sharona E. Gordon

[1]These authors contributed equally to this work.

This chapter is a reproduction of a published manuscript.

2.1 Abstract

Membrane asymmetry is essential for generating second messengers that act in the cytosol and for trafficking of membrane proteins and membrane lipids, but the role of asymmetry in regulating membrane protein function remains unclear. Here we show that the signaling lipid phosphoinositide 4,5-bisphosphate ($PI(4,5)P_2$) has opposite effects on the function of TRPV1 ion channels depending on which leaflet of the cell membrane it resides in. We observed potentiation of capsaicin-activated TRPV1 currents by $PI(4,5)P_2$ in the intracellular leaflet of the plasma membrane but inhibition of capsaicin-activated currents when $PI(4,5)P_2$ was in both leaflets of the membrane, although much higher concentrations of $PI(4,5)P_2$ in the extracellular leaflet were required for inhibition compared with the concentrations of $PI(4,5)P_2$ in the intracellular leaflet that produced activation. Patch clamp fluorometry using a synthetic $PI(4,5)P_2$ whose fluorescence reports its concentration in the membrane indicates that $PI(4,5)P_2$ must incorporate into the extracellular leaflet for its inhibitory effects to be observed. The asymmetry-dependent effect of $PI(4,5)P_2$ may resolve the long standing controversy about whether $PI(4,5)P_2$ is an activator or inhibitor of TRPV1. Our results also underscore the importance of membrane asymmetry and the need to consider its influence when studying membrane proteins reconstituted into synthetic bilayers.

2.2 Introduction

The signaling lipid $PI(4,5)P_2$(Cao et al., 2013a) is universally accepted to play an essential role in regulation of TRPV1 ion channels. However, whether $PI(4,5)P_2$ activates or inhibits TRPV1 has been

debated for over a decade and remains unresolved(Collins and Gordon, 2013b, Cao et al., 2013a, Prescott and Julius, 2003, Chuang et al., 2001, Lukacs et al., 2007, Yao and Qin, 2009, Ufret-Vincenty et al., 2011, Mercado et al., 2010, Gordon-Shaag et al., 2008, Klein et al., 2008, Stein et al., 2006, Cao et al., 2013b, Liao et al., 2013, Collins and Gordon, 2013a, Devaux, 1992). As an activator, $PI(4,5)P_2$ has been proposed to associate with TRPV1 under basal conditions, acting as a cofactor for channel activation. As part of a negative feedback loop in response to Ca^{2+} influx into a cell, Ca^{2+} activation of phospholipase C would lead to depletion of $PI(4,5)P_2$ and a consequent reduction in TRPV1 activity. In contrast, $PI(4,5)P_2$ has also been proposed to tonically inhibit TRPV1 under basal conditions. In this scenario, depletion of $PI(4,5)P_2$ by phospholipase C would remove the inhibition, giving an increase in channel activity. This mechanism has been proposed to underlie the potentiation of TRPV1 in response to Gαq-coupled G protein-coupled receptors(Chuang et al., 2001, Lukacs et al., 2007). Interestingly, a dual effect of $PI(4,5)P_2$ has also been proposed in which $PI(4,5)P_2$ potentiates activation at high concentrations of the agonist capsaicin but inhibits activation at low concentrations of capsaicin(Lukacs et al., 2007).

The disparate roles proposed for $PI(4,5)P_2$ may arise, at least in part, from different experimental preparations used to study it. In whole cells, $PI(4,5)P_2$ levels can be reduced by converting it to either inositol trisphosphate and diacylglycerol (by phospholipase C) or phosphoinositol 4-phosphate (PI(4)P) by a lipid phosphatase. Do the products of $PI(4,5)P_2$ degradation influence the functional effects observed? We have shown that inositol trisphosphate antagonizes the activating effects of $PI(4,5)P_2$ in excised patches(Ufret-Vincenty et al., 2011), but, of course, this important second messenger can have a variety of targets in intact cells. More recently we have shown that PI(4)P directly activates TRPV1 but that this activation requires at least 20-fold higher concentrations of PI(4)P than $PI(4,5)P_2$ (Collins and Gordon, 2013b, Klein et al., 2008) so that it is unlikely to be a factor under typical experimental conditions.

In excised patches from either isolated sensory neurons or cultured cells expressing TRPV1, the activating effect of $PI(4,5)P_2$ on TRPV1 is somewhat less controversial. The application of natural or synthetic $PI(4,5)P_2$ to the intracellular side of inside-out excised patches from cells produces TRPV1 activation in all reported studies(Klein et al., 2008, Lukacs et al., 2007, Ufret-Vincenty et al., 2011, Stein et al., 2006). One popular form of $PI(4,5)P_2$ used extensively in excised patches is a short-chain, water-soluble

synthetic version with octanoyl chains at the sn-1 and sn-2 positions (diC8-PI(4,5)P_2,Fig. 2.1). Recent characterization of the partition coefficient of diC8-PI(4,5)P_2 into bilayers designed to resemble the intracellular leaflet of the plasma membrane allowed the apparent affinity of TRPV1 for diC8-PI(4,5)P_2 to be calculated, giving an EC50 of a few tenths of one mole percent(Collins and Gordon, 2013b). Resting levels of PI(4,5)P_2 have been measured to be about 1 mol % (Cheng et al., 2007). Although we have not measured the apparent affinity of TRPV1 for natural PI(4,5)P_2, it is still unclear whether PI(4,5)P_2 levels in the membrane are ever reduced sufficiently to cause its dissociation from TRPV1 under physiological conditions.

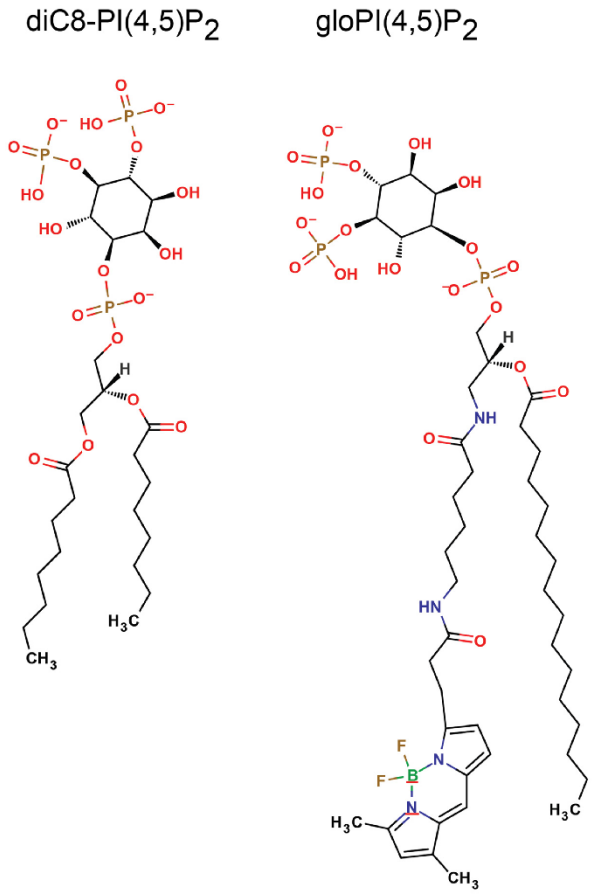

Fig. 2.1 Illustrations of diC8-PI(4,5)P_2 and gloPI(4,5)P_2 used in this study.

In a reduced system in which TRPV1 channels were purified and reconstituted into synthetic vesicles, TRPV1 in excised patches from liposomes prepared with 4 mol % $PI(4,5)P_2$ were shown to be inhibited relative to TRPV1 in patches from liposomes prepared without $PI(4,5)P_2$ (Cao et al., 2013a). Could this inhibition have been due to the extremely high concentration of $PI(4,5)P_2$ in the liposome membrane patches? Or could the structure of the synthetic liposome, compared with the structure of a cell plasma membrane, contribute to $PI(4,5)P_2$ inhibition of TRPV1? Alternatively, is a reevaluation of the effect of $PI(4,5)P_2$ on TRPV1 in excised patches warranted?

We hypothesized that the symmetry of the synthetic liposomes used for studies of reconstituted TRPV1 might explain the observed inhibition by $PI(4,5)P_2$. Cell membranes are asymmetric. That is, their intracellular leaflets and extracellular leaflets are composed of different lipids. Generally, the intracellular leaflet is dominated by phosphatidylethanolamine and phosphatidylserine (PS, about 15 mol %) with about 1 mol % of $PI(4,5)P_2$ and 1 mol % of PI(4)P. The intracellular leaflet, thus, has an overall surface potential of about −25 mV (Peitzsch et al., 1995). In contrast, the extracellular leaflet is dominated by phosphatidylcholine, with no phosphoinositides (Downes and Michell, 1982, Gascard et al., 1993, Burriss Garrett and Redman, 1975), and has an overall positive charge relative to the intracellular leaflet (Cheng et al., 2007). Thus, membrane proteins see a very different environment in the two leaflets (see Fig. 2.2). Here, we examined whether this asymmetry matters with respect to regulation of TRPV1 by $PI(4,5)P_2$. We found that $PI(4,5)P_2$ localized to the intracellular leaflet activated TRPV1. Importantly, $PI(4,5)P_2$ symmetrically localized to both leaflets inhibited TRPV1, although this required a very high concentration of $PI(4,5)P_2$ in the extracellular leaflet. These findings may explain the anomalous inhibition of reconstituted TRPV1 channels by $PI(4,5)P_2$ in symmetric liposome patches and emphasize the importance of membrane asymmetry when using reduced systems for studies of membrane proteins.

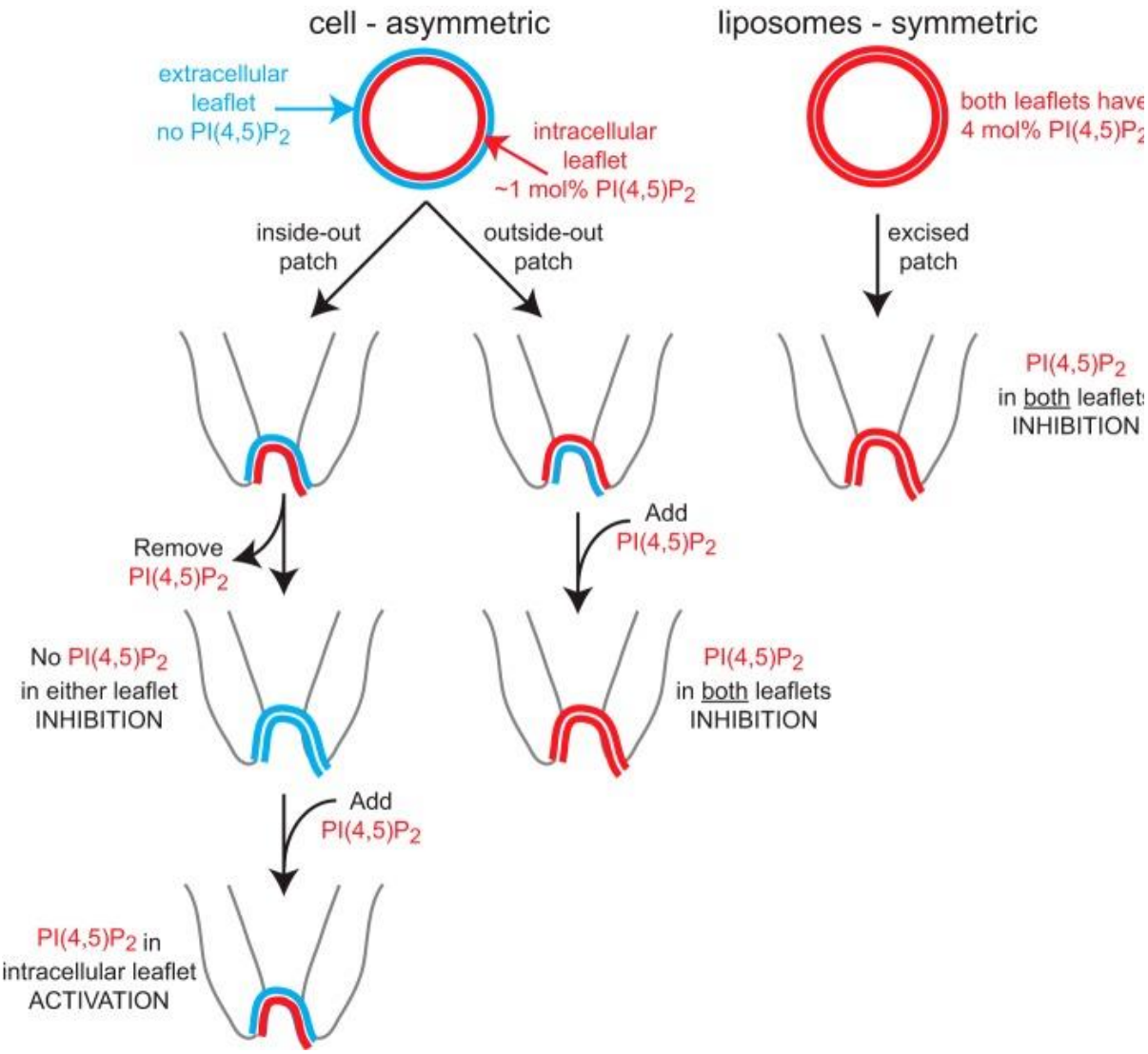

Fig. 2.2 Schematic of the relationship between membrane asymmetry and regulation of TRPV1. Blue represents a leaflet of the bilayer that does not contain $PI(4,5)P_2$, and red represents a leaflet of the bilayer that contains $PI(4,5)P_2$.

2.3 Results

2.3.1 PI(4,5)P_2 Activates TRPV1 When in the Intracellular Leaflet of the Plasma Membrane

To test the hypothesis that the asymmetry of PI(4,5)P_2 localization in the plasma membrane is important for regulation of TRPV1, we compared the effects of diC8-PI(4,5)P_2 (Lukacs et al., 2007, Ufret-Vincenty et al., 2011, Klein et al., 2008, Stein et al., 2006) on inside-out versus outside-out patches from HEK293T/17 cells transiently transfected with TRPV1. The exogenous agonist capsaicin freely equilibrates across the membrane so that it is equally effective when applied to the extracellular face of an outside-out patch as it is when applied to the intracellular face of an inside-out patch(Jung et al., 1999). No difference between the patch configurations was observed in the average current amplitude in response to 500 nm capsaicin (inside-out, 1410 pA ± 544 pA, n = 5; outside-out, 1070 pA ± 128 pA, n = 46; $p > 0.05$).

We have shown previously that TRPV1 is associated with PI(4,5)P_2 in inside-out excised patches and that sequestering the PI(4,5)P_2 using the nonselective scavenger polylysine leads to dissociation of PI(4,5)P_2 from the channels and inhibition of capsaicin-activated current (Stein et al., 2006). PI(4,5)P_2 in the intracellular leaflet of plasma membranes is expected to be at a concentration of roughly 1 mol % (Cheng et al., 2007, Wenk et al., 2003, Nasuhoglu et al., 2002, Ozato-Sakurai et al., 2011). We have shown recently that a solution concentration of about 50 μm diC8-PI(4,5)P_2 is required to give 1 mol % in a synthetic bilayer modeled after the intracellular leaflet of the plasma membrane of dorsal root ganglion neurons (Collins and Gordon, 2013b). As shown in Fig. 2.3, a and perfusion of 50 μm diC8-PI(4,5)P_2 onto inside-out patches enhanced TRPV1 activation by capsaicin (after pretreatment of patches with polylysine). Activation of TRPV1 by diC8-PI(4,5)P_2 applied to the intracellular leaflet of patches reversed upon removal of diC8-PI(4,5)P_2 from the bath (Ufret-Vincenty et al., 2011, Klein et al., 2008, Stein et al., 2006).

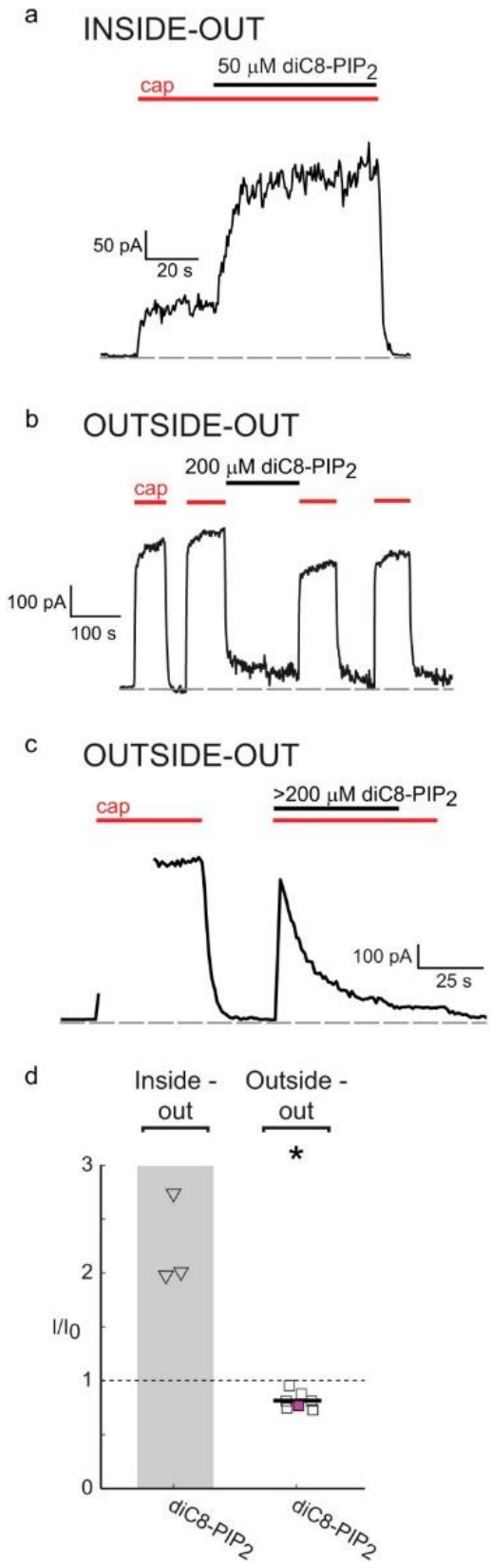

Fig. 2.3 Opposite regulation of TRPV1 by diC8-PI(4,5)P_2 applied to the opposite leaflets of the plasma membrane.

Currents during a jump to +60 mV from a holding potential of 0 mV with 500 nMcapsaicin (cap) or diC8-PI(4,5)P_2 in the bath, as indicated by the red or black bars, respectively. a, example of a current trace from an inside-out patch pretreated with polylysine and then treated with diC8-PI(4,5)P_2. b, representative current trace of an outside-out patch treated with diC8-PI(4,5)P_2. After two sequential perfusions of 500 nM capsaicin, a solution concentration of 200 μM diC8-PI(4,5)P_2 was used for ≥100 s, equivalent to the expected concentration of ≤~9 mol % in the extracellular leaflet of the membrane(Collins and Gordon, 2013b). c, current trace of outside-out patch with 500 nM capsaicin applied in the presence of a high concentration of >200 μMdiC8-PI(4,5)P_2. The missing portion of the trace during capsaicin perfusion is due to I-V curve acquisition. Dashed lines represents zero current. d, potentiation or inhibition of TRPV1 currents by application of diC8-PI(4,5)$P_2$to the intracellular (inside-out, initial capsaicin current (I_0) determined just prior to perfusion with diC8-PI(4,5)P_2 and final current (I) recorded between 60 and 1135 s after diC8-PI(4,5)P_2 was added to the bath, as described in Ref.(Klein et al., 2008) or extracellular (outside-out, only experiments using perfusion protocol shown in b are included where capsaicin current (I_0) determined just prior to perfusion with diC8-PI(4,5)P_2 and final current (I) recorded at 30 s after the end of diC8-PI(4,5)P_2 perfusion) leaflet. ▽, diC8-PI(4,5)P_2applied to inside-out patch; □, diC8-PI(4,5)P_2 applied to outside-out patch, median I/I_0 = 0.81 (n = 7, p = 0.016); purple square, I/I_0 of representative trace in b. Statistical significance (*) was determined by Wilcoxon signed-rank test, p <

2.3.2 $PI(4,5)P_2$ Inhibits TRPV1 When in Both Leaflets of the Plasma Membrane

In excised patches, native $PI(4,5)P_2$ is present only in the intracellular leaflet (i.e. the membrane is asymmetric, Fig. 2.2). To test the effect of symmetric $PI(4,5)P_2$ in the plasma membrane, we examined the effects of diC8-$PI(4,5)P_2$ applied to the bath on TRPV1 channels in outside-out patches (Fig. 2.3, b–d). These patches would then have native $PI(4,5)P_2$ in the intracellular leaflet and diC8-$PI(4,5)P_2$ in the extracellular leaflet (Fig. 2.2). A solution concentration of 50 μm diC8-$PI(4,5)P_2$ did not significantly alter the capsaicin-activated current when applied to outside-out patches. However, application of ≥200 μm diC8-$PI(4,5)P_2$ onto outside-out patches produced robust inhibition of the capsaicin-activated current (Fig. 2.3, b–d). A solution concentration of 200 μm is expected to produce ≤~9 mol % in the extracellular leaflet of the patch (Collins and Gordon, 2013b). Interestingly, the recent report showing inhibition of TRPV1 by symmetric $PI(4,5)P_2$ used bilayers with 4 mol % $PI(4,5)P_2$ (Cao et al., 2013a).

An important technical consideration was noted when high concentrations of diC8-$PI(4,5)P_2$ were applied to patches in the presence of ≥500 nm capsaicin. Under these conditions, the effect of diC8-$PI(4,5)P_2$ on the capsaicin-activated current was highly variable (compare Fig. 2.3, b and c) and not always observed. We suspected that the detergent-like qualities of capsaicin could decrease the critical micellar concentration of diC8-$PI(4,5)P_2$, thereby limiting the concentration of diC8-$PI(4,5)P_2$ monomers in solution and, thus, the mole fraction of diC8-$PI(4,5)P_2$ achieved. On the basis of our previous work, we expect the critical micellar concentration of diC8-$PI(4,5)P_2$ to be greater than ~3 mm (Collins and Gordon, 2013b). Although this is a factor of 10 or more greater than the concentration of diC8-$PI(4,5)P_2$ used here, it seemed possible that the addition of capsaicin could reduce the free concentration of diC8-$PI(4,5)P_2$ in solution below that required to inhibit TRPV1. Our collected data (Fig. 2.3, d), therefore, reflect only experiments in which diC8-$PI(4,5)P_2$ was applied in the absence of capsaicin. Note that applying diC8-$PI(4,5)P_2$ to outside-out patches and measuring subsequent capsaicin-activated channel activity was only possible because the inhibition produced by diC8-$PI(4,5)P_2$ reversed very slowly upon its removal from the bath (Fig. 2.4).

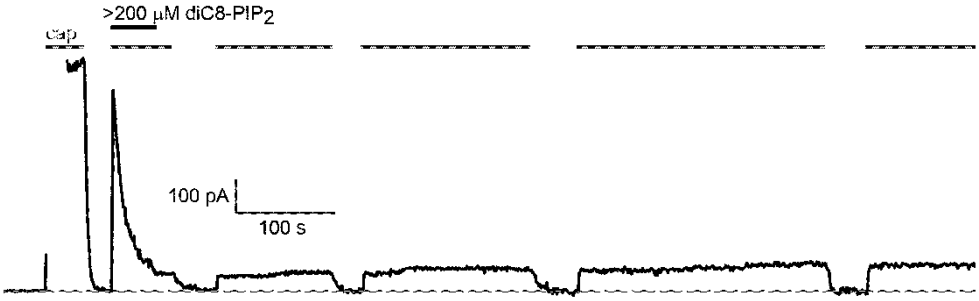

Fig. 2.4 Recovery of current in outside-out patch from inhibition by diC8-PI(4,5)P_2 applied to extracellular leaflet.

Figure is full current trace of Fig. 2.3 c in main text. Dashed line represents zero current.

2.3.3 Inhibition of TRPV1 by PI(4,5)P_2 in the Extracellular Leaflet Involves PI(4,5)P_2 Incorporation into the Bilayer

We next examined whether partitioning of diC8-PI(4,5)P_2 into the extracellular leaflet of the plasma membrane was required for its inhibition of TRPV1. Perhaps the headgroup of the phosphoinositide interacted with TRPV1 while in solution without need for its incorporation into the bilayer. A form of PI(4,5)P_2 that reports its partitioning into the membrane would allow us to determine whether this is the case.

To determine whether inhibition of TRPV1 by PI(4,5)P_2 involves partitioning of PI(4,5)P_2 into the extracellular leaflet of the plasma membrane, we used patch clamp fluorometry (Zheng and Zagotta, 2003). We used a long-chain PI(4,5)P_2, called gloPI(4,5)P_2, with a terminal BODIPY-FL moiety at the sn-1 position (Fig. 2.1). The properties of the BODIPY-FL moiety are particularly advantageous. Its fluorescence is quenched in aqueous solution, and it becomes fluorescent upon partitioning into the membrane (Bai and Pagano, 1997) (see “Experimental Procedures”). By recording the BODIPY-FL fluorescence simultaneous with the capsaicin-activated current in an outside-out excised patch, we could determine whether the change in fluorescence we observed tracked the change in current. Of course, for the fluorescence of gloPI(4,5)P_2 to be useful, its functional effects must mirror those of diC8-PI(4,5)P_2. As shown in Fig. 2.4, gloPI(4,5)P_2 activated TRPV1 when applied to inside-out patches and inhibited TRPV1 when applied to outside-out patches. Thus, gloPI(4,5)P_2 is an appropriate surrogate for diC8-PI(4,5)P_2, and its fluorescence in patches can be used to measure its partitioning into the extracellular leaflet of the plasma membrane.

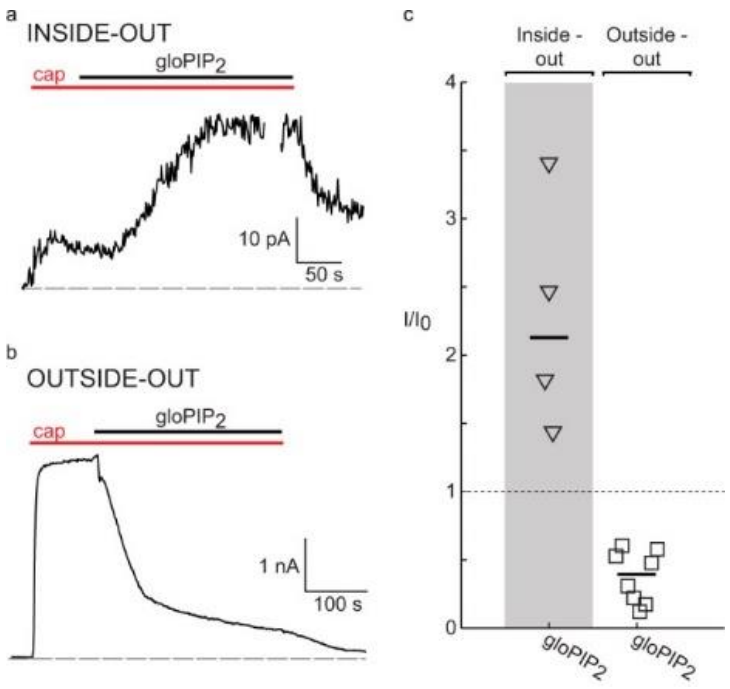

Fig. 2.5 Opposite regulation of TRPV1 by gloPI(4,5)P_2 applied to the opposite leaflets of the plasma membrane. Currents measured during a pulse to +60 mV from a holding potential of 0 mV with 500 nM capsaicin (cap) in the absence and presence of 1 μMgloPI(4,5)P_2 in the bath, as indicated by the red and black bars, respectively. a, inside-out patch pretreated with polylysine. b, outside-out patch. The dashed line represents zero current. c, collected data from inside-out (n = 4, median I/I_0 = 2.1) (▽) and outside-out (n = 8, median I/I_0 = 0.39) (□) patches with the current in the presence of gloPI(4,5)P_2 (I), determined between 152–529 s after the start of gloPIP2 perfusion depending on the patch, normalized to the current in the absence of gloPI(4,5)P_2 (I_0), determined just prior to addition of gloPIP_2.

As shown in Fig. 2.5, inset, upon addition of gloPI(4,5)P_2 to the patch, the patch fluorescence increased even though little background fluorescence was observed in the bath. We calculated the mole percent of gloPI(4,5)P_2 in the patch membrane from the fluorescence in the patch (see Fig. 2.7 and "Experimental Procedures") and plotted one minus mole percent (blue trace) on the same time scale as we plotted the current (black trace). We found that the inhibition of TRPV1 by gloPI(4,5)P_2 occurred with the same time course as the partitioning of gloPI(4,5)P_2 into the extracellular leaflet of the plasma membrane. The simplest interpretation of the coincidence between partitioning of gloPI(4,5)P_2 into the membrane and inhibition of TRPV1 by gloPI(4,5)P_2 is that TRPV1 is inhibited by gloPI(4,5)P_2 incorporated into the extracellular leaflet of the plasma membrane.

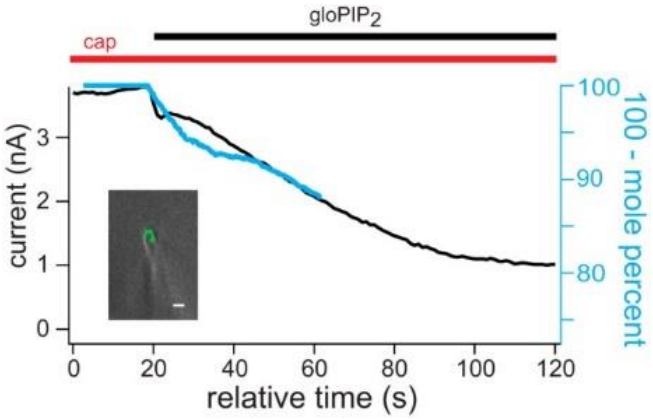

Fig. 2.6 The fluorescence of gloPI(4,5)P_2 reports its concentration in the membrane. Shown is 100 − mol % (blue) and current (black) versus the time from the patch shown in the inset. Calculation of mole percent from fluorescence was as described under "Experimental Procedures." The experiment was repeated in four patches. Inset, image of an outside-out excised patch in bright-field (grayscale) and epifluorescence (green). Scale bar = 5 μm. cap, capsaicin.

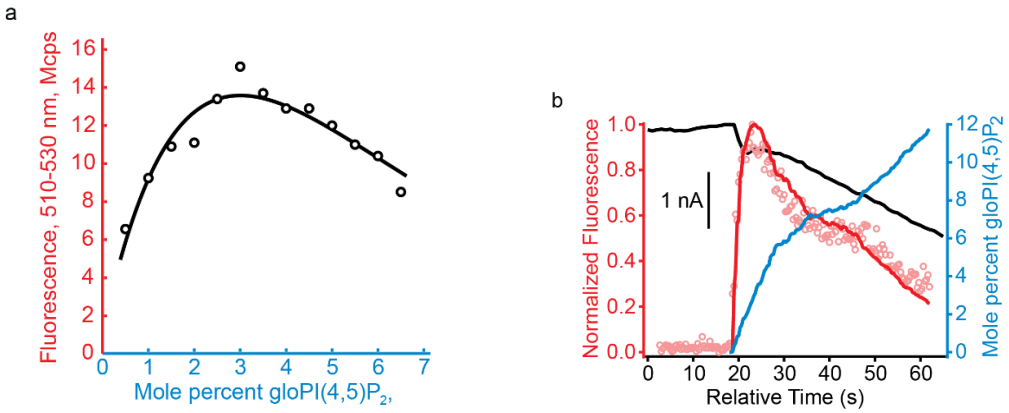

Fig. 2.7 Conversion of gloPI(4,5)P_2 fluorescence into mole percent. (a) Fluorescence from gloPI(4,5)P_2 in POPC liposomes (circles) and a model fit to that fluorescence, as described in the Methods (black curve). (b) Capsaicin and gloPI(4,5)P_2 evoked current (black curve) and fluorescence (red circles) in outsideout patches, as in Fig. 2.6 of the main text. The blue curve is an estimate of the mole percent of gloPI(4,5)P_2 in the patch membrane, derived by fitting the expected fluorescence (red curve) — itself calculated from the model shown in (a) — to the experimentally determined fluorescence, using a heuristic procedure described in the Methods.

The inhibition of the capsaicin-activated current by gloPI(4,5)P_2 became significant above ~4 mol % (Fig. 2.6 and Fig. 2.7, b). This could be an underestimate, however, because the binding of gloPI(4,5)P_2

to TRPV1 may not have reached steady state. Even with this caveat, we can conclude that the apparent affinity of TRPV1 for diC8-PI(4,5)P_2 (up to between roughly 4 and 9 mol % or between 50 and 200 μm in solution, Fig. 2.3) and gloPI(4,5)P_2 (about 4 mol %, Fig. 2.6) in the extracellular leaflet are on the same order of magnitude.

2.3.4 Other diC8 Lipids Affect TRPV1 Activity When Applied to the Extracellular Surface of Outside-out Patches

Like PI(4,5)P_2, significant amounts of phosphatidylinositol (PI), PI(4)P, and PS are present in the intracellular leaflet of the plasma membrane at rest. PI and PI(4)P are each believed to comprise ~1 mol % of phospholipids and PS ~10% of phospholipids in the intracellular leaflet of the plasma membrane (Gascard et al., 1993, Ozato-Sakurai et al., 2011, Gascard et al., 1991, Devaux, 1992). In addition, like PI(4,5)P_2, PI and PI(4)P have been shown to inhibit TRPV1 reconstituted into liposomes when these phospholipids are present in both leaflets of the bilayer (Cao et al., 2013a). Therefore, we examined whether the addition of diC8-PI, diC8-PI(4)P, diC8-PG, or diC8-PS to outside-out patches would alter the activity of TRPV1 (Fig. 2.8).

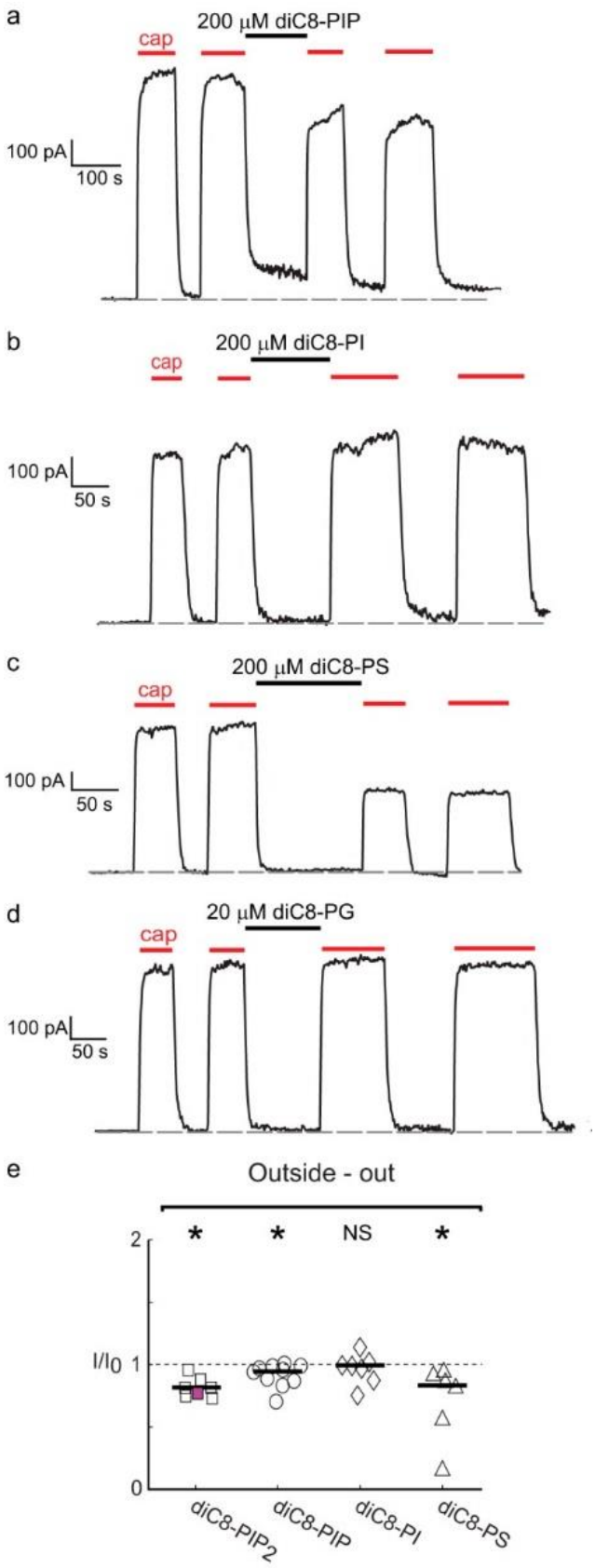

Fig. 2.8 Representative traces of currents from outside out patches elicited by capsaicin before and after perfusion with diC8 phospholipids. a, 200 μM diC8-PI(4)P treatment. cap, capsaicin. b, 200 μM diC8-PI treatment. c, 200 μM diC8-PS treatment. d, 20 μM diC8-PG treatment. The dashed linerepresents zero current. e, inhibition of TRPV1 currents by application of different diC8 phospholipids to the extracellular (outside-out, only experiments using perfusion protocol shown in Fig. 2.3b are included, and calculation of I/I_0 is as described for outside-out patches in Fig. 2.3 d) leaflet. □, diC8-PI(4,5)P_2, median I/I_0 = 0.81 (n = 7, p = 0.016). The purple square is I/I_0 of the representative trace in Fig. 2.3 b. ○, diC8-PI(4)P, median I/I_0 = 0.95 (n = 10, p = 0.004). ◊, diC8-PI, median I/I_0 = 0.99 (n = 7, p = 0.470). ▵, diC8-PS, median I/I_0 = 0.83 (n = 6, p = 0.031). Statistical significance (*) or non-significance (NS) of inhibition was determined by Wilcoxon signed-rank test, p < 0.05

As shown in Fig. 2.8e, application of 200 μm diC8-PI(4)P and diC8-PS produced a small but statistically significant inhibition of the capsaicin-activated current, whereas application of diC8-PI did not. The experiments with application of diC8-PS showed a broader distribution of responses than the other short-chain phospholipids we tested, and five of 11 patches were lost during the perfusion of diC8-PS (Fig. 2.6a). Ordinarily, PS is asymmetrically distributed on the intracellular leaflet of the plasma membrane. However, in a population of cells, we expect that there is some natural variability to the amount of PS that resides in their extracellular leaflets, and this could broaden our distribution of diC8-PS results (Devaux, 1992, Bevers and Williamson, 2010). Addition of 200 μm diC8-PG to outside-out patches resulted in loss of the patch seal in three consecutive experiments (Fig. 2.6b), and when we reduced the concentration of diC8-PG to 20 μm, there was no apparent inhibition (n = 3, Fig. 2.8d). Even when the solution concentrations of each of these short-chain phospholipids were the same, we expect that they would be present in the extracellular leaflet at somewhat higher mole fractions than the cognate concentration of diC8-PI(4,5)P_2 because of their lower charge density. We have shown previously that diC8-PI(4)P partitions into a synthetic bilayer modeled to represent the overall charge and saturation of the intracellular leaflet about twice as well as diC8-PI(4,5)P_2 (Collins and Gordon, 2013b). Without similar measurements of the partition coefficients of diC8-PI(4)P, diC8-PI, and diC8-PS into synthetic bilayers modeled to represent the overall charge and saturation of the extracellular leaflet, we cannot quantitatively compare the effects of these lipids to those of diC8-PI(4,5)P_2.

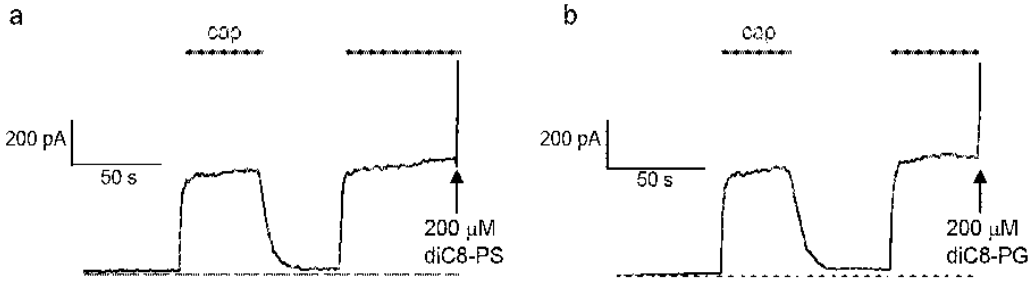

Fig. 2.9 Representative traces of currents from outside out patches lost after treatment with (a) 200 uM diC8-PS or (b) 200 uM diC8-PG.
Dashed line represents zero current.

2.4 Discussion

The controversy surrounding whether $PI(4,5)P_2$ in the intracellular leaflet activates or inhibits TRPV1 has important consequences for how we think about its physiological role. Viewed as an activator, $PI(4,5)P_2$ depletion has been proposed to underlie Ca^{2+}-dependent desensitization (Lukacs et al., 2007, Yao and Qin, 2009, Ufret-Vincenty et al., 2011). Viewed as an inhibitor, $PI(4,5)P_2$ depletion has been proposed to underlie G protein-coupled, receptor-mediated sensitization (Chuang et al., 2001). Thus, whether $PI(4,5)P_2$ depletion is activating or inhibitory directs our thinking about whether changes in its concentration produce desensitization or sensitization.

We favor the view that $PI(4,5)P_2$ in the intracellular leaflet of the plasma membrane is an activator of, or at least cofactor for, TRPV1 on the basis of a the following evidence. Application of either short-chain, long-chain, or natural $PI(4,5)P_2$ to the intracellular leaflet of excised patches or to one side of a planar bilayer containing reconstituted TRPV1 potentiates activation of TRPV1 (Lukacs et al., 2007, Stein et al., 2006, Lukacs et al., 2013). Application of purified, recombinant pleckstrin homology domain protein from phospholipase Cδ1, a $PI(4,5)P_2$-selective binding protein, to inside-out excised patches inhibits the capsaicin-activated current(Klein et al., 2008). Depletion of $PI(4,5)P_2$ by either a voltage-sensitive phosphatase or a chemically inducible phosphatase inhibits capsaicin-activated currents (Klein et al., 2008, Lukacs et al., 2007). The nonspecific anion-sequestering agent polylysine, which is expected to sequester all anionic lipids in the membrane, inhibits capsaicin-activated currents (Lukacs et al., 2007, Stein et al., 2006). Inclusion of diC8-$PI(4,5)P_2$ in the whole-cell patch pipette reduces desensitization (Lishko et al., 2007). Ca^{2+} influx through TRPV1 produces simultaneous $PI(4,5)P_2$ depletion and inhibition of the current (desensitization) (Mercado et al., 2010).

$PI(4,5)P_2$ in the intracellular leaflet has also been proposed to directly inhibit TRPV1. An intriguing new set of findings adds to the evidence for $PI(4,5)P_2$ as an inhibitor of TRPV1. Purified TRPV1 channels were reconstituted into synthetic liposomes of defined composition and analyzed with patch clamp electrophysiology (Cao et al., 2013a). The temperature and capsaicin dependence were measured in liposomes that included either no phosphoinositides or 4% $PI(4,5)P_2$. TRPV1 in the $PI(4,5)P_2$-containing

liposomes showed a significantly higher temperature threshold for activation, increasing from about 27 °C (no $PI(4,5)P_2$) to about 38 °C (4% $PI(4,5)P_2$).

A consequence of lipid mixing during liposome production is the symmetric distribution of lipids in the bilayer. In a recent reconstitution experiment with TRPV1, Lukacs et al. generated an asymmetric lipid bilayer by introducing diC8-$PI(4,5)P_2$ to the cis compartment of a painted bilayer (Cao et al., 2013a). These reconstitution experiments convincingly demonstrate that $PI(4,5)P_2$ asymmetry in the plasma membrane is a critical necessity and not inhibitory to TRPV1 function (Lukacs et al., 2013).

The inhibition of TRPV1 by $PI(4,5)P_2$ in the extracellular leaflet we report here may reconcile the physiological role of $PI(4,5)P_2$ as an activator of TRPV1 with $PI(4,5)P_2$ inhibition of TRPV1 observed in the reconstituted system of Cao et al. Of course, a number of other experimental differences between our work with channels in biological membranes and observations made using purified channels reconstituted into synthetic bilayers may further contribute to the differences in channel properties measured. However, the $PI(4,5)P_2$ inhibition we report here indicates that the presence of $PI(4,5)P_2$ in both leaflets of the bilayer would be expected to contribute to the $PI(4,5)P_2$ inhibition observed in that system.

Is the inhibition of TRPV1 observed when $PI(4,5)P_2$ is located in both leaflets of the bilayer a general indictment of efforts to reconstitute membrane proteins into membranes of defined composition? We view such well controlled experiments as essential for studies of how membrane properties affect membrane protein function. Nonetheless, the nonphysiological inhibition of TRPV1 produced by symmetric $PI(4,5)P_2$ in synthetic bilayers serves as a reminder that membrane asymmetry matters and challenges us to mimic biologically relevant properties of the membrane when studying reconstituted membrane proteins.

2.5 Experimental procedures

2.5.1 Cell Culture and Transfection

HEK 293T/17 cells were cultured at 37 °C, 5% CO2, in Dulbecco's modified Eagle's medium (Invitrogen) containing 25 mm glucose, 1 mm sodium pyruvate, and 4 mm l-glutamine. Culture medium was supplemented with 10% fetal bovine serum and penicillin/streptomycin. Cells were transfected using Lipofectamine 2000 according to the instructions of the manufacturer. 12 h after transfection, cells were

placed on 25-mm glass coverslips (coated with polylysine to aid cell attachment) and left in culture until used for experimentation 12–48 hours later.

2.5.2 Electrophysiology Recording

Currents were recorded using filamented borosilicate glass pipettes (1.2-mm outer diameter, 1.0-mm inner diameter) heat polished to a resistance of 3–6 MΩ. Symmetrical solutions were used, containing 130 mm NaCl, 0.2 mm EDTA, and 3 mm HEPES (pH 7.2). Outside-out patches were formed by first using suction to achieve electrical continuity with the cytosol and then slowly moving the pipette away from the cell. Perfusion was achieved by positioning the pipette directly in front of a barrel through which solutions flowed, controlled by an RSC-200 rapid solution changer device (Biologic Instruments). The dioctanoyl phosphoinositides, diC8-PI(4,5)P_2, diC8-PI(4)P, diC8-PI (all from Echelon Biosciences), diC8-PS, and diC8-PG (both from Avanti Lipids) were applied in this manner. To prepare aliquots of phospholipids from Echelon Biosciences, we weighed the shipping vials before and after removing the lyophilized product with water to accurately determine the amount supplied to us. Methods to measure TRPV1 current potentiation with diC8-PI(4,5)P_2 from inside-out patches have been described previously (Klein et al., 2008). Inhibition of TRPV1 current in outside-out patches by diC8 phospholipid was determined by calculating a ratio (I/I0) of the current during capsaicin perfusion 30 s after ≥100 s of phospholipid exposure (I) to the current during capsaicin perfusion just prior to phospholipid exposure (I0). GloPI(4,5)P_2 (Echelon Biosciences,Fig. 2.1) was applied manually as follows. First, most of the solution in the chamber was removed via suction, leaving just enough to immerse the tip of the patch pipette. GloPI(4,5)P_2 was then added to the chamber with a glass pipette to an estimated final concentration of 1 μm. This procedure was meant to reduce adherence of the long-chain phosphoinositide to the Teflon and polyethylene perfusion tubing. In all experiments, patches were held at a potential of 0 mV and jumped to +60 mV and −60 mV for between 80–100 ms. Currents shown are difference currents in which the current in the absence of capsaicin has been subtracted. Patches with a seal resistance of <1 GΩ were not used.

2.5.3 Patch Clamp Fluorometry

Experiments were performed using a Nikon TiE microscope equipped with a Photometrics QuantEM camera. Excitation with the 488-nm line of an argon laser was attenuated with an acousto-optic modulator. The emission light was filtered through a 495-nm long-pass filter. Exposure time was 100 ms. Data were analyzed using ImageJ (Schneider et al., 2012). Data shown are the difference in mean intensity within a region of interest including the patch and mean intensity within an adjacent background region.

The fluorescence of gloPI(4,5)P_2 was converted to mole fraction of membrane lipids as follows. BODIPY fluorescence self-quenches at high densities because of excimer formation(Bai and Pagano, 1997) so that small aggregates or vesicles found in solution fluoresce little. As the gloPI(4,5)P_2 inserts into the bilayer, it is diluted, and its fluorescence increases. However, as the concentration of gloPI(4,5)P_2 in the bilayer increases further, the fluorescence per fluorophore decreases as excimer formation becomes more likely. Above a concentration in the membrane of about 3 mol %, self-quenching dominates, and total fluorescence decreases with increasing concentrations. We measured the fluorescence from gloPI(4,5)P_2 in 1,2-dioleoyl-sn-glycero-3-phosphocholine liposomes at concentrations from 0.5–6.5 mol %. The lipids were mixed in 2:1 chloroform-methanol, dried under a vacuum, resuspended in 155 mm KCl, 25 mm HEPES (pH 7.4) at ~0.25 mm, and then sonicated in a high-power bath sonicator for 10 min to produce small unilamellar liposomes. 100 μl of each sample and 200 μl of the original buffer were mixed in the wells of a 96-well plate. Fluorescence spectra (500–700 nm) were recorded using 488-nm excitation in a Horiba FluorLog 3 with a plate reader attachment. Fluorescence intensity was integrated from 510–530 nm (to cover the peak which shifts slightly with fluorophore concentration, and this was fit to a model for BODIPY quenching(Dahim et al., 2002), $F = Q_m \Gamma \exp(-\pi R_m^2 \Gamma)$, where Γ is the area density of the fluorophore, Q_m accounts for quantum efficiency and geometric factors, and R_m characterizes fluorescence quenching versus distance. The model and data are shown in Fig. 2.7a. We found that R_m = 2.6 nm, which is indistinguishable from that for other related BODIPY-labeled lipids (Bai and Pagano, 1997, Dahim et al., 2002).

To estimate the mole percent of gloPI(4,5)P_2 in the patch membranes, we fit a model to the fluorescence recorded from excised outside-out patches. Fluorescence was calculated from the model

parameters (the mole percent of gloPI(4,5)P_2 at each time) and the F versus Γ model above. Given the number of parameters, it is necessary to apply a "soft" constraint that the concentration of gloPI(4,5)P_2 in the membrane increases at each time step. This is implemented in the fitting function as a finite penalty for the mole fraction decreasing from one time point to the next. The final model fit depends on the strength of the penalty, which is chosen qualitatively. Although the quantification shown is, thus, a rough estimate only, for every choice of the penalty strength we obtain very similar results. The results are shown in Fig. 2.6 and in more detail in Fig. 2.3b. Finally, it should be noted that, although this is a reasonable estimate of mole percent gloPI(4,5)P_2 in the membrane, the interaction between gloPI(4,5)P_2 and TRPV1 may not have achieved steady state. Therefore, the apparent concentration dependence for inhibition may underestimate the apparent affinity of TRPV1 for gloPI(4,5)P_2.

2.6 Acknowledgments

We thank Drs. William N. Zagotta, Roger Hardie, and Tamara Rosenbaum for comments on an early version of the manuscript.

This work was supported, in whole or in part, by NIGMS, National Institutes of Health Grant R01GM100718; by NEI, National Institutes of Health Grants R01EY017564 and P30EY001730; by the National Center for Research Resources, National Institutes of Health Grant S10RR025429; and by NIDDK, National Institutes of Health Grants P30DK017047, T32EY007031, and T32HL007312.

3 Reciprocal regulation among TRPV1 channels and phosphoinositide 3-kinase in response to nerve growth factor

Anastasiia Stratiievska, Sara Nelson, Eric N Senning, Jonathan D Lautz, Stephen EP Smith, Sharona E Gordon

University of Washington, United States; Seattle Children's Research Institute, United States

This chapter is a reproduction of a published manuscript with addendums.

3.1 Abstract

Although it has been known for over a decade that the inflammatory mediator NGF sensitizes pain-receptor neurons through increased trafficking of TRPV1 channels to the plasma membrane, the mechanism by which this occurs remains mysterious. NGF activates phosphoinositide 3-kinase (PI3K), the enzyme that generates $PI(3,4)P_2$ and PIP_3, and PI3K activity is required for sensitization. One tantalizing hint came from the finding that the N-terminal region of TRPV1 interacts directly with PI3K. Using two-color total internal reflection fluorescence microscopy, we show that TRPV1 potentiates NGF-induced PI3K activity. A soluble TRPV1 fragment corresponding to the N-terminal Ankyrin repeats domain (ARD) was sufficient to produce this potentiation, indicating that allosteric regulation was involved. Further, other TRPV channels with conserved ARDs also potentiated NGF-induced PI3K activity. Our data demonstrate a novel reciprocal regulation of PI3K signaling by the ARD of TRPV channels.

3.2 Introduction

Although the current opioid epidemic highlights the need for improved pain therapies, in particular for pain in chronic inflammation (Johannes et al., 2010), too little is known about the mechanisms that mediate increased sensitivity to pain that occurs in the setting of injury and inflammation (Ji et al., 2014). Inflammatory hyperalgesia, the hypersensitivity to thermal, chemical, and mechanical stimuli (Cesare and McNaughton, 1996), can be divided in two phases, acute and chronic (Dickenson and Sullivan, 1987). Locally released inflammatory mediators, including growth factors, bradykinin, prostaglandins, ATP and

tissue acidification, (Kozik et al., 1998, Lardner, 2001, Tissot et al., 1989, Burnstock, 1972), directly stimulate and sensitize nociceptive fibers of primary sensory neurons (Cesare and McNaughton, 1996, Bevan and Yeats, 1991, Trebino et al., 2003, Hamilton et al., 1999, McMahon et al., 1995).

One of the proteins that has been studied for its role in hyperalgesia is Transient Receptor Potential Vanilloid Subtype 1 (TRPV1). TRPV1 is a non-selective cation channel that is activated by a variety of noxious stimuli including heat, extracellular protons, and chemicals including capsaicin, a spicy compound in chili pepper (Caterina et al., 1999). TRPV1 is expressed in sensory nociceptive neurons, which are characterized by cell bodies located in the dorsal root ganglia (DRG) and trigeminal ganglia (Caterina et al., 1999). Sensory afferents from these neurons project to skin and internal organs, and synapse onto interneurons in the dorsal horn of the spinal cord (Willis WJ, 1978). TRPV1 activation leads to sodium and calcium influx, which results in action potential generation in the sensory neuron and, ultimately, pain sensation (Caterina et al., 1997).

The importance of TRPV1 in inflammatory hyperalgesia was demonstrated by findings that the TRPV1 knock-out mouse showed decreased thermal pain responses and impaired inflammation-induced thermal and chemical hyperalgesia (Caterina et al., 2000b). TRPV1 currents are enhanced during inflammation which leads to increased pain and lowered pain thresholds (Davis et al., 2000, Zhang et al., 2005, Shu and Mendell, 1999). TRPV1 is modulated by G-protein coupled receptors (GPCRs) and receptor tyrosine kinases (RTKs), but the mechanisms by which these receptors modulate and sensitize TRPV1 are controversial (Suh and Oh, 2005, Shu and Mendell, 1999, Cesare and McNaughton, 1996).

Nerve growth factor (NGF) is one of the best studied RTK agonists involved in inflammatory hyperalgesia (Vetter et al., 1991). NGF acts directly on peptidergic C-fiber nociceptors (Donnerer et al., 1992), which express RTK receptors for NGF: Tropomyosin-receptor-kinase A (TrkA) (McMahon et al., 1995) and neurotrophin receptor $p75_{NTR}$ (Lee et al., 1992). NGF binding to TrkA/$p75_{NTR}$ induces receptor auto-phosphorylation and activation of downstream signaling pathways including phospholipase C (PLC), mitogen-activated protein kinase (MAPK), and Type IA phosphoinositide 3-kinase (PI3K) (Vetter et al., 1991, Raffioni and Bradshaw, 1992, Dikic et al., 1995). We and others have previously shown that the acute phase of NGF-induced sensitization requires activation of PI3K, which increases trafficking of TRPV1

channels to the PM (Stein et al., 2006, Bonnington and McNaughton, 2003). In chronic pain, NGF also produces changes in the protein expression of ion channels such as TRPV1 and NaV1.8 (Ji et al., 2002, Thakor et al., 2009, Keh et al., 2008). The acute and chronic phases of the NGF response result in increased “gain” to painful stimuli.

Type 1A PI3K is a lipid kinase, which phosphorylates the signaling lipids Phosphatidylinositol (4) phosphate (PI4P) and Phosphatidylinositol (4,5) bisphosphate (PIP_2) into Phosphatidylinositol (3,4) bis phosphate ($PI(3,4)P_2$) and Phosphatidylinositol (3,4,5) trisphosphate (PIP_3) (Auger et al., 1989). $PI(3,4)P_2$ and PIP_3 are signaling lipids as well, and their role in membrane trafficking and other downstream signaling is well-established (Insall and Weiner, 2001, Hawkins and Stephens, 2016). PI3K is an obligatory heterodimer that includes the catalytic p110 subunit (with α, β, and ϒ isoforms) and regulatory p85 subunit (with α, β isoforms) (Hiles et al., 1992, Vanhaesebroeck et al., 2010). The p85 subunit contains two Src homology 2 (SH2) domains (Escobedo et al., 1991), which recognize the phospho-tyrosine motif Y-X-X-M of many activated RTKs and adaptor proteins (Songyang et al., 1993). In the resting state, p85 inhibits the enzymatic activity of p110 via one of its SH2 domains (Miled et al., 2007). This autoinhibition is relieved when p85 binds to a phospho-tyrosine motif (Miled et al., 2007). NGF-induced PI3K activity leads to an increase in the number of TRPV1 channels at the PM (Bonnington and McNaughton, 2003, Stein et al., 2006).

We have previously shown that TRPV1 and p85 interact directly (Stein et al., 2006). We localized the TRPV1/p85 interaction to the N-terminal region of TRPV1 and a region including two SH2 domains of p85 (Stein et al., 2006). However, whether the TRPV1/p85 interaction contributes to NGF-induced trafficking of TRPV1 is unknown. Here, we further localized the functional interaction site for p85 to the region of TRPV1 N-terminus containing several conserved Ankyrin repeats (Ankyrin repeat domain (ARD)). Remarkably, we found that TRPV1 potentiated the activity of PI3K and that a soluble TRPV1 fragment corresponding to the ARD was sufficient for this potentiation. Because the ARD is structurally conserved among TRPV channels, we tested whether other TRPV channels could also potentiate NGF-induced PI3K activity. We found that TRPV2 and TRPV4 both potentiated NGF-induced PI3K activity and trafficked to the PM in response to NGF. Together, our data reveal a previously unknown reciprocal regulation among TRPV

channels and PI3K. We speculate that this reciprocal regulation could be important wherever TRPV channels are co-expressed with PI3K-coupled RTKs.

3.3 Results

3.3.1 NGF-induced trafficking of TRPV1 channels to the PM is preceded by activation of PI3K.

To study events that underlie NGF-induced trafficking of TRPV1 to the PM, we used TIRF microscopy to visualize fluorescently labeled TRPV1 (rat) (YFP-fusion, referred to as TRPV1) in transiently transfected F-11 cells. Cells were also transfected with the NGF receptor subunits TrkA and $p75_{NTR}$ (referred to as TrkA/ $p75_{NTR}$). TIRF microscopy isolates ~100 nm of the cell proximal to the coverslip (Ambrose, 1961, Axelrod, 1981), capturing the PM-proximal fluorescent signals. A change in TRPV1 fluorescence reflects a change in the number of TRPV1 channels at the PM.

We examined NGF-dependent changes in PM-associated TRPV1 before Fig. 3.1A, time point 1), during, and following (Fig. 3.1A, time point 2) a 10-minute exposure of the cells to NGF (100 ng/ml) via its addition to the bath (bar with gray shading in Fig. 3.1B, C). Fig. 3.1 A, bottom panel shows representative TIRF images of TRPV1 fluorescence of an individual F-11 cell footprint. Consistent with previous findings (Stein et al., 2006), upon addition of NGF, TRPV1 levels at the PM increased, with time point 2 depicting the cell footprint intensity at steady state. For each cell, we normalized the mean fluorescence intensity within the footprint at each time point to the mean between 0- and 60 s prior to the application of NGF. The signal for TRPV1 for the cell in Fig. 3.1 A is shown in Fig. 3.1 B, and the collected data, showing the mean and standard error of the mean, are illustrated in Fig. 3.1 C.

To evaluate NGF-induced PI3K activity, we used fluorescently tagged Btk-PH and Akt-PH, PH (Pleckstrin Homology) domain probes, that recognize primarily PIP_3 or both $PI(3,4)P_2$ and PIP_3, respectively (James et al., 1996). Btk-PH and Akt-PH are soluble proteins that localize to the cytosol at rest, when $PI(3,4)P_2/PIP_3$ levels are very low, and are recruited to the PM upon stimulation with NGF, when PI3K becomes active and generates $PI(3,4)P_2/PIP_3$ (Hawkins et al., 2006, Lemmon, 2008). A change in PH domain probe fluorescence reflects a change in $PI(3,4)P_2/PIP_3$ concentration at the PM, thus serving as an

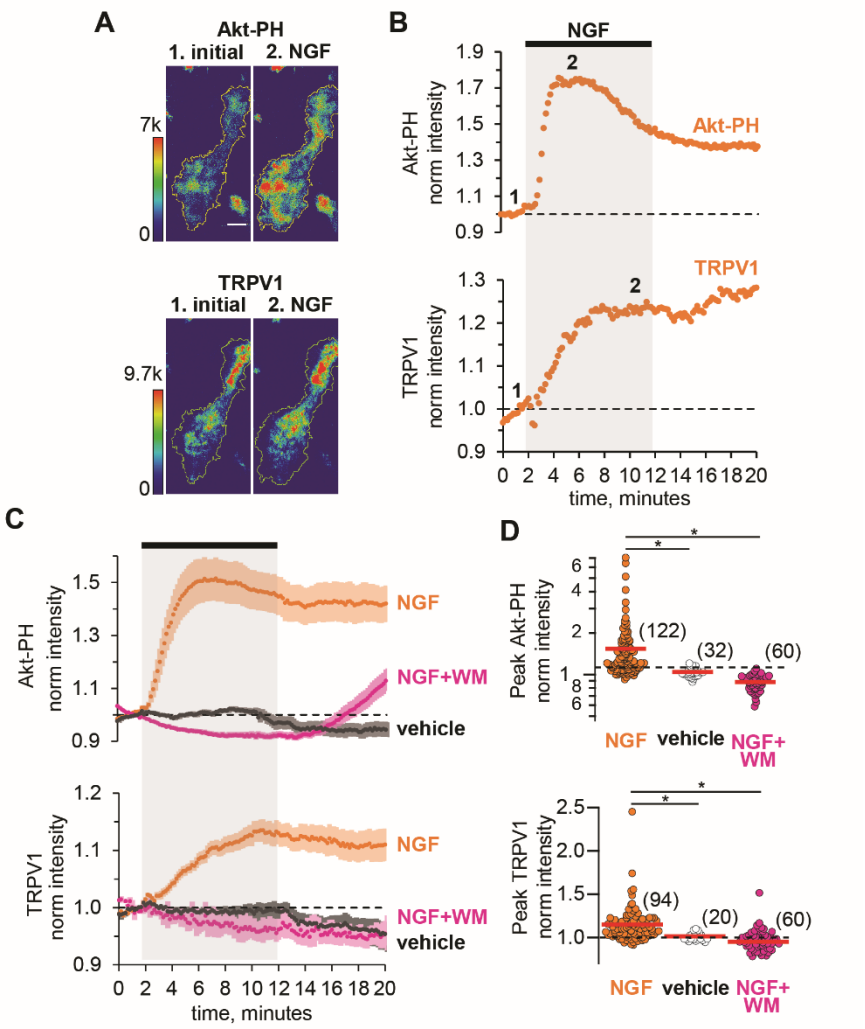

Fig. 3.1 NGF increases PIP3 and recruits TRPV1 to the PM.

(A) TIRF images of a representative F-11 cell transfected with TrkA/p75NTR, TRPV1 and Akt-PH. Images labeled 1 were collected before NGF application and those labeled 2 were collected at the plateau during NGF application, as indicated by the time points labeled in B. Scale bar is 10 µm. LUT bars represent background-subtracted pixel intensities. The yellow border represents the outline of the cell footprint. (Top) Fluorescence intensity from Akt-PH. (Bottom) Fluorescence intensity from TRPV1.

(B) Time course of NGF-induced changes in fluorescence intensity for the cell shown in A. NGF (100 ng/mL) was applied during the times indicated by the black bar/gray shading. Intensity at each time point was measured as the mean gray value within the footprint (yellow outline in A). Data were normalized to the mean intensity values during the two minutes prior to NGF application.

(C) And (D) Collected data for the group of cells tested.

(C) Time course of NGF-induced changes in fluorescence intensity. Averaged time courses of TIRF intensity normalized as in B. Cells treated with either NGF (orange), vehicle (black) or NGF + wortmannin (NGF+WM, magenta), as indicated. TRPV1 (bottom) and Akt-PH (top). Error bars are SEM

indirect measure of PI3K activity. Because PH domain probes have been reported to interfere with PI3K signaling (Varnai et al., 2005), we tested whether Btk-PH and Akt-PH are compatible with NGF signaling to TRPV1. We found that Btk-PH completely abrogated NGF-induced trafficking of TRPV1 to the PM (Fig. 3.2). In contrast, Akt-PH was fully compatible with NGF-induced trafficking of TRPV1 (Fig. 3.2).

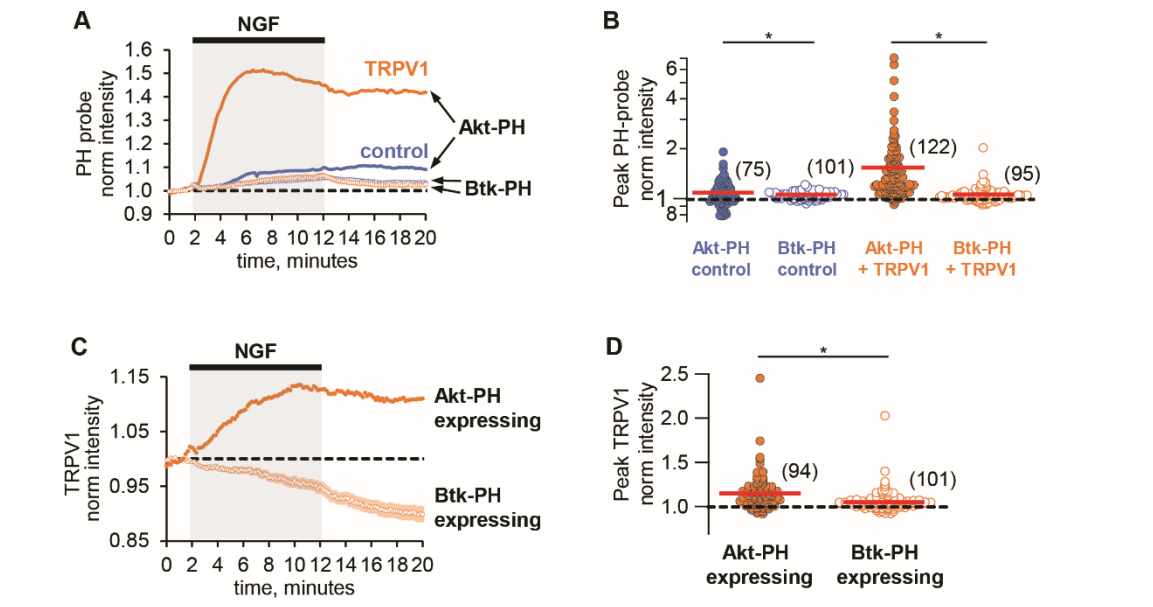

Fig. 3.2 Btk-PH is not compatible with NGF signaling to TRPV1.

(A) Time course of NGF-induced changes in PH-probe fluorescence intensity. TRPV1 (orange) and control cells (blue) are shown expressing either Akt-PH (filled symbols, traces as in Fig. 3.1C, error bars removed for clarity) or Btk-PH (open symbols; error bars are SEM).

(B) NGF-induced change in peak PH-probe fluorescence intensity. TRPV1 (orange) and control cells (blue) are shown expressing either Akt-PH (filled symbols, data same as in Fig. 3.1D) or Btk-PH (open symbols). Peak referes to averaged normalized TIRF Akt-PH or Btk-PH intensity during NGF application (6-8 minutes). The red bars indicate the mean. Asterisks indicate significance of Wilcoxon rank test p value <0.05.

(C) Time course of NGF-induced changes in TRPV1 fluorescence intensity. Averaged time courses of TIRF intensity normalized as in Fig. 3.1B. Cells expressing TRPV1 and either Btk-PH (open symbols, error bars are SEM) or Akt-PH (filled symbols, trace as in Fig. 3.1C, error bars removed for clarity).

(D) NGF-induced change in peak TRPV1 fluorescence intensity. Cells expressing TRPV1 and either Btk-PH (open symbols) or Akt-PH (filled symbols, data same as in Fig. 3.1D). Peak refers to averaged normalized TIRF TRPV1 intensity during NGF application (10-12 minutes). The red bars indicate the mean. Asterisks indicate significance of Wilcoxon rank test p value <0.05.

As an additional control, we used an orthogonal approach to evaluate the compatibility of the Akt-PH probe with NGF signaling in our cell system. Phosphorylation of the protein kinase Akt (also known as

PKB) is a well-studied signaling event downstream of PI3K (Burgering and Coffer, 1995, Kohn et al., 1995). Akt is phosphorylated in a PI(3,4)P_2/PIP_3-dependent manner at two sites, T308 and S473, by PDK1 (Alessi et al., 1997, Stokoe et al., 1997, Frech et al., 1997) and mTORC2 respectively (Sarbassov et al., 2005). Phosphorylation of Akt at these two sites leads to full activation of Akt, regulating a variety of cellular processes, including the inflammatory response to NGF (Xu et al., 2007, Sun et al., 2007, Xu et al., 2011). Therefore, we tested whether co-expression of the Akt-PH probe, altered NGF-induced Akt phosphorylation. We performed western blot analysis using anti- pAKTt308, anti-pAKTs473, and anti-pan Akt antibodies. Fig. 3.3 shows that NGF-induced Akt phosphorylation was preserved in cells expressing the Akt-PH probe. We therefore utilized the Akt-PH probe as a readout of PI3K activity in the remaining experiments.

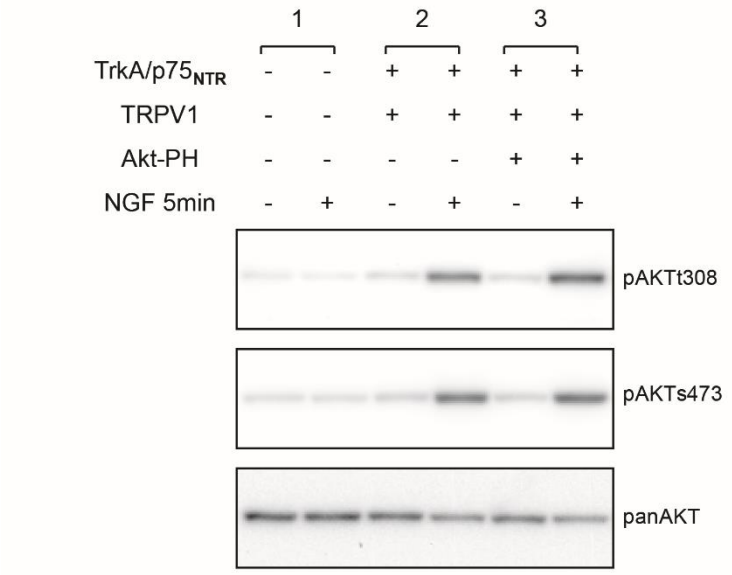

Fig. 3.3 Akt-PH expression does not interfere with NGF-induced Akt phosphorylation.
Immunoblot analysis for Akt-phosphorylation in cells lacking TrkA/p75NTR (pair of lanes #1) treated with vehicle or NGF 100 ng/ml for 5 min. Cells lacking Akt-PH (pair of lanes #2) have comparable NGF-induced Akt-phosphorylation to cells transfected with Akt-PH (pair of lanes #3).

We used two-color TIRF microscopy to measure PI3K activity and TRPV1 trafficking to the PM simultaneously. Treatment of cells with NGF produced an increase in plasma-membrane associated Akt-

PH, indicating that $PI(3,4)P_2/PIP_3$ levels in the PM increased. The increase was relatively rapid, with kinetics determined by both PI3K activity and the affinity of Akt-PH for $PI(3,4)P_2/PIP_3$. The increased Akt-PH signal partially decreased over time even in the continued presence of NGF (Fig. 3.1 B and C orange, top), possibly due to $TrkA/p75_{NTR}$ receptor internalization (Grimes et al., 1996, Ehlers et al., 1995) and activation of phosphoinositide 3-phosphatases, e.g. PTEN (Malek et al., 2017). NGF treatment also increased the PM TRPV1 signal without an apparent reversal to baseline over the duration of our experiments (Fig. 3.1 B and C orange, bottom). The peak levels of Akt-PH and TRPV1 for all cells, represented as the normalized intensities measured at 4-6 minutes (for Akt-PH) and 8-10 minutes (for TRPV1) after the start of NGF application, are shown in the scatterplot of Fig. 3.1 D. The distributions were not normal, but skewed towards larger values. This distribution shape is characteristic of NGF-induced TRPV1 sensitization reported previously in DRG neurons (Stein et al., 2006, Bonnington and McNaughton, 2003), indicating that our cell expression model behaves similarly to isolated DRG neurons. NGF induced a significant increase in Akt-PH levels compared to vehicle (Mean ± SEM: 1.54 ± 0.08, n=122 compared to 1.01 ± 0.01, n=32, Wilcoxon rank test $p = 10^{-12}$, Fig. 3.1 C, top panel, orange and black symbols respectively, see also Fig. 3.4), and a significant increase in TRPV1 levels compared to vehicle (Mean ± SEM: 1.15 ± 0.02, n=94 compared to 0.99 ± 0.01, n=20, Wilcoxon rank test $p = 10^{-6}$; Fig. 3.1 C, bottom panel, orange and black symbols respectively, see also Fig. 3.4). Consistent with a PI3K-dependent mechanism, the NGF-induced increases in both PM-associated Akt-PH and TRPV1 were prevented by the PI3K inhibitor wortmannin (20nM) (Fig. 3.1 C and D, magenta, n=60, Mean ± SEM for Akt-PH – 0.88 ± 0.01 and for TRPV1 – 0.95 ± 0.01; Wilcoxon rank test p value for Akt-PH – 10^{-13} and for TRPV1 – 10^{-10}).

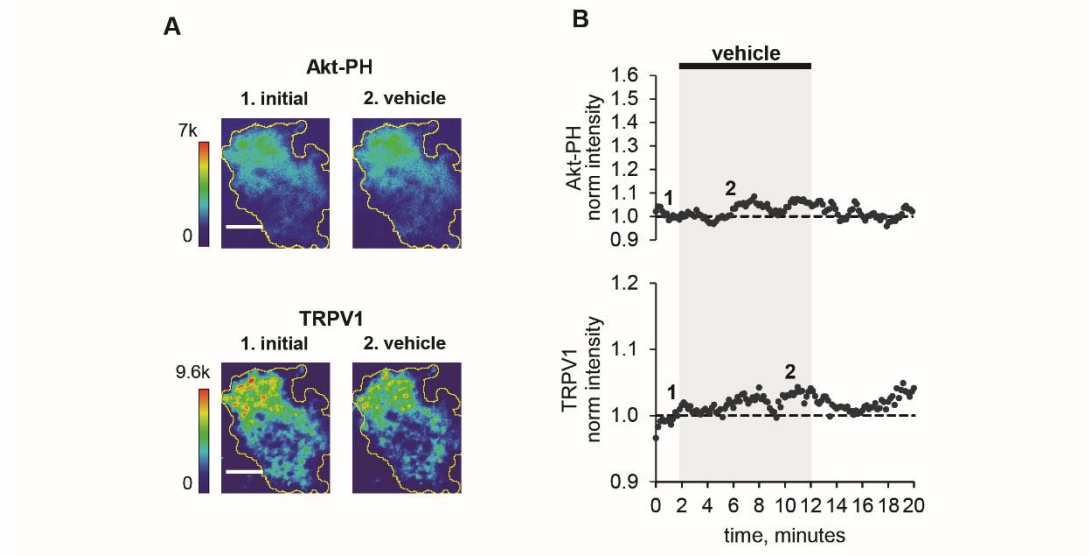

Fig. 3.4 Vehicle does not increase PIP3 or recruit TRPV1 to PM.

(A) TIRF images of a representative F-11 cell transfected with TrkA/p75NTR, TRPV1 and Akt-PH. Images labeled 1 were collected before vehicle application and those labeled 2 were collected at the time points labeled in B. Scale bar is 10 µm. LUT bars represent background-subtracted pixel intensities. The yellow border represents the outline of the cell footprint. (Top) Fluorescence intensity from Akt-PH. (Bottom) Fluorescence intensity from TRPV1.

(B) Time course of vehicle-induced changes in fluorescence intensity for the cell shown in A. Vehicle was applied during the times indicated by the black bar/gray shading. Intensity at each time point was measured as the mean gray value within the footprint (yellow outline in A). Data were normalized to the mean intensity values during the two minutes prior to vehicle application.

TIRF microscopy is often discussed as a method that isolates a fluorescence signal at the PM (Axelrod, 1981). Indeed, illumination falls off exponentially with distance from the coverslip (Ambrose, 1961). Nevertheless, with a typical TIRF setup such as that used for this study (see Materials and Methods) ~90% of the signal comes from the cytosol (Fig. 3.5, also see Methods), assuming the incidence of light was at the critical angle and that the membrane bilayer and associated protein layer extends up to ~10 nm from the coverslip. The contamination of the TIRF signal with fluorescence from the cytosol leads to an underestimation of the change in PM-associated fluorescence from Akt-PH and TRPV1. Under our experimental conditions, we estimate that the ratio of the total fluorescence intensity measured after and before NGF application, F_{NGF}, of 1.54 translates into about a 10-fold increase in PM-associated fluorescence, R_m (Fig. 3.5; see Methods), although this should be considered just a rough estimate.

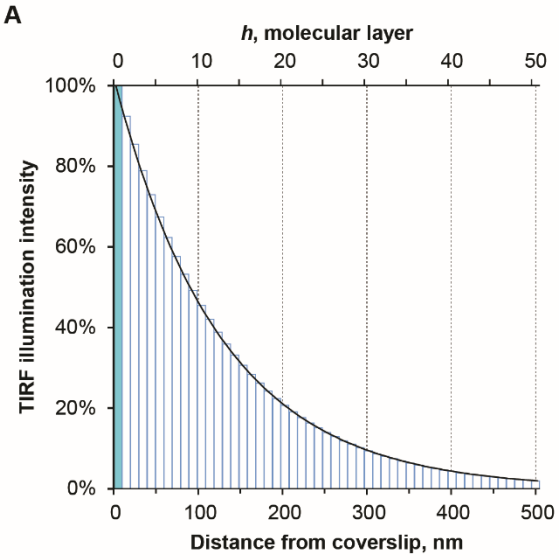

B

Akt-PH	$F_{NGF}/F_{initial}$	R_m
Control	1.08	2
+TRPV1	1.54	10
+TRPV1-ARD	1.32	7
vehicle	1.01	1.1

Fig. 3.5. Model for TIRF illumination and estimation of Akt-PH translocation to the PM. (A) TIRF illumination intensity over distance in nanometers and molecular layers according to our model, see Materials and Methods. Refractive indexes of solution, coverslip and an incidence angle were all determined by our experimental conditions. Bars represent molecular layers, solid fill – membrane layer, open – cytosol layers. (B) Table for measured Akt-PH TIRF fluorescence (FNGF / Finitial), and estimated ratio of molecules at the membrane after NGF to that before NGF (Rm) TRPV1 and vehicle are measurements of data in Fig. 3.1, control and TRPV1-ARD – from Fig. 3.6. We consider the membrane and associated proteins to reside in layer h0. At rest, we assume that Akt-PH molecules are distributed evenly throughout layers h0-h49. We also assumed a fixed number of molecules in the field and that the only NGF-induced change was a redistribution of molecules among layers.

3.3.2 TRPV1 potentiates NGF-induced PI3K activity

Comparing the NGF-induced increase in Akt-PH in control cells that did not express TRPV1 to that in cells expressing TRPV1, we made an unexpected observation: TRPV1 appeared to potentiate NGF-induced PI3K activity. Comparing the time course of the NGF response in cells without TRPV1 (Fig. 3.6 A, blue trace) to cells expressing TRPV1 (Fig. 3.6 A, orange), we found a pronounced increase in Akt-PH fluorescence intensity in TRPV1-expressing cells. This increase was statistically significant, with the peak

normalized Akt-PH intensity value of 1.08 ± 0.03 (n=75) in cells without TRPV1 and 1.54 ± 0.08 (n=122) in cells expressing TRPV1 (Fig. 3.6 B, Wilcoxon rank test p = 10^{-12}, see also Fig. 3.7 A). Interestingly, the dynamics of NGF-induced PI(3,4)P_2/PIP_3-generation in the absence of TRPV1 were also different in that PI(3,4)P_2/PIP_3 levels were sustained. As in TRPV1-expressing cells, the NGF-induced increases in PI(3,4)P_2/PIP_3 levels in control cells were prevented by treatment of cells with wortmannin (Fig. 3.1, Mean ± SEM: 0.81 ± 0.02, n=53; Student's t-test p-value was 10^{-16}).

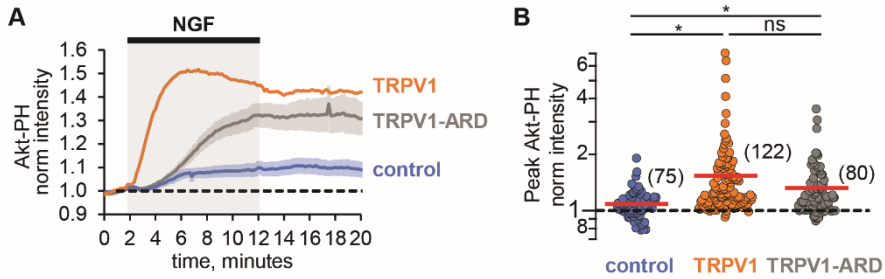

Fig. 3.6 TRPV1-ARD is necessary and sufficient for potentiation of NGF-induced PI3K activity.

(A) Time course of NGF-induced changes in Akt-PH fluorescence intensity. NGF (100 ng/mL) was applied during the times indicated by the black bar/gray shading. Averaged normalized TIRF intensity from cells transfected with TrkA/p75NTR and Akt-PH: control cells without TRPV1 (blue, n=75), TRPV1 (orange, n=122), or TRPV1-ARD (gray, n=80). Traces represent the mean and error bars represent the SEM. TRPV1 data are the same as in Fig. 3.1C, error bars removed for clarity.

(B) NGF-induced changes in Akt-PH fluorescence intensity for control cells (blue), cells expressing TRPV1 (orange data are the same as in Fig. 3.1D) and cells transfected with TRPV1-ARD (gray). Averaged normalized TIRF intensity during NGF application (6-8 minutes). Red bars indicate mean (see Table 1 for values). Asterisks indicate significance of Holm-Bonferroni post-hoc adjusted Wilcoxon rank test p value <0.001 (see Table 1 for values).

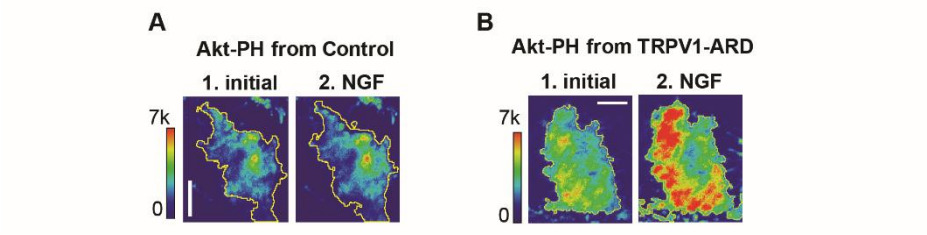

Fig. 3.7 Representative images of NGF-induced recruitment Akt-PH and TRP channels to the PM. Representative images of Akt-PH fluorescence from F-11 cells transfected with TrkA/p75NTR, and Akt-PH without TRPV1 – control (A) and cells additionally transfected with TRPV1-ARD (B). Timing of images and labels as in Fig. 3.1A. Scale bar is 10 µm. LUT bar is background subtracted pixel intensities. Yellow outline represents the cell footprint.

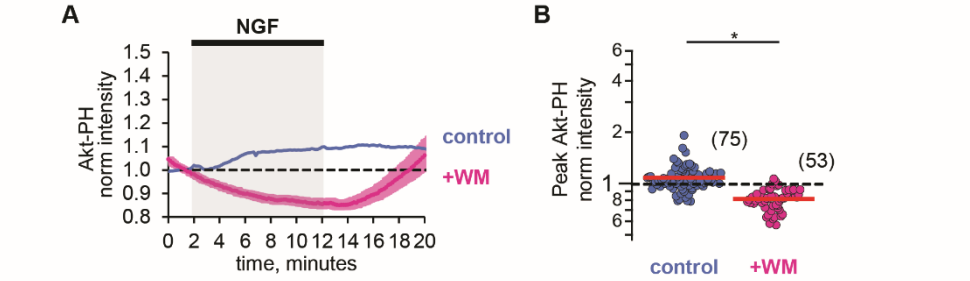

Fig. 3.8 PI(3,4)P2/PIP3 generation is diminshed by PI3K inhibitor wortmannin.

(A) Time course of NGF-induced changes in Akt-PH fluorescence intensity. Averaged normalized TIRF intensity from control cells transfected with TrkA/p75NTR and Akt-PH but no TRPV1 treated with NGF (blue, n=75, data are the same as in Fig. 3.6A, error bars removed for clarity) or NGF + wortmannin (WM, magenta, n=53). Traces represent the mean and error bars represent the SEM. control data are the same as in Fig. 3.6A, error bars removed for clarity.

(B) NGF-induced changes in averaged normalized TIRF Akt-PH fluorescence intensity for control cells treated with NGF (blue data are the same as in Fig. 3.6B) or NGF+Wortmannin (WM, magenta, n=53). Peak referes to averaged normalized TIRF intensity during NGF application (6-8 minutes). Red bars indicate mean. Asterisks indicate significance of Student's T-test p value <0.001.

One possible cause for the potentiation of NGF-induced PI3K activity we observed in TRPV1-expressing cells could be a change in PI3K expression levels in TRPV1 vs. control cells. To determine whether this was the case, we performed western blot analysis with an anti-p85α antibody to quantify the PI3K protein levels across transfection conditions. As shown in Fig. 3.9 A, expression of TRPV1 did not

alter the expression level of the p85α subunit of PI3K. We quantified protein expression levels using densitometry, and normalized expression to tubulin, giving the relative expression levels shown in Fig. 3.9 B. Average relative p85α expression levels were similar between non-TRPV1 expressing cells and cells expressing TRPV1 (n=5, Student's t-test p value was 0.95). We conclude that a difference in PI3K expression in TRPV1-expressing vs. control cells did not account for the observed TRPV1-induced potentiation of NGF-stimulated PI3K activity.

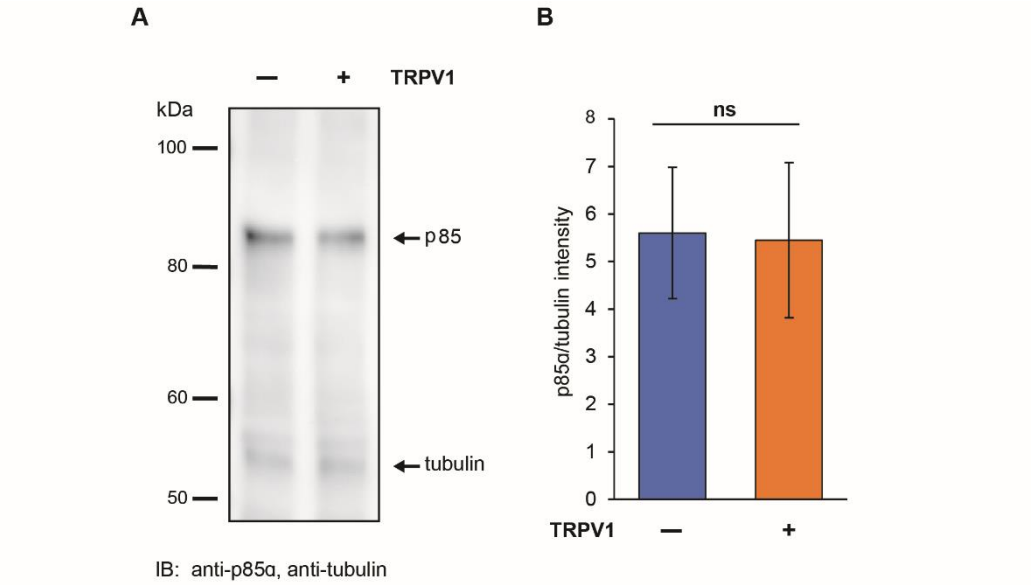

Fig. 3.9 TRPV1 co-expression does not alter PI3K expression.

(A) Representative immunoblot for p85 expression in F-11 cells expressing -/+ TRPV1. Membrane was stained for p85 and tubulin simultaneously.

(B) Relative p85 expression in F-11 cells expressing -/+ TRPV1. Immunoblots were quantified as described in Methods (n = 5 independent experiments). Mean ± SEM pixel intensity are plotted normalized to the tubulin band on each blot. Student's t-test two-tailed p=0.95.

3.3.3 The ARD of TRPV1 is sufficient for potentiation of NGF-induced PI3K activity

We have previously shown that the N-terminal region of TRPV1, consisting of 110 amino acids followed by the ankyrin repeat domain (TRPV1-ARD) interacts directly with the p85 subunit of PI3K, in yeast 2-hybrid assays, co-immunoprecipitation from cells, and using recombinant fragments *in vitro* (Stein et al., 2006). We hypothesized that the TRPV1-ARD might also mediate NGF-induced potentiation of PI3K. To

determine whether the ARD is sufficient for potentiation of NGF-induced PI3K activity, we expressed the ARD as a fragment and then measured NGF-induced PI3K activity. As shown in Fig. 3.6 A (gray trace), NGF induced PI3K activity that was greater in TRPV1-ARD expressing cells than in control cells (blue trace). The increase in peak Akt-PH normalized intensity was statistically significant compared to control cells, with a mean of 1.32 (± 0.02, n=80; Fig. 3.6 B; Wilcoxon rank test $p = 10^{-5}$, see also Fig. 3.7B). The kinetics of this potentiation were somewhat slower with TRPV1-ARD compared to TRPV1 (Fig. 3.1 and Fig. 3.6 A, orange trace), so that Akt-PH reached steady-state levels somewhat later during NGF treatment. Nevertheless, the potentiation of NGF-induced PI3K activity by the ARD fragment was nearly as great as observed with full-length TRPV1 (Wilcoxon rank test p = 0.08). In addition, the ability of a soluble TRPV1 fragment to reconstitute potentiation suggests that the mechanism of potentiation is at least partly allosteric, involving more than just a tethering of PI3K at the membrane by TRPV1.

3.3.4 An orthogonal PI3K assay confirms that TRPV1 potentiates NGF-induced PI3K activity and generation of $PI(3,4)P_2/PIP_3$

We used the Akt phosphorylation assay described above as an orthogonal method of examining the potentiation of NGF-induced PI3K activity in TRPV1-expressing cells. We performed western blot analysis using phospho-specific Akt antibodies, reprobing the blots with a pan Akt antibody for normalization purposes (Fig. 3.10 A). Because phosphorylation at T308 and S473 are differentially regulated, we used three concentrations of NGF (5, 25, and 100 ng/mL) and two incubation times (1 and 5 minutes). We observed increased phosphorylation at both T308 and S473 in TRPV1-expressing cells compared to control cells for almost all trials with all three NGF concentrations and both time points (Fig. 3.10 B, C). The enhanced NGF-induced Akt phosphorylation was statistically significant for both T308 and S473 sites for all conditions pooled together (Fig. 3.10 D, E; paired Student's t-test for T308 p = 0.02 and S473 p=0.008). Thus, TRPV1 potentiation of NGF-induced PI3K activity is sufficient to enhance $PI(3,4)P_2$ and/or PIP_3 levels to increase Akt phosphorylation.

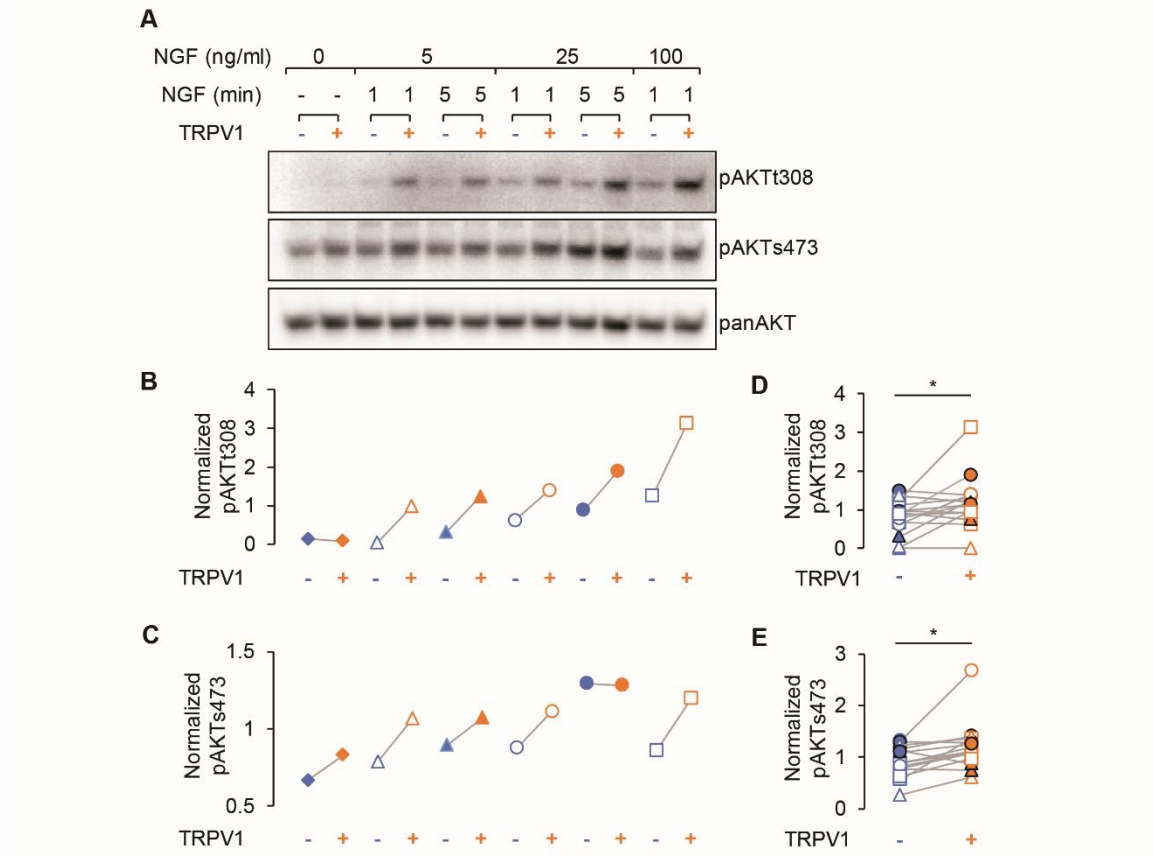

Fig. 3.10. TRPV1 enhances NGF-induced Akt phosphorylation.

(A) Representative immunoblot staining for analysis of Akt phosphorylation in F-11 cells transfected same as in imaging experiments. Cells were treated with indicated dose of NGF for an indicated amounts of time, lysed and loaded on SDS-PAGE. The same membrane was probed with pS473-Akt, stripped and re-probed with pT308-Akt and again with panAKT antibodies (See Methods).

(B) and (C) Analysis of the representative blots shown in (A). Each band average intensity was normalized to the average of the blot and then divided by that of the corresponding lane of the pan-Akt blot. Akt phosphorylated at T308 (B) and S473 (C) from control cells (blue symbols) and cells expressing TRPV1 (orange symbols) treated with NGF (5, 25 or 100ng/ml) for 1 or 5 minutes as indicated in (A). Triangles represent treatment with NGF 5 ng/ml, circles – 25 ng/m, squares – 100 ng/ml. Open symbols represent treatments for 1 min and filled symbols – 5 min.

(D) and (E) Normalized phospho-Akt intensities from all indicated conditions are pooled together for the n=3 of independent experiments. Paired Student's t-test for pT308-Akt p = 0.02 and for pS473-Akt p = 0.008.

Finally, Fig. 3.10 shows that the extent of Akt phosphorylation in unstimulated cells was indistinguishable in control vs. TRPV1-expressing cells at both S308 ($Intensity_{pAkt/pan\ Akt}$: 0.075 ± 0.004 for control and 0.076 ± 0.004 for TRPV1, Mean ± SEM, n=3, paired Student's t-test p = 0.95) and T473 sites ($Intensity_{pAkt/pan\ Akt}$: 0.3 ± 0.24 for control and 0.23 ± 0.14 for TRPV1, Mean ± SEM, n=3, paired Student's t-

test p = 0.44), indicating that TRPV1 did not perturb the levels of $PI(3,4)P_2/PIP_3$ at rest. Importantly, we examined whether NGF-induced phosphorylation at both T308 and S473 required expression of $TrkA/p75_{NTR}$. NGF-induced phosphorylation of Akt was not observed in cells in which $TrkA/p75_{NTR}$ were not expressed (Fig. 3.3). Together with the data using Akt-PH in TIRF microscopy experiments, these data indicate that NGF-induced PI3K activity is greater, and $PI(3,4)P_2/PIP_3$ production is greater, in TRPV1-expressing cells than in those that do not express TRPV1.

3.3.5 Potentiation of PI3K and NGF-induced trafficking are conserved among TRPV channels

The ARD of TRPV1 is highly conserved among other members of the TRPV family of ion channels (Gaudet, 2008). Given the sufficiency of the TRPV1 ARD in potentiation of NGF-induced PI3K activity, we postulated that reciprocal regulation among other TRPV family members and PI3K would occur as well. We examined whether other ARD-containing TRP channels, TRPV2 (rat) and TRPV4 (human) were trafficked to the plasma membrane in response to NGF. Using TRPV2 and TRPV4 fused to fluorescent proteins, we found that they were both trafficked to the PM in response to NGF compared to vehicle (Holm-Bonferroni post-hoc adjusted Wilcoxon rank test $p < 0.05$ see Fig. 3.1, Fig. 3.11 C,D, see also Fig. 3.12 for representative images). In addition, we found that the NGF-induced increase in Akt-PH was significantly greater in TRPV2- and TRPV4-expressing cells compared to control cells (Holm-Bonferroni post-hoc adjusted Wilcoxon rank test $p < 0.05$ see Fig. 3.6, Fig. 3.11 A,B). The effects of TRPV2 and TRPV4 on $PI(3,4)P_2/PIP_3$ levels were significantly smaller than those elicited by TRPV1 (Holm-Bonferroni post-hoc adjusted Wilcoxon rank test $p < 0.05$ see Fig. 3.1 and Fig. 3.11). Further experiments would be required to determine whether the differences were due to differences in expression level, differences in the affinity of PI3K for the TRPV ARDs, or differences in the effect of each ARD on the catalytic activity of PI3K. We conclude that potentiation of NGF-induced PI3K activity and traffic to the PM in response to NGF are conserved among TRPV1, TRPV2, and TRPV4.

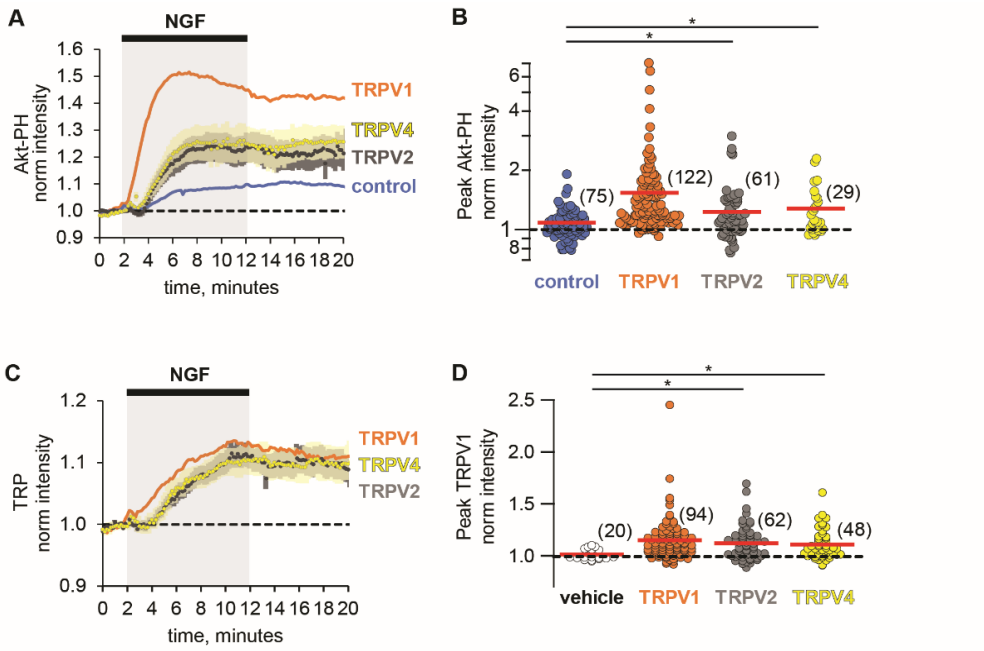

Fig. 3.11 Potentiation of PI3K and NGF-induced trafficking are conserved among TRPV channels.

Time course of NGF-induced changes in fluorescence intensity. NGF (100 ng/mL) was applied during the times indicated by the black bar/gray shading. Traces represent the mean, error bars are SEM. Control and TRPV1 data same as in Fig. 3.6 with error bars removed for clarity.

(A) Averaged normalized TIRF intensity of Akt-PH from cells transfected with TrkA/p75NTR and Akt-PH and: (A) no channel (control; blue; n=75); TRPV1 (orange; n=122); TRPV2 (black; n=61); TRPV4 (yellow; n=29).

(B) Averaged normalized Akt-PH intensity during NGF application (6-8 minutes). The red bars indicate the mean. Asterisks indicate significance (Holm-Bonferroni post-hoc adjusted Wilcoxon rank test $p < 0.05$, see Table 1 for values).

(C) Averaged normalized TIRF intensity of individual TRP channels. Color scheme as in (A) with the cell numbers as follows: TRPV1 (n=94); TRPV2 (n=62); TRPV4 (n=48).

(D). Averaged normalized TRP channel intensity during NGF application (8-10 minutes). The red bars indicate the mean. Asterisks indicate significance (Holm-Bonferroni post-hoc adjusted Wilcoxon rank test $p < 0.05$, see Table 2 for values)

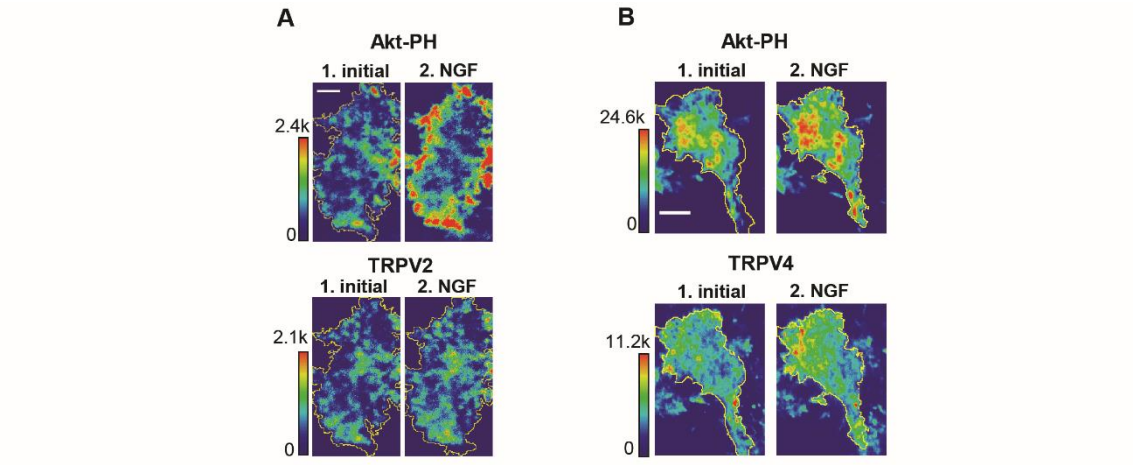

Fig. 3.12 Representative images of NGF-induced recruitment Akt-PH and TRP channels to the PM. Representative images of F-11 cells transfected with TrkA/p75NTR, Akt-PH and one of the following: (A) TRPV2; (B) TRPV4. Timing of images and labels as in Fig. 3.1A. Scale bar is 10 µm. LUT bar is background subtracted pixel intensities. Yellow outline represents the cell footprint.

Increased trafficking of TRPV1 to the cell surface is essential for sensitization to noxious stimuli produced by NGF and other inflammatory mediators (Morenilla-Palao et al., 2004, Ferrandiz-Huertas et al., 2014). Although the involvement of PI3K in NGF-induced sensitization has been known for over a decade (Bonnington and McNaughton, 2003, Stein et al., 2006), the role, if any, of direct binding of TRPV1 and PI3K was unclear. Here we show that ARD region of TRPV1 that binds PI3K is sufficient to potentiate NGF-induced PI3K activity. Although it is possible that TRPV1 inhibition of the $PI(3,4)P_2/PIP_3$ phosphatase PTEN (Malek et al., 2017) could contribute to TRPV1 potentiation of NGF-induced increases in $PI(3,4)P_2/PIP_3$ levels, this and other more complex models are not needed to explain are data. In addition, whereas the present work does not rule out that the potentiation of PI3K we describe requires an effector that mediates signaling between the TRPV1 ARD and PI3K, we favor a simpler model in which the previously described direct interaction between TRPV1 and PI3K mediates the signaling. We speculate that, without TRPV1 potentiation of PI3K, NGF signaling would not produce sufficient $PI(3,4)P_2/PIP_3$ to promote channel trafficking during inflammation. Future studies that decouple potentiation of PI3K activity from the expression of TRPV channels will be needed to determine whether the reciprocal regulation between ARD-containing TRPV channels and PI3K serves an obligate role in channel sensitization.

Is reciprocal regulation among TRPV channels and PI3K relevant beyond pain signaling? TRPV channels have been proposed to be involved in RTK/PI3K signaling in a variety of cell types (Reichhart et al., 2015, Katanosaka et al., 2014, Jie et al., 2015, Sharma et al., 2017). For example, TRPV2 is co-expressed in muscle cells with the insulin like growth factor receptor and is known to be important in muscle loss during muscular dystrophy (Iwata et al., 2003). The mechanism is believed to involve insulin like-growth factor receptor activation leading to increased trafficking of TRPV2 to the sarcolemma, Ca^{2+} overload/cytotoxicity, and cell death (Iwata et al., 2003, Perálvarez-Marín et al., 2013, Katanosaka et al., 2014). Whether TRPV2 potentiates insulin like growth factor-induced PI3K activity remains to be determined. The co-expression of TRPV channels with RTK/PI3K in other tissues, including nerve (TRPV1/NGF) (Tanaka et al., 2016), muscle (TRPV2/IGF) (Katanosaka et al., 2014) and lung (TRPV4/TGFβ1) (Rahaman et al., 2014) raises the question of whether reciprocal regulation among TRPV channels and PI3K plays a role in RTK signaling in cell development, motility, and/or pathology.

3.4 Addendums

3.4.1 ARD containing TRPA1channel traffics to the PM but does not potentiate PI3K

The ARD are highly conserved among other members of the TRP superfamily of ion channels (Gaudet, 2008) (see also section 1.2.2). Given the conservation of the reciprocal regulation among three TRPV family members tested above and PI3K (section 3.3.5), we next addressed whether reciprocal regulation of PI3K activity and channel trafficking extends to TRPA1, which contains an N-terminal ARD with a very different structure compared to the TRPV channels (Fig. 1.5, discussed in section 1.2.2). We examined whether another ARD-containing TRP channel, TRPA1 (zebrafish) was trafficked to the plasma membrane in response to NGF. Using TRPA1 fused to GFP, we found that it was trafficked to the PM in response to NGF compared to vehicle (Wilcoxon rank test $p < 0.05$, see Fig. 3.13C,D, see also Fig. 3.14 for representative images). TRPA1 did not potentiate NGF-induced PI3K activity (Fig. 3.13B, Mean ± SEM: 1.14 ± 0.03, Wilcoxon rank test p value=0.13, see Fig. 3.13). Poor expression of TRPA1 may contribute to the apparent lack of significance in potentiation of NGF-induced PI3K activity (Mean ± SEM: 1518 ± 321 au

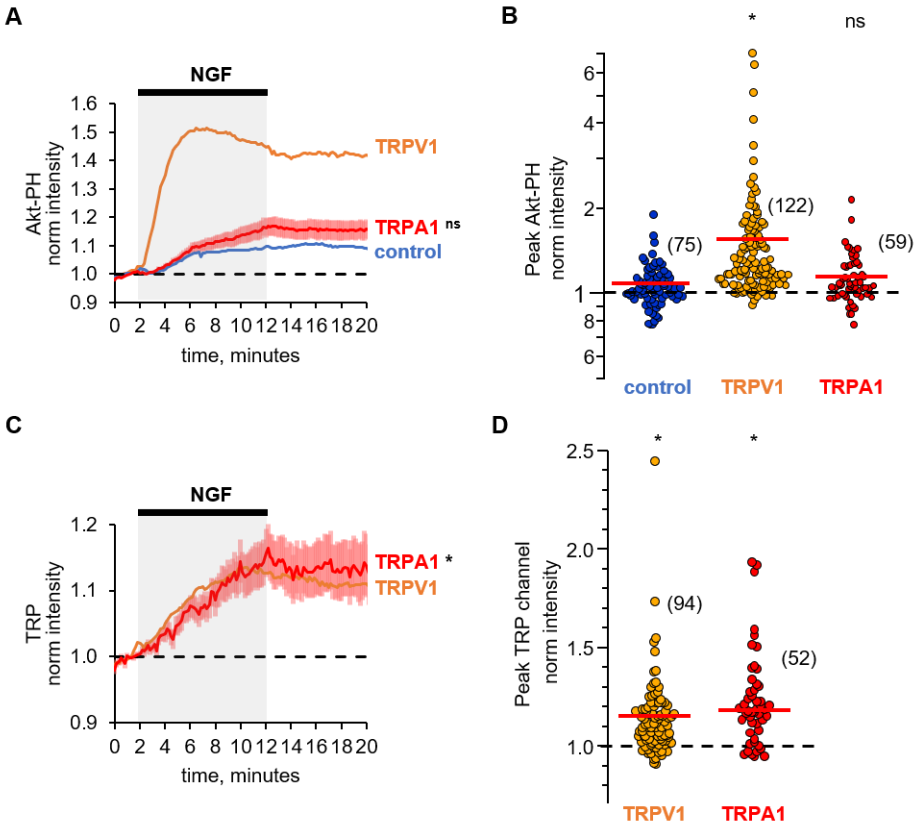

Fig. 3.13 Potentiation of NGF-induced PI3K activity is conserved in ARD-containing TRPA1 channels

Averaged normalized TIRF intensity of Akt-PH (A,B) and TRP channel (C,D) from cells transfected with TrkA/p75NTR and Akt-PH and: no channel (control; blue); TRPV1 (orange); TRPA1 (red).

A) Time course of NGF-induced changes in Akt-PH fluorescence intensity. NGF (100 ng/mL) was applied during the times indicated by the black bar/gray shading. Traces represent the mean, error bars are SEM. Control and TRPV1 data same as in Fig. 3.6A & B with error bars removed for clarity.

B) Averaged normalized Akt-PH intensity during NGF application (6-8 minutes). The y-axis is logarithmic. Asterisks represent statistical significance from Wilcoxon rank test, comparing each TRP dataset to control with $p<0.05$, (values listed in Table 3.1). Each data point represents one cell. The red bars indicate the mean. Values in parenthesis indicate n.

C) Time course of NGF-induced changes in TRP channel fluorescence intensity. NGF (100 ng/mL) was applied during the times indicated by the black bar/gray shading. Traces represent the mean, error bars are SEM. Control and TRPV1 data same as in Fig. 3.6A & B with error bars removed for clarity.

D) Averaged normalized TRP fluorescence intensity during NGF application (8-10 minutes). Asterisks represent statistical significance from Wilcoxon rank test comparing each TRP dataset to vehicle, $p<0.05$ (values listed in Table 3.2). Each data point represents one cell. The red bars indicate the mean. Values in parenthesis indicate n.

for TRPA1 compared to 3039 ± 296 au for TRPV1). Another possibility for the lack of apparent potentiation of PI3K by TRPA1, compared to TRPV1, may lie in a different morphology and a number of Ankyrin repeats (see figure Fig. 1.5). It is also feasible that PI3K and TRPA1 from different species (mouse and zebrafish, respectively) may not interact as well as within the species, this possibility needs to be further investigated.

We favor an interpretation when the ARD of TRPA1 does somewhat potentiate NGF-induced PI3K activity at least to the extent required for its trafficking to the PM. More sensitive cell assays for PIP_3 and in vitro studies will be required to test this hypothesis. We conclude that trafficking of ARD-containing TRP channels to the PM in response to NGF is conserved. We were unable to observe potentiation of NGF-induced PI3K activity by TRPA1 but this does not rule out the possibility of reciprocal regulation.

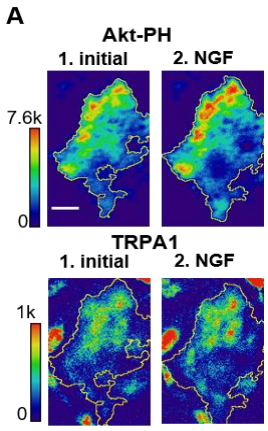

Fig. 3.14 Representative images of NGF-induced recruitment Akt-PH and TRPA1 channels to the PM Representative images of F-11 cells transfected with TrkA/p75$_{NTR}$, Akt-PH and TRPA1. Timing of images and labels as in Fig. 3.6A. Scale bar is 10 µm. LUT bar is background subtracted pixel intensities. Yellow outline represents the cell footprint.

3.4.2 Effects on PI3K activity by TRPM channels

To eliminate the possibility of reciprocal effect dependent on other domains conserved among TRP channels we tested TRPM8 members of TRPM family (rat) which do not contain ARD (Yin et al., 2017). We found that they did not show reciprocal regulation with both PI3K activity and channel trafficking. TRPM8 channels did not potentiate PI3K activity, although they transiently trafficked to the PM in response to NGF

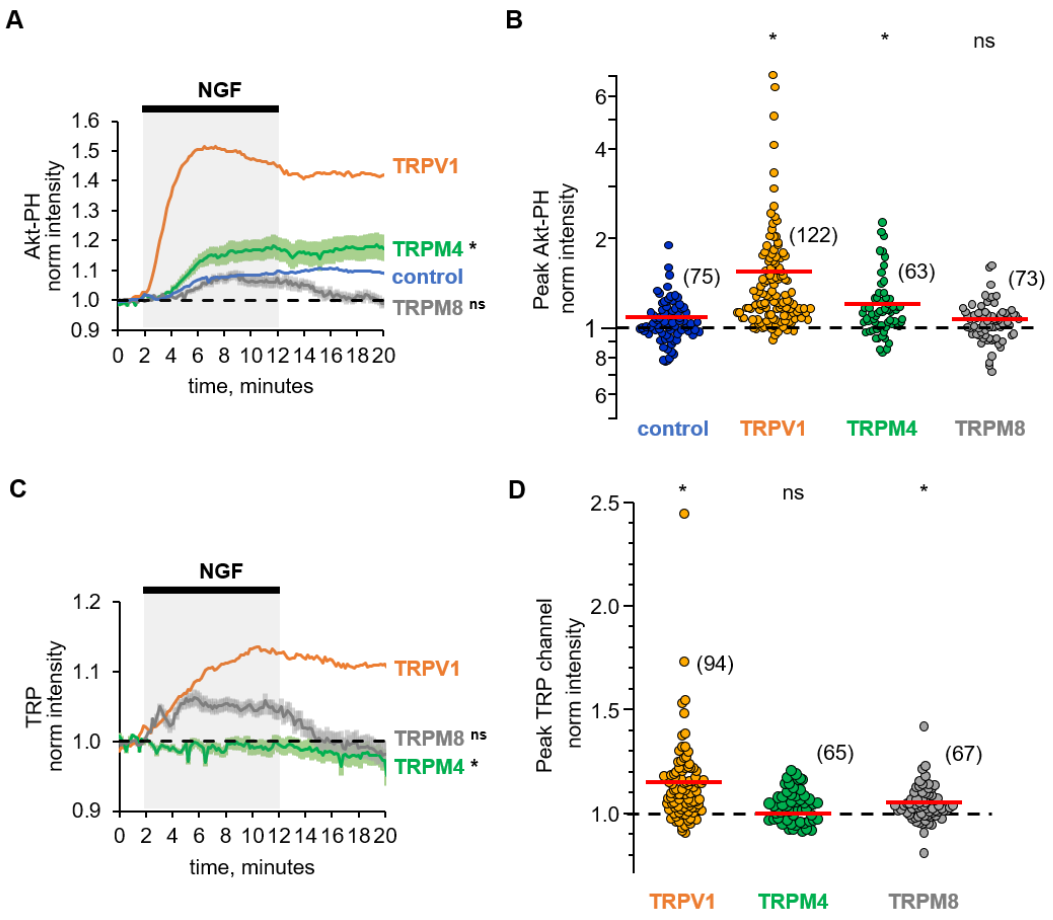

Fig. 3.15 NGF-induced trafficking is not conserved among non-ARD TRP channels

Averaged normalized TIRF intensity of Akt-PH (A,B) and TRP channel (C,D) from cells transfected with TrkA/p75$_{NTR}$ and Akt-PH and: no channel (control; blue); TRPV1 (orange); TRPM4 (green); TRPM8 (gray). A) Time course of NGF-induced changes in Akt-PH fluorescence intensity. NGF (100 ng/mL) was applied during the times indicated by the black bar/gray shading. Traces represent the mean, error bars are SEM. Control and TRPV1 data same as in Fig. 3.6A & B with error bars removed for clarity.

B) Averaged normalized Akt-PH intensity during NGF application (6-8 minutes). The y-axis is logarithmic. Asterisks represent statistical significance from Wilcoxon rank test, comparing each TRP dataset to control with p<0.05 (values listed in Table 3.1). Each data point represents one cell. The red bars indicate the mean. Values in parenthesis indicate n.

C) Time course of NGF-induced changes in TRP channel fluorescence intensity. NGF (100 ng/mL) was applied during the times indicated by the black bar/gray shading. Traces represent the mean, error bars are SEM. Control and TRPV1 data same as in Fig. 3.6A & B with error bars removed for clarity.

D) Averaged normalized Akt-PH intensity during NGF application (6-8 minutes). Asterisks represent statistical significance from Wilcoxon rank test, comparing each TRP dataset to vehicle p<0.05 (values listed in Table 3.2). Each data point represents one cell. The red bars indicate the. Values in parenthesis indicate n.

of activity (Fig. 3.15, see also for values Table 3.1). These data suggest that whereas the reciprocal regulation PI3K activity and channel trafficking are conserved among ARD-containing TRPV channels, this conservation does not extend to other TRP channels with different N-terminal domain structures.

It was believed that all channels of the TRPM family do not contain an ARD. Unexpectedly, a recent TRPM4 Cryo-EM structure revealed two ARD-like domains in the N-terminus, which were not predicted for poor sequence similarity with other ARDs (Winkler et al., 2017). Interestingly, we show that TRPM4 channels potentiated NGF-induced PI3K activity (Fig. 3.15C, Fig. 3.16, see also Table 3.1 for values). Despite significant potentiation of PI3K, TRPM4 did not traffic to the PM in response to NGF (Fig. 3.15D, Fig. 3.16, see also Table 3.2 for values). This suggests that despite poor sequence similarity, ARD may exhibit conserved effects on PI3K activity.

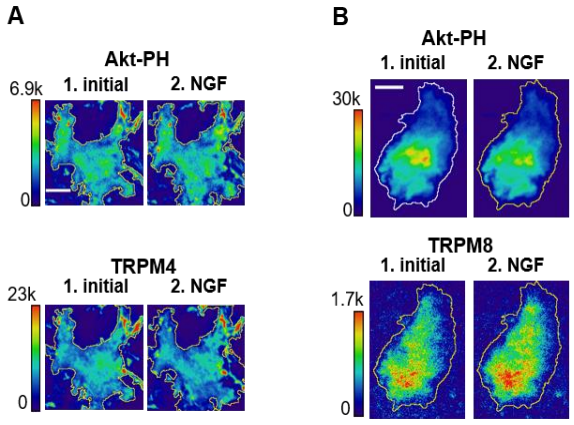

Fig. 3.16 Representative images of NGF-induced recruitment Akt-PH and TRP channels to the PM
Representative images of F-11 cells transfected with TrkA/p75$_{NTR}$, Akt-PH and one of the following: (A) TRPM4; (B) TRPM8. Timing of images and labels as in Fig. 3.1A. Scale bar is 10 µm. LUT bar is background subtracted pixel intensities. Yellow outline represents the cell footprint.

3.4.3 Calcium imaging in DRG cells expressing TRPV1 shows sensitization of TRPV1 with NGF

It has been previously shown that inflammatory mediators, such as NGF, lead to hyperalgesia, an increased sensitivity to painful stimuli. Although both central and peripheral mechanisms contribute to hyperalgesia, it can be measured in the peripheral sensory afferents as an increase in the response of

TRPV1 ion channels to noxious chemical and thermal stimuli (i.e. sensitization). We examined NGF-induced sensitization in freshly isolated mouse DRG neurons. Cells were loaded with the calcium sensitive dye Fluo-4-AM (3μM Invitrogen Cat# F14201 at 37°C at 5% CO_2 in the dark of incubator for 30 min, and 30 more min in the wash). The intensity of the Ca^{2+} signal was measured in response to repeated bath applications of the TRPV1 agonist capsaicin. In contrast to multiple published studies (Bonnington and McNaughton, 2003, Zhu and Oxford, 2007), NGF application between 1st and 2nd application of capsaicin did not produce robust sensitization of TRPV1 responses (Fig. 3.17A). We hypothesized that calcium-induced desensitization of TRPV1 may be required to observe NGF-induced TRPV1 sensitization. In order to obtain robust NGF-induced sensitization of TRPV1-dependent calcium influx – a phenomenon that has been termed desensitization or tachyphylaxis, we utilized longer experimental protocol with multiple capsaicin applications. Fig. 3.17 B shows representative trace of Fluo-4 fluorescence intensity from a DRG neuron alternately perfused with saline solution or saline + capsaicin (100 nM) for 7 cycles. Repeated applications of capsaicin produced diminishing Ca^{2+} responses due to Ca^{2+}-induced desensitization of TRPV1. Cells were treated with NGF (100 ng/ml) between the 5th and 6th cycle. We quantified the amplitude of TRPV1-dependent Ca^{2+} responses by measuring the Fluo-4 fluorescence intensity in response to 4th, 5th and 6th capsaicin applications normalized to immediately preceding capsaicin application (Fig. 3.17 C, n=27, asterisks indicate significance of Wilcoxon rank test). In accordance with previously reported findings, we observed strong sensitization of capsaicin-induced Ca^{2+} responses in DRG cells upon treatment with NGF.

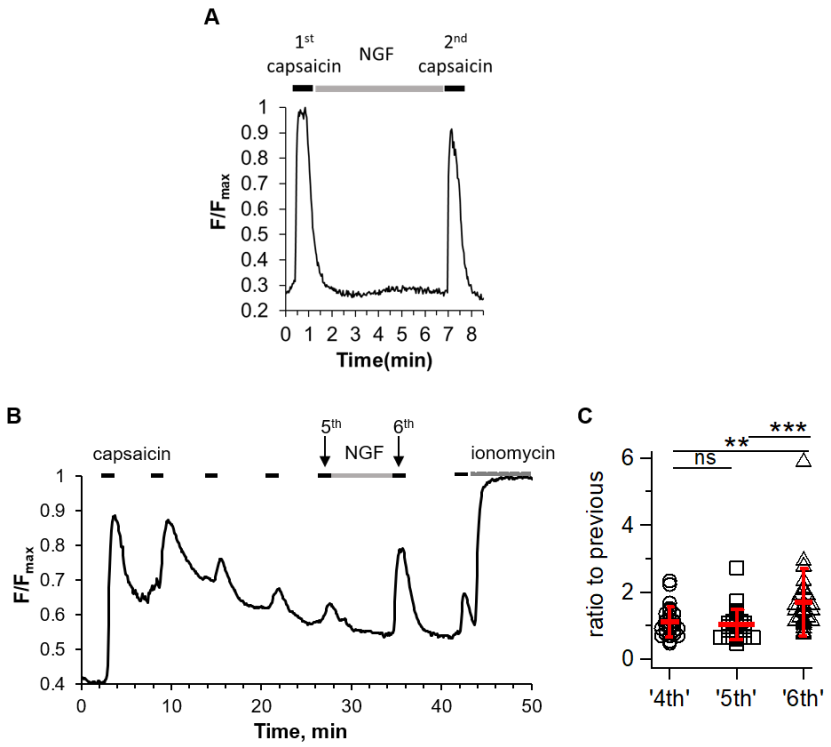

*Fig. 3.17 Calcium imaging in DRG cells expressing TRPV1 shows sensitization of TRPV1 with NGF. A) Fluo4-AM fluorescence of a representative DRG neuron in response to two capsaicin applications (100nM). NGF (100ng/ml) was applied to bath between 1st and 2nd capsaicin applications. B) Fluo4-AM fluorescence of a representative DRG neuron during modified protocol of 7 consecutive capsaicin applications to achieve desensitization. NGF was applied to bath between 5th and 6th applications of capsaicin. Ionomycin (10uM) was added in the end of the recording to achieve F_{max}. C) Scatterplot showing capsaicin response amplitudes in response to 4th, 5th and 6th applications normalized to immediately preceding application (n=27). Asterisks indicate significance levels of Wilcoxon rank test (*** - p< 0.001, ** - p<0.005, ns - p>0.05)*

One explanation for these findings is that the TRPV1 must be in desensitized state in order to observe NGF-induced potentiation. Our TIRF imaging experiments described in section 3.3.1 do not support this hypothesis, because we did not apply capsaicin and never repetitively increased intracellular calcium concentrations in order to detect NGF-induced increase in TRPV1 trafficking to the PM. Alternatively, in our calcium imaging experiments the increase in number of functional TRPV1 at the PM may be cancelled out by desensitization of existing TRPV1 channels.

3.5 Conclusions and further directions.

Our conclusions are summarized in the illustration of Fig. 3.18. In cells that do not express TRPV1, NGF-induced PI3K activity is moderate, generating moderate levels of PIP_3 (Fig. 3.18 A). We speculate that these moderate levels of PIP_3 are not sufficient to support increased trafficking of membrane protein-containing vesicles to the PM. In contrast, co-expression of TRPV1 potentiates NGF-induced PI3K activity, generating higher levels of PIP_3 (Fig. 3.18 B). We propose that these higher levels of PIP_3 are necessary to support trafficking of TRPV1-continaing vesicles to the PM.

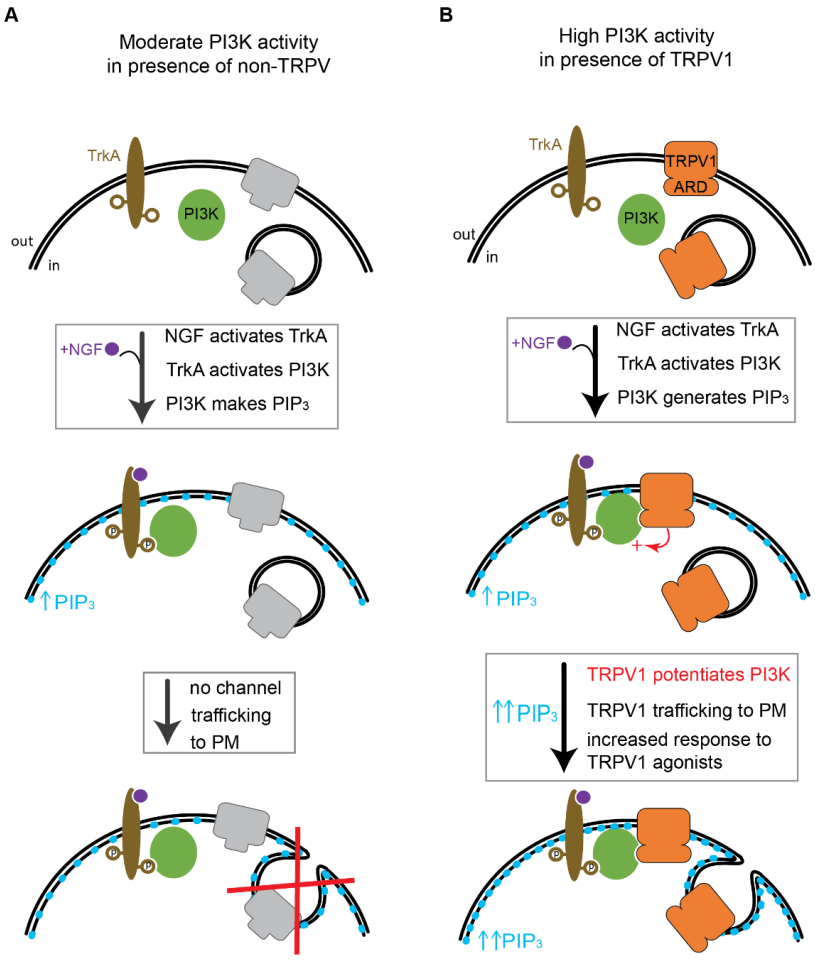

Fig. 3.18 Cartoon representation for reciprocal regulation of PI3K by ARD-containing TRP channels. (A) We speculate that moderate PI3K activity levels in presence of the non-TRPV channel are not sufficient to promote channel trafficking to the PM. (B) In presence of TRPV1 (and other TRPV channels) PI3K activity is potentiated which results in sufficient PIP_3 levels for channel trafficking to the PM.

Two possible mechanisms for NGF-induced potentiation of PI3K activity by TRPV1 are depicted in fig 4A. In one mechanism, binding to the integral membrane protein TRPV1 may stabilize the association of PI3K with the membrane. The stabilization could occur at rest, in the absence of NGF, and/or upon NGF stimulation, after activated TrkA recruits PI3K to the membrane (Fig. 3.19, left). There are precedents for an association mechanism. A mutation in the p110 catalytic subunit of PI3K (H1047R) increases membrane association, thereby increasing activity (Gabelli et al., 2014, Carson et al., 2008). In addition, the membrane-bound version of the small GTPase H-Ras associates with PI3K, accelerating formation of a PI3K-phosphotyrosine complex and modestly slowing its off rate (Buckles et al., 2017, Burke and Williams, 2015). A second possible mechanism is that TRPV1 allosterically enhance the catalytic activity of NGF-activated PI3K (Fig. 3.19, right). The two mechanisms are not mutually exclusive, but do make different predictions about potentiation of PI3K by a soluble fragment of TRPV1 that is not bound to the PM. In the first case, we would expect that a TRPV1 fragment corresponding to the PI3K binding site would not be sufficient for potentiation, as it would not localize PI3K at the PM in resting cells. In the second case, the fragment would produce potentiation of PI3K activity via an allosteric mechanism.

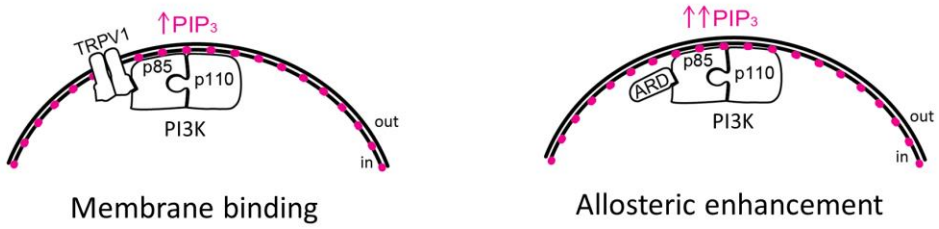

Fig. 3.19 Two proposed mechanisms for TRPV1 potentiation of PI3K.

Together, our data indicate that potentiation of NGF-induced PI3K activity by TRPV1 is mediated by its ARD and that the mechanism of potentiation likely involves an allosteric enhancement of the catalytic activity of PI3K by its direct interaction with the TRPV1 ARD (Fig. 3.19, left). Whether the slower NGF-induced increase in Akt-PH observed with TRPV1-ARD compared with full-length TRPV1 (Fig. 3.6) arises from a missing component of membrane binding of PI3K (Fig. 3.19, right) remains to be determined.

Several questions remain to be investigated.

1) Invitro studies of PI3K activity in presence of ARDs will elucidate key properties of potentiation, such as affinity of the interaction, effects on PI3K kinase activity and substrate selectivity.

2) Mutagenesis will allow for identification of the PI3K – ARD interaction site, and potentially for disruption of the interaction, which may prove useful for application in various disease states such as inflammatory hyperalgesia and Duchenne muscular dystrophy.

3) Lack of clear potentiation of PI3K activity by TRPA1 along with clear NGF-induced trafficking of TRPA1 may provide useful insight into properties of ARD-PI3K interaction.

4) Potentiation by TRPM4 may elucidate key features of ARD-like domains important for potentiation of PI3K but not trafficking of the channels.

3.6 Methods

3.6.1 TIRF Microscopy and analysis

For imaging, we used an inverted microscope (NIKON Ti-E) equipped for total internal fluorescence (TIRF) imaging with a 60x objective (NA 1.49). Glass coverslips with adherent cells were placed in a custom-made chamber. The chamber volume (~1 ml) was exchanged using a gravity-driven perfusion system. Cells were acclimated to flow for at least 15 min prior to NGF application. Akt-PH fused to Cyan Fluorescent Protein (CFP) was imaged using excitation from a 447 nm laser and a 480/40 emission filter. TRPV1 fused to Yellow Fluorescent Protein (YFP) was imaged using the 514 nm line of an argon laser and a 530 long pass emission filter. Time-lapse images were obtained by taking consecutive CFP and YFP images every 10 seconds. Movies were then processed using ImageJ software (NIH) (Rasband, 1997-2016). Regions of interest (ROI) were drawn around the footprint of individual cells and the average ROI pixel intensity was measured. Measurements were analyzed using Excel 2013 (Microsoft Corporation), by subtracting the background ROI intensity from the intensity of each cell ROI. Traces were normalized by the average intensity during the 1 min time period prior to NGF application.

3.6.2 Depth of TIRF field and membrane translocation estimation

Because $PI(3,4)P_2/PIP_3$ levels reported by the Akt-PH fluorescence measured with TIRF microscopy include significant contamination from free Akt-PH in the cytosol, we used the characteristic decay of TIRF illumination to estimate the fraction of our signal due to Akt-PH bound to the membrane. We first estimated the fraction of the illumination at the membrane in resting cells, assuming that free Akt-PH is homogeneously distributed throughout the evanescent field. After stimulation with NGF, we then used this fraction of illumination at the membrane to determine the fraction of the emission light originating from this region. The estimation approach used below was not used to quantitatively evaluate our data. Rather, it demonstrates the general issue of cytosolic contamination causing underestimation of changes in membrane-associated fluorescence even when using TIRF microscopy.

The depth of the TIRF field was estimated as described in the literature (Axelrod, 1981, Mattheyses and Axelrod, 2006). Briefly, when laser light goes through the interface between a coverslip with refractive index n_2 and saline solution with refractive index n_1, it experiences total internal reflection at angles less than the critical incidence angle, θ_c, given by

$$\theta_c = sin^{-1}(\frac{n_1}{n_3}).$$

The characteristic depth of the illuminated field *d* is described by

$$d = \frac{\lambda_0}{4\pi n_3}(sin^2\theta - sin^2\theta_c)^{-\frac{1}{2}},$$

where λ_0 is laser wavelength. The illumination decay τ, depends on depth of field as follows:

$$\tau = \frac{1}{d}.$$

TIRF illumination intensity, *I*, is described in terms of distance from the coverslip, *h,* by

$$\mathrm{I} = e^{-\tau h}$$

For simplicity, we measured the distance *h* in “layers”, with the depth of each layer corresponding to physical size of Akt-PH, which was estimated to be approximately 10 nm based on the sum of longest dimensions of Akt-PH and GFP in their respective crystal structures (PDB ID: 1UNQ and 1GFL). We solved

for TIRF illumination intensity using the following values for our system: refractive indexes of solution n_1=1.33 and coverslip n_3=1.53, critical incidence angle θ_C =60.8 degrees. The laser wavelength used in our experiments was λ_0 =447 nm, and the experimental angle of incidence was θ_{exp}=63 degrees. This produces a characteristic depth of d_{63} =127 nm and an illumination decay of τ_{63} =0.008 nm^{-1}. We plot TIRF illumination intensity over distance in molecular layers and nanometers in Fig. 3.5.

The values determined above allow us to estimate the contributions to our TIRF signal from the membrane vs. the cytosol. According to our calculation, the TIRF illumination intensity approaches 0 at around 500 nm, or layer h_{49}. We consider the membrane and associated proteins to reside in layer h_0. Under these conditions, at rest, 5% of total recorded TIRF fluorescence arises from h_0, with the remainder originating from h_1-h_{49}. At rest, we assume that Akt-PH molecules are distributed evenly throughout layers h_0-h_{49}, with no Akt-PH bound to the membrane because the concentration of $PI(3,4)P_2/PIP_3$ in the PM is negligible at rest. Total fluorescence intensity measured before NGF application, $F_{initial}$, depends on m, the number of molecules per layer at rest, B, the brightness of a single molecule of CFP, and TIRF illumination intensity, I:

$$F_{initial} = \mathrm{B} * \sum_{0}^{49} mI_i$$

Normalizing our time traces to $F_{initial}$, sets $F_{initial}$ = 1. We solved for m numerically using Excel (Microsoft, Redmond, WA), and determined a value of 0.08. We assumed a fixed number of molecules in the field and that the only NGF-induced change was a redistribution of molecules among layers. The total fluorescence intensity measured after NGF application, F_{NGF}, will reflect the redistribution of Δm molecules between membrane layer h_0 and all layers h_0-h_{49}, with free Akt-PH homogeneously distributed among these layers. Therefore, F_{NGF} is a sum of fluorescence intensities of the number of bound molecules in the membrane layer h_0 and the free molecules in layers h_1-h_{49}:

$$F_{NGF} = \mathrm{B} * \ [(\Delta m)I_0 + \textstyle\sum_0^{49}(m - \frac{\Delta m}{50})I_i]$$

We solved for Δm using Excel, constraining F_{NGF} to the values we measured for control and TRPV1-expressing cells (data listed in the table in Fig. 3.5B). Finally, we estimated the NGF-induced change in Akt-PH bound to the membrane as R_m, the ratio of molecules in h_0 after NGF to that before NGF:

$$R_m = \frac{(m + \Delta m)I_0}{mI_0}$$

We compared R_m values to the F_{NGF} values listed in the table Fig. 3.5B. For example, in cells expressing TRPV1, F_{NGF} of 1.54 led to 10 times more membrane-associated Akt-PH molecules. Note, that if we instead allow the number of molecules in cytosolic layers to remain constant as m_0 increases with NGF treatment, we calculate an R_m value of 8, very similar to the value of 10 obtained with redistribution of a fixed number of molecules across all layers. Both of these scenarios are independent of the initial Akt-PH fluorescence intensity in a given cell.

3.6.3 Cell culture /transfection/ DNA constructs/ solutions

F-11 cells (a gift from M.C. Fishman, Massachusetts General Hospital, Boston, MA; (Francel et al., 1987)) were cultured at 37°C, 5% CO_2 in Ham's F-12 Nutrient Mixture (#11765-054; Gibco) supplemented with 20% fetal bovine serum (#26140-079; Gibco, Grand Island, NY), HAT supplement (100 µM sodium hypoxanthine, 400 nM aminopterin, 16 µM thymidine; #21060-017; Gibco), and penicillin/streptomycin (#17-602E, Lonza, Switzerland). F-11 cells were tested negative for mycoplasma contamination using Universal Mycoplasma Detection Kit (# ATCC 30-1012K, ATCC, Manassas, VA). F-11 cells for imaging experiments were plated on Poly-Lysine (#P1274, Sigma, St. Louis, MO) coated 0.15 mm x 25 mm coverslips (#64-0715 (CS-25R15), Warner Instruments, Hamden, CT) in a 6-well plate. Cells were transfected with Lipofectamine 2000 (4ul/well, Invitrogen, Grand Island, NY) reagent using 1-3 ug of cDNA per well. 24 hrs post-transfection, media was replaced with HEPES-buffered saline (HBR, double deionized water and in mM: 140 NaCl, 4 KCl, 1 $MgCl_2$, 1.8 $CaCl_2$, 10 HEPES (free acid) and 5 glucose) for at least 2 hrs prior to the imaging. During experiments, cells were treated with 100 ng/ml NGF 2.5S (#13257-019, Sigma), vehicle (HBR) or 20 nM wortmannin (Sigma W1628).

TRPV1-cYFP (rat) (Ufret-Vincenty et al., 2015), TRPV1-ARD-ctagRFP (rat), TRPV2-cYFP (rat) (Mercado et al., 2010) DNA constructs were made in the pcDNA3 vector (Invitrogen), where "-n" or "-c" indicates that the fluorescent protein is on the N- or C-terminus, respectively. TRPV4-EGFP (human) in pEGFP was obtained from Tim Plant (Charite-Universitatsmedizine, Berlin) (Strotmann et al., 2003). TrkA (rat) in the pcCMV5 vector and $p75_{NTR}$ (rat) in the pcDNA3 vector were obtained from Mark Bothwell

(University of Washington, Seattle). PH-Akt-cCerulean in the pcDNA3-k vector was made based on the construct in the pHR vector from the Weiner Lab (Toettcher et al., 2011). The function of the ion channels tested were confirmed using Ca^{2+} imaging and/or patch clamp electrophysiology (data not shown).

3.6.4 Western blotting

For detection of relative expression of PI3K p85α subunit, cells were transfected as described above for imaging experiments. 24 hrs after transfection, cells were scraped off the bottom of 10 cm plates, washed with PBS 4 times and homogenized in Lysis buffer (1% Triton 25 mM Tris-HCl, 150 mM NaCl, 1 mM EDTA, pH 7.4) for 2 hrs with mixing at 4°C. Lysates were spun down at 14000 rpm for 30 min at 4°C to remove the cell nuclei and debris. Cleared lysates were mixed with Laemmli 2x SDS sample buffer (#161-0737, Bio-Rad, Hercules, CA), boiled for 10 minutes and subjected to SDS PAGE to separate proteins by size. Gels were then transferred onto the PDVF membrane using Trans-Blot SD semi-dry transfer cell (Bio-Rad) at 15 V for 50 min. Membranes were blocked in 5% BSA Tris-Buffered Saline, 0.1% Tween (TBS-T) for 1 hr and probed with primary antibody for 1 hr at RT. Next, membranes were washed 6x times with TBS-T and probed with secondary antibodies conjugated with Horse Radish Peroxidase (HRP) for 1 hr. After another set of 6 washes membranes were developed by addition of the SuperSignal™ West Femto HRP substrate (#34096, Thermo, Grand Island, NY) and imaged using CCD camera-enabled imager. For quantification, blot images were analyzed in ImageJ. ROIs of the same size were drawn around the bands for p85 and tubulin, then mean pixel intensity was measured. Mean p85 intensities were normalized by dividing by mean tubulin intensities and plotted in Fig. 3.9. Experiments were repeated with n=5 independent samples. Primary antibodies used were: anti-PI3K (alpha) polyclonal (#06-497 (newer Cat#ABS234), Upstate/Millipore, Burlington, MA) at 1:600 dilution; β Tubulin (G-8) (#sc-55529, Santa Cruz, Dallas, TX) at 1:200 dilution. Secondary antibodies used: Anti-Rabbit IgG (#074-1506, KPL/SeraCare Life Sciences, Milford, MA) at 1:30,000 dilution; Anti-Mouse IgG (#NA931, Amersham/ GE Healthcare Life Sciences, United Kingdom) at 1:30,000 dilution.

For detection of phosphorylated Akt, cells plated in six-well plates were treated for the indicated amount of time (Fig. 3.10, Fig. 3.3) in the CO_2 incubator at 37°C. Immediately after treatment, wells were aspirated and scraped in ice-cold lysis buffer (H_2O, TBS, 1% NP-40, 5 mM NaF, 5 mM Na_3VO_4, with added

Protease inhibitors (#P8340, Sigma) and Phosphatase Inhibitor Cocktail 2 (#P5726, Sigma). After incubation on ice for 15 min, lysates were cleared by centrifugation at 15k g for 15 min at 4°C. Protein contents of cleared lysates were measured using the BCA assay (#23225 Pierce) according to manufacturer's protocol. Volumes of lysates were adjusted according to these measurements and subjected to SDS-PAGE. Gels were transferred onto PVDF membranes using wet-transfer. Membranes were blocked in TBS-T with 5% milk for 1 hr and incubated overnight at 4°C with one of the following primary antibodies: pAKTs473 clone D9E (#4060, Cell Signaling), pAKTt308 clone 244F9 (#4056, Cell Signaling) or panAKT clone 40D4 (#2920, Cell Signaling) at 1:2500 dilution. Further procedures were as indicated in the previous paragraph. After development membranes were stripped using Pierce Restore Western Blot strip- ping buffer (#21059, Thermo Fisher), reprobed with the other anti-phospho-AKT antibody and then stripped and re-probed with panAKT clone 40D4 (#2920, Cell Signaling) antibody at 1:2500 dilution. Data was normalized by diving the average intensity of a band by the average intensity of a blot and then dividing by that of a pan-Akt blot (Fig. 3.10).

3.7 Tables

Table 3.1 Normalized Akt-PH fluorescence intensities measured during NGF application for all discussed conditions.

The number of cells in the data set collected over at least three different experiments is given by n. Non-adjusted Wilcoxon rank test two tail p values for pairwise comparisons as indicated.

Akt-PH from	Mean ± SEM during NGF	n=	P value, comparison against control	P value, comparison against TRPV1
control	1.08 ± 0.03	75	-	-
TRPV1	1.54 ± 0.8	122	10^{-12}	-
TRPV1-ARD	1.32 ± 0.2	80	10^{-5}	0.08
TRPV2	1.23 ± 0.18	61	0.04	0.0002
TRPV4	1.28 ± 0.14	29	0.02	0.02
TRPA1	1.14 ± 0.03	59	0.13	10^{-7}
TRPM4	1.2 ±0.04	63	0.01	10^{-5}
TRPM8	1.07 ± 0.02	73	0.8	10^{-14}

Table 3.2 Normalized TRP channel fluorescence intensities measured during NGF application for all discussed conditions.

The number of cells in the data set collected over at least three different experiments is given by n. Non-adjusted Wilcoxon rank test two tail p values was performed for pairwise comparisons as indicated.

	Mean ± SEM during NGF	**n=**	**P value, comparison against TRPV1**	**P value, comparison against vehicle**
TRPV1	1.15 ± 0.02	94	-	-
vehicle	1.01 ± 0.01	20	10^{-6}	-
TRPV2	1.12 ± 0.02	62	0.24	0.002
TRPV4	1.11 ± 0.02	48	0.13	0.002
TRPA1	1.17 ± 0.04	53	0.4	0.0007
TRPM4	0.99 ±0.01	65	10^{-12}	0.3
TRPM8	1.05 ± 0.01	67	10^{-5}	0.02

3.8 Acknowledgements

We thank Mika Munari, Gilbert Martinez, Mark Bothwell, Bertil Hille, William N. Zagotta, Shao-En Ong, Tamara Rosenbaum and Gaby Bergollo for helpful discussions. We are grateful to the following individuals for providing cDNA constructs: Tim Plant (Charite-Universitatsmedizine, Berlin) for TRPV4; Marc Simard (University of Maryland, College Park) for TRPM4; Mark Bothwell (University of Washington, Seattle) for TrkA and $p75_{NTR}$; Ajay Dhaka (University of Washington) for TRPA1; and Orion Weiner (UCSF) for Akt-PH.

Research reported in this publication was supported by the National Eye Institute of the National Institutes of Health under award numbers R01EY017564 (to SEG), by the National Institute of General Medical Sciences of the National Institutes of Health under award numbers R01GM100718 and R01GM125351 (to SEG), by the National Institute of Mental Health under award number R01MH113545 (to SEPS), by the National Institute of Biomedical Imaging and Bioengineering of the National Institutes of Health under award number T32EB001650 (to AS), and by the following additional awards from the National Institutes of Health: S10RR025429, P30DK017047, and P30EY001730, and by a Royalty Research Fund Award from the University of Washington (to SEG). The content is solely the responsibility of the authors and does not necessarily represent the official views of the National Institutes of Health. The authors declare no competing financial interests.

4 TRPV1 retains and sustains PI3K at the plasma membrane: insights from a light-controlled opto-PI3K system

4.1 Introduction

We have recently demonstrated reciprocal regulation of NGF-induced PI3K activity by TRPV1 (Stratiievska et al., 2018). NGF-induced PI3K activity was potentiated in presence of the TRPV1 channels and was accompanied by channel trafficking to the plasma membrane. Conversely, we and others have previously shown that inhibition of PI3K prevents the NGF-induced increase in plasma membrane levels of TRPV1 (Stein et al., 2006, Zhuang et al., 2004, Bonnington and McNaughton, 2003). However, it is not known whether PIP_3 synthesis is sufficient to trigger this increase or whether contributions from other pathways downstream of NGF, such as PLC and MAPK, play a role. In order to distinguish PI3K activity from other NGF downstream signaling events, we are developing an optogenetic approach to activate PI3K specifically with light.

Stimulus-induced dimerization is a common approach used to manipulate various cell signaling events, such as protein localization and activation (Putyrski and Schultz, 2012). Two types of such systems include light-induced and chemically-induced dimerization. Chemically-induced dimerization systems, such as rapamycin-induced dimerization of FRB-FKBP (Rivera et al., 2019), are based on the properties of small molecules called chemical inducers of dimerization (CIDs) to bind two proteins simultaneously (Putyrski and Schultz, 2012). Dimerization partners are usually genetically modified to be fused to target proteins or to sub-cellular localization signals. Such systems are extensively used in studies of protein expression, cell survival and motility (for extensive review refer to (Voss et al., 2015)). CIDs generally suffer from a major disadvantage; namely, once CIDs are added, dimerization may not be rapidly reversed, unless a competing ligand is added (Feng et al., 2014), or CID is photocleaved (Ahmed et al., 2014). Small CID molecules must be able to penetrate the cell. In addition, all of the CID approaches allow for just a one-time activation of the target protein. Another downside of CIDs is that the small molecules added to activate dimerization may also have off-target effects, which may be hard to control and account for in the experimental design

(Clackson et al., 1998)., Finally, CID approach may only be applied to the entire cell or a population of cells, so no precise subcellular activation may be achieved.

Using light to control the dimerization addresses the disadvantages of CIDs. Multiple light-inducible dimer (LIDs) systems were developed to utilize proteins from light-sensitive organisms, such as LOV-domain (Krauss et al., 2010), CRY2 (Kennedy et al., 2010) or Phytochrome B (Shimizu-Sato et al., 2002). Such systems allow for rapid dimerization and dissociation of partner proteins. Rapid induction and ablation of signaling with great spatio-temporal precision is achieved by the use of genetically modified dimerization partners fused to target proteins (Levskaya et al., 2009). Such approaches are extensively used to control phosphoinositide signaling, activity of small GTP-ases, protein degradation, secretion and transcription (Idevall-Hagren et al., 2012, Toettcher et al., 2011, Levskaya et al., 2009, Chen et al., 2013, Hughes et al., 2012).

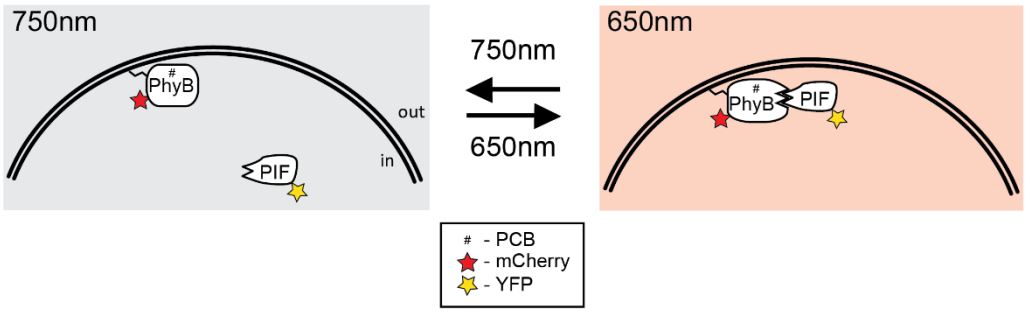

Fig. 4.1 Cartoon representation for light-induced PhyB-PIF dimerization.
Membrane-localized PhyB fused to mCherry (PhyB-mCherry-CAAX) and supplied with PCB (#), interacts with PIF fused to YFP upon illumination with 650 nm light. This results in membrane recruitment of PIF-YFP. Upon subsequent illumination with 750 nm PhyB is photo-switched into a conformation with low affinity to PIF, which leads to PIF dissociation into the cytoplasm.

The opto-PI3K light-controlled dimerization system was based on the light-sensitive protein PhyB (Phytochrome B) and its interacting partner PIF (Phytochrome B interacting factor) (Shimizu-Sato et al., 2002, Levskaya et al., 2009). PhyB in the presence of the co-factor PCB (Phycocyanobilin, in Fig. 4.1 indicated by "#") undergoes photo-switchable conformational changes dependent on the wavelength of red-light illumination. 650 nm light illumination drives PhyB into a conformation with high affinity for PIF forcing PhyB and PIF to interact, and 750 nm light instantly reverses this interaction. The advantages of the opto-

PI3K light-controlled dimerization system include a rapid reversibility and a spatial control over the PhyB-PIF interaction (Toettcher et al., 2011).

In order to achieve reversible activation of PI3K, Toettcher and colleagues genetically modified PhyB by addition of membrane localizing sequence CAAX and fusion to fluorescent protein mCherry (this construct will be further referred to simply as PhyB, Fig. 4.2, bottom). In addition, the iSH domain from PI3K regulatory subunit p85 was fused to PIF tagged with yellow fluorescent protein YFP (further referred to as $p85^{iSH}$-PIF, Fig. 4.2, bottom).

In order to record PI3K activity in response to light, a fluorescent probe that recognized the PI3K product – PIP_3 was used. In addition to the components of opto-PI3K system, cells expressed the PIP_3-specific Pleckstrin homology (PH) domain (James et al., 1996) from the enzyme Akt fused to CFP (referred to as Akt-PH (Frech et al., 1997), Fig. 4.2, bottom).

PI3K is an enzyme that upon recruitment to the membrane by Receptor Tyrosine Kinases (RTKs) phosphorylates PIP_2 into PIP_3 (see section 1.3 for details). The catalytic PI3K subunit p110 always exists as a heterodimer with its regulatory subunit p85 (Geering et al., 2007). Under physiological conditions, PI3K is activated by interactions between the nSH2 domain of the p85 subunit and membrane-localized phospho-tyrosine motifs of receptor tyrosine kinases. These interactions release autoinhibition of the p110 catalytic subunit by the nSH2 domain (Miller et al., 2014).

The iSH domain of the p85 subunit is responsible for binding to p110, therefore in $p85^{iSH}$-PIF transfected cells it is presumed to always exist as heterodimer with endogenous p110 (Fig. 4.2, bottom). Upon 650 nm light illumination $p85^{iSH}$-PIF/p110 interacts with membrane localized PhyB (Fig. 4.2, bottom). Since $p85^{iSH}$-PIF used in the opto-PI3K system doesn't contain the autoinhibitory nSH2 domain, endogenous p110 bound to $p85^{iSH}$-PIF is instantly active when localized to the PM via the PIF-PhyB interaction. This translocation leads to activation of PI3K via co-localization with the lipid substrate and results in an increase in PIP_3 concentration at the plasma membrane, which in turn, is detected by Akt-PH probe. Alternatively, illumination with 750 nm light induces a conformation in PhyB with low affinity for PIF. This leads to dissociation of $p85^{iSH}$-PIF from the membrane-localized PhyB, leading to "deactivation": of

PI3K and gradual decrease of PIP_3 concentration by phosphatases. In summary, 650 nm light illumination results in activation of PI3K and 750 nm light turns the PI3K off (Fig. 4.2, top).

The Opto-PI3K system was developed by Weiner and Lim groups at UCSF (Toettcher et al., 2011). After this original publication, this group was the only one to keep reporting on research using it. Here we developed an approach useful for troubleshooting implementation of opto-PI3K in transiently transfected cells. Using this approach, other groups will be enabled to implement PI3K in any cell line of their interest. We predict that our troubleshooting approach will help to give rise to a large number of publications using this elegant opto-PI3K system and developing other PhyB-PIF based systems for light activation.

We aimed to utilize the opto-PI3K approach to isolate PI3K signaling events from PLC and MAPK that accompany NGF-induced PI3K activation. By directly activating PI3K and therefore, bypassing TrkA signaling, we aimed to gain better understanding of PI3K signaling involved in TRPV1 sensitization during inflammation.

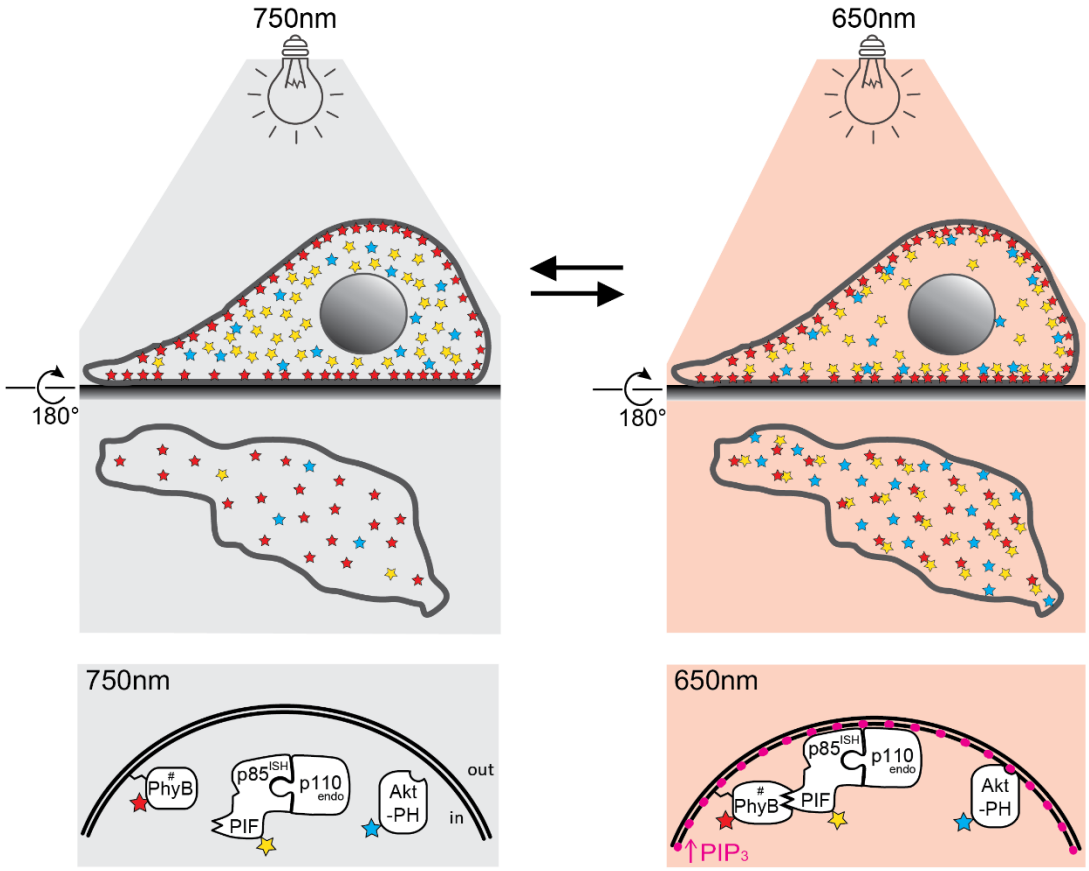

Fig. 4.2 Cartoon representation for activation of the opto-PI3K system.

Cell expressing components of opto-PI3K system on the surface of Poly-K coated glass coverslip.

Top: PhyB is membrane tethered (red V-shape) and $p85^{ISH}$-PIF is free diffusing in cytoplasm (yellow circles). Under de-activating 750 nm light illumination, $p85^{ISH}$-PIF is in cytoplasm (left, gray background). Upon illumination with activating 650 nm light, $p85^{ISH}$-PIF rapidly translocates to the membrane (right, red background).

Middle: view from the bottom of the cell footprint. Upon translocation of cytoplasmic proteins to the PM in response to 650nm light the number of fluorescent molecules increases.

Bottom: zoomed in view on the plasma membrane. Star shapes indicate fluorescent proteins of the corresponding color (red – mCherry, yellow – YFP, cyan – CFP). # indicates PhyB with a co-factor PCB. Magenta indicates PIP_3 molecules. $P110_{endo}$ indicates endogenous p110.

4.2 Results:

4.2.1 Implementing an optogenetic approach to generate PIP_3 in the plasma membrane.

As a proof of principle for PhyB-PIF light-induced dimerization, we first used a NIH3T3 cell-line previously generated by the Weiner Lab, stably expressing genetically modified PhyB (NIH3T3-PhyB-mCherry-CAAX) (Toettcher et al., 2011). In order to visualize a light-induced interaction of PIF with PhyB, we utilized scanning confocal microscopy. NIH3T3-PhyB-mCherry-CAAX were plated on PolyK-treated glass coverslips and transfected with PIF-YFP (without $p85^{iSH}$) 24 hours prior the experiment. On the day of an experiment cells were loaded with PCB for 1 hr at 37°Cin the dark. Cells were equilibrated under de-activating 750 nm light for at least 5 min before recording. Next, cells were placed in the experimental chamber with HBR in the dark. Immediately after placing the coverslip on the microscope stage, cells were illuminated with 750 nm de-activating light from above through the filter cube with 760/40 nm bandpass filter using an overhead condenser lamp at maximum voltage output of 12V as a light source (see Fig. 4.21).

In order to record light-induced translocation of PIF to the plasma membrane via interaction with membrane-tethered PhyB, confocal cross-section images of the PIF-YFP fluorescence excited with 514 nm argon laser and emission at 535 nm were collected at 5 second intervals. Fig. 4.3 A shows a series of representative PIF-YFP confocal images of NIH3T3-PhyB-mCherry-CAAX cell being alternately illuminated with de-activating 750 nm light or activating 650 nm light. Fig. 4.3 B, shows the ratio of the PIF-YFP fluorescence measured using a small region of interest (ROI) drawn at the plasma membrane (F_m) and the cell cytoplasm (F_c). Initially, under de-activating 750 nm illumination PIF-YFP is evenly distributed within the cytoplasm which results in ratio F_m/F_c ~1. Upon 650 nm illumination, PIF-YFP is rapidly translocated to the plasma membrane which leads to the increase in the value of F_m/F_c. Repeated 650/750 nm illumination results in reversible translocation of PIF to the PM/cytoplasm for multiple cycles (Fig. 4.3 B). This indicated that we were able to reproduce light-inducible PhyB-PIF translocation and dissociation using our experimental set up.

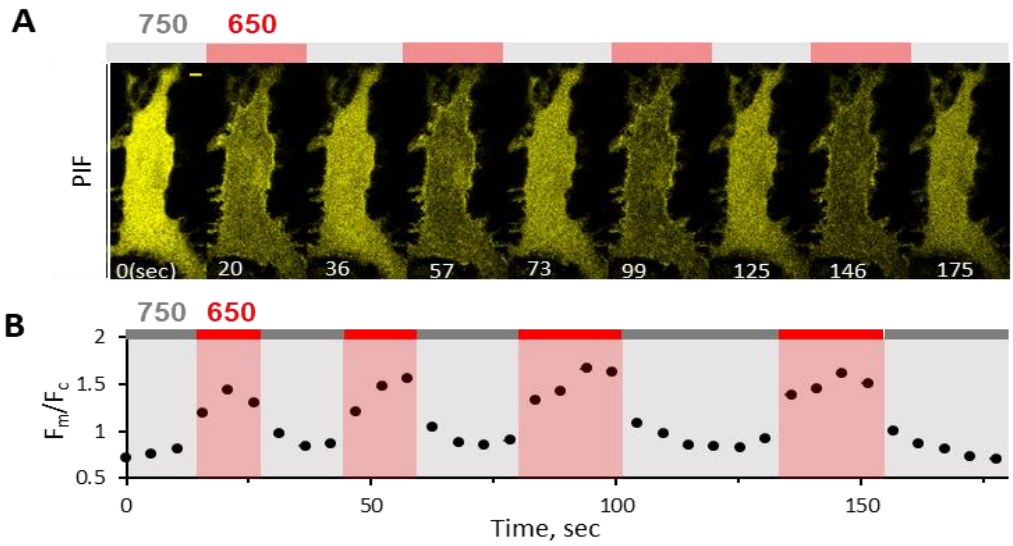

Fig. 4.3 PhyB – PIF light inducible interaction is fully reversible on the time scale of ~10 sec and can be repeated multiple times.

A) Representative PIF fluorescence confocal images of NIH3T3 cell stably expressing PhyB-CAAX transfected with PIF. Time stamps as in B.

B) Ratio of measured PIF fluorescence at ROI placed at the membrane (F_m) and cytoplasm (F_c) from the cell in A.

Next we set out to control PI3K activity with light using NIH3T3 cells stably expressing PhyB-mCherry-CAAX, PIF fused to the iSH domain from PI3K regulatory subunit p85and YFP; and the Akt-PH domain fused to CFP (also previously generated by the Weiner Lab). Translocation of $p85^{iSH}$-PIF-YFP brings the p110 catalytic subunit to the PM which results in activation of PI3K and generation of PIP_3. Increase in PIP_3 concentration at the PM leads to translocation of the PIP_3-sensitive probe from the Plekstrin homology domain of Akt fused to CFP to the PM. To record near-membrane fluorescence of $p85^{iSH}$-PIF and Akt-PH FP-fusion proteins transfected in NIH3T3-PhyB-mCherry-CAAX cells, we first utilized confocal microscopy as described above. It was especially difficult to obtain reliable measurements of plasma membrane fluorescence for extended period of time, because robust PI3K activation is a signal for cell membrane remodeling and motility.

In order to overcome the problem of cell motility after activation of PI3K, we used dual-color TIRF microscopy. TIRF microscopy allows for illumination of ~300 nm of the cell adjacent to the coverslip, which

results in excitation of only the fluorophore molecules in close proximity to the plasma membrane. The advantage of TIRF over confocal microscopy is that TIRF produces fluorescent images of the isolated cell footprint with a better signal to noise ratio. In addition, cell motility does not affect the measurements of PM fluorescence using TIRF, because a region of interest may be drawn to exclude the moving parts of cell footprint. This results in more reliable measurements of the plasma membrane fluorescence of the cell (Fig. 4.4 A).

To mimic PI3K activation by NGF we switched to 650 light illumination for 2 min (Fig. 4.4, red bars with shading). Cells were equilibrated under de-activating 750 nm light for at least 5 min. The average fluorescence intensity was measured within the ROI drawn around entire cell footprint and normalized to the intensity of the ROI in the first frame (Fig. 4.4 B, norm intensity over time). Illumination with activating 650 nm light led to fast translocation of $p85^{iSH}$-PIF to the plasma membrane as seen from the increase in the normalized intensity (Fig. 4.4, top). Once switched to deactivating 750 nm light $p85^{iSH}$-PIF rapidly dissociated from the plasma membrane as seen from the decreased fluorescence intensity to basal levels. This indicates that we successfully recruited opto-PI3K to the plasma membrane with light in a reversible manner.

This was followed by the slower increase in the Akt-PH fluorescence that reached a steady state over a 3 min illumination period (Fig. 4.4, bottom). To maintain the PIP_3 balance at low basal levels, PI3K activity is counteracted by phosphatases such as PTEN, that de-phosphorylate PIP_3. Therefore, the 650 nm light-induced increase in PIP_3, was followed by a decrease in PIP_3 concentration after illumination with 750 nm light, as seen from the slow decrease in Akt-PH. Intervals of at least 3 min between the 650 nm illumination cycles were required to allow for full restoration of basal PIP_3 concentration. The changes in PIP_3 levels at the PM indicate that we successfully activated opto-PI3K with light in a reversible manner.

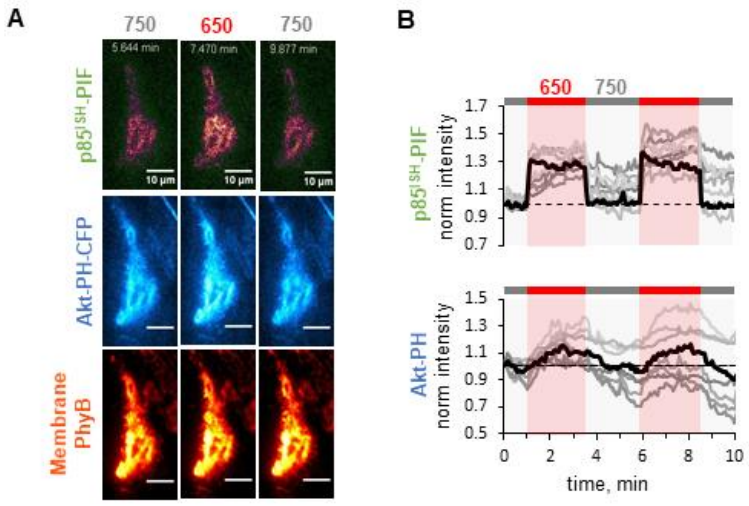

Fig. 4.4 Opto-PI3K system observed using TIRF microscopy

TIRF fluorescence images of a representative NIH3T3 cell stably expressing PhyB-mCherry-CAAX, p85ISH-PIF and Akt-PH illuminated with 750 nm or 650 nm light as indicated. Scale bar is 10 µm.

Collected traces of normalized p85ISH-PIF (top) and Akt-PH (bottom) TIRF fluorescence intensity measured within the ROI drawn around the entire cell footprint of the cell (n=8).

4.2.2 Troubleshooting opto-PI3K Implementation

Our motivation was to use opto-PI3K in a neuronal cell line F-11, because it is believed to be more physiologically relevant to NGF signaling and hyperalgesia (Francel et al., 1987). Once we have shown that opto-PI3K system works in the NIH3T3 cells in which it was first developed, we asked if it would extend to a variety of cell lines. This includes commonly used HEK293T/17 cells and a neuronal cell line F-11, a hybridoma between rat neuroblastoma and mouse DRG neurons. We started with transfecting HEK293T/17 cells with plasmids deposited to Addgene by Weiner group (pal149 for PhyB-mCherry-CAAX Addgene #22275, pal175 for PIF-YFP Addgene #22276). Unfortunately, we were not able to observe reversible translocation of PIF-YFP to the plasma membrane with light.

We performed a series of experiments aimed to troubleshoot each of the three components of PhyB-PCB-PIF system in transfected cells. First, we validated the quality of a co-factor phycocyanobilin (PCB, ChemPrep Inc.), that interacts with PhyB and is required for light-sensitivity. PCB is a small light-sensitive molecule which is purified from Spirulina algae. PCB was stored at -20°Cin the dark, but it was previously reported that its reactivity decays over time (Levskaya et al., 2009). We generated a membrane-

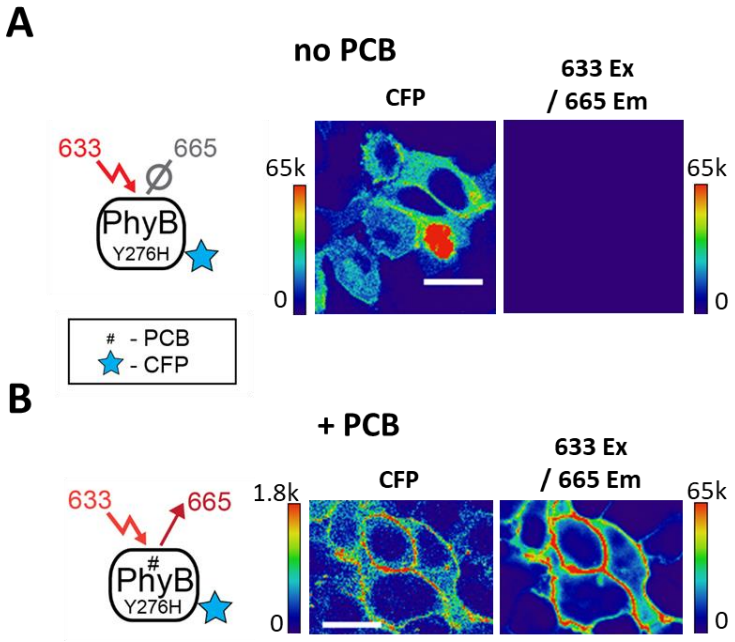

Fig. 4.5 Troubleshooting the quality of PCB. PhyB-Y276H-CFP gained red fluorescence upon PCB incorporation. Representative confocal images of HEK293T/17 cells transfected with PhyB-Y276H fused to CFP (blue star) without (A) or with 10uM PCB treatment (B). CFP fluorescence and 633 nm excitation / 665 nm emission fluorescence from PhyB-Y276H-CFP is shown in false color using heat map LUT. Scale bar 10 μm.
A) PhyB-Y276H-CFP does not have 633 nm excitation / 665 nm emission fluorescence in the absence of PCB.
B) In cells loaded with PCB PhyB-Y276H-CFP gained 633 nm excitation / 665 nm emission fluorescence.

tethered via CAAX sequence PhyB construct containing mutation at Y276H (based on pal113 obtained from Addgene, #22471 (Levskaya et al., 2009)). Upon PCB incorporation, PhyB-Y276H mutant gains far red (665 nm) fluorescence excited using 633 nm laser and cannot be activated by light (Su and Lagarias, 2007). This construct can be used as quality control for PCB. We added 10μM PCB to the cell medium in the dark at 37°Cfor 1 hr. Fig. 4.5, shows representative fluorescence images of HEK293T/17cells transfected with PhyB-Y276H-CFP-CAAX at both CFP and red emission wavelengths, loaded with either vehicle or PCB, obtained by scanning confocal microscopy. Compared to cells treated with vehicle (Fig. 4.5, A) cells treated with PCB were fluorescent at both CFP (Fig. 4.5, B, left panel) and red fluorescence from PhyB-PCB (Fig. 4.5, B, right panel). This validates that the PCB compound interacts with PhyB-Y276H-CFP-CAAX in HEK293T/17 cells.

Next step in troubleshooting is to validate the PIF for the ability to interact with PhyB. We took advantage of the fact that the PhyB-Y276H mutant constitutively binds PIF regardless of light exposure (Su

and Lagarias, 2007). HEK293T/17 cells were co-transfected with membrane-tethered PhyB-Y276H-CFP-CAAX and PIF-YFP (Levskaya et al., 2009). PIF-YFP was evenly distributed in the cytoplasm in control cells treated with vehicle (Fig. 4.6, A). In contrast, in cells treated with PCB, (Fig. 4.6, B) PIF-YFP was recruited to the PM by membrane-tethered PhyB-Y276H mutant. This validated the ability of PIF-YFP to interact with PhyB that is bound to PCB.

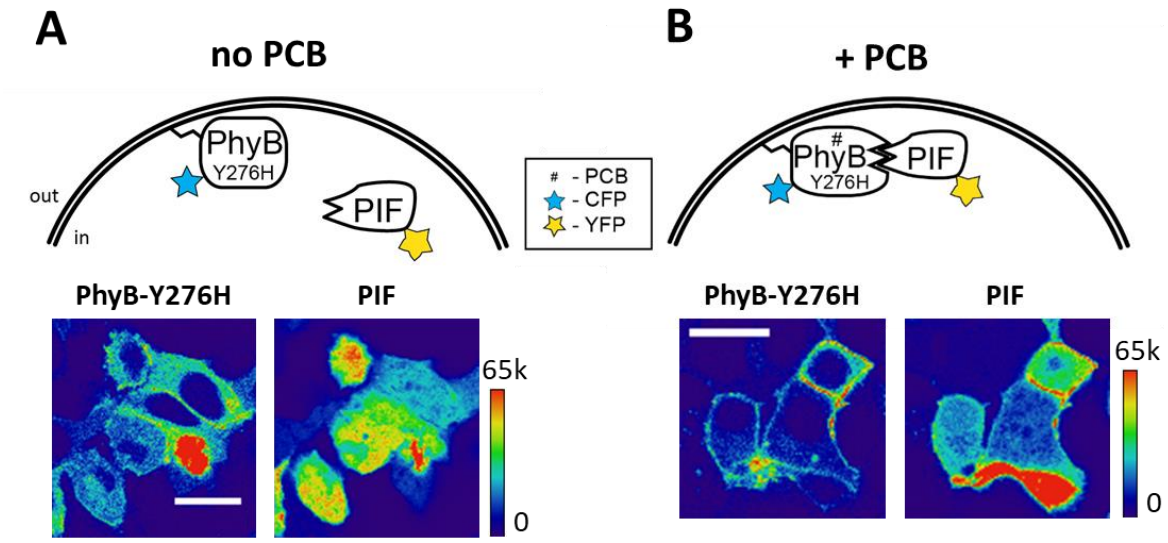

Fig. 4.6 Troubleshooting the ability of PIF to interact with PhyB. PhyB-Y276H constitutively binds PIF upon PCB incorporation.

A) Top: cartoon representing PhyB-Y276H fused to CFP (blue star) and PIF fused to YFP (yellow star) localization in the absence of PCB. Bottom: representative confocal images of HEK293T/17 cells transfected with PhyB-Y276H-CFP and PIF-YFP (false color using heat map LUT). Scale bar 10 μm.

B) In cells loaded with PCB PIF fluorescence is localized to the plasma membrane. Top: cartoon representing PhyB-Y276H and PIF localization in the presence of PCB (10μM, indicated by #). Bottom: representative confocal images of HEK293T/17 cells transfected with PhyB-Y276H-CFP and PIF-YFP (false color using heat map LUT). Scale bar 10 μm.

Thus, we confirmed the quality of the PCB stock and the ability of PIF-YFP to interact with PhyB. Still, we could not reproduce the light-induced PIF translocation in cells other than those stably expressing NIH3T3-PhyB-mCherry-CAAX that we had obtained from Weiner Lab. The only possible explanation to this was some unknown differences between the stably expressed gene for PhyB-CAAX in the NIH3T3 cell line and pal149-Cherry.pcDNA3 (Levskaya et al., 2009) plasmid which we used for transient transfections

(obtained from Addgene, #22275). In order to test this, we sequenced the genes from pal149 in pcDNA3 vector and PhyB-mCherry-CAAX in pHR vector (used to generate stable expressing NIH3T3 cells). Sequence comparison indicated two significant differences (Fig. 4.7). First, PhyB gene from NIH3T3 was codon-optimized for mammalian expression (with 75% nucleotide sequence similarity to pal149). Second, PhyB from the NIH3T3 cell line and the pal149 plasmid had different linkers between the PhyB and Cherry fluorescent protein. We hypothesized, that the linker from pal149 was interfering with light-activation of PhyB-PIF interaction in transfected cells.

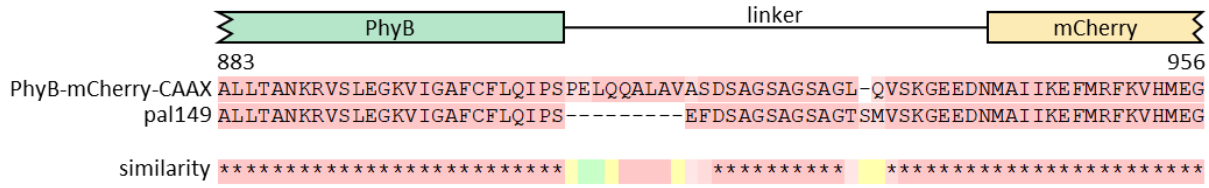

Fig. 4.7 Sequence differences in PhyB-mCherry-CAAX constructs define opto-PI3K system functionality. Amino-acid sequence comparison using T-COFFEE. PhyB-mCherry-CAAX was sequenced from stably expressing NIH3T3 cell line. pal149 was obtained from Addgene. PhyB and mCherry domains are identical. Constructs utilize different linkers. Nucleotide sequences are also different due to codon optimization

Next, we aimed to create a mammalian expression vector containing a PhyB-mCherry-CAAX- gene identical to that expressed in NIH3T3-PhyB-mCherry-CAAX cell line which exhibited robust reversible PhyB-PIF interaction. We purified DNA from the stable NIH3T3-PhyB-mCherry-CAAX cell line using the Wizard® SV Genomic DNA Purification System. Briefly, we set up a PCR using Herculase II Fusion DNA Polymerase, and ran the products on the DNA gel. We purified the band using QIAX II gel extraction kit. Purified linear DNA was sequenced by Operon (EurofinsGenomics, Luxembourg). Sequence analysis verified that the sequence of the extracted gene was identical to PhyB-mCherry-CAAX in lentiviral expression pHR vector used to make NIH3T3 stable cell line.

To generate a mammalian expression plasmid for transient transfections using F-11 cells, we cloned PhyB-mCherry-CAAX gene into the pcDNA3 mammalian expression vector. We used PhyB-mCherry-CAAX from pHR vector as a template in PCR reaction to amplify the gene using primers introducing unique restriction enzyme sites that were used for ligation. The ligation product was transformed in DH5α strain of *E. coli* cells using heat shock. The plasmid DNA was purified from a single colony using

QIAprep Spin Miniprep Kit (Qiagen, Cat# 27104) then screened through restriction analysis. Positive plasmids were sequenced to confirm absence of any secondary mutation.

In order to study PI3K activation in a cell line that was more physiologically relevant to NGF signaling, we transfected F-11 cells with a newly generated PhyB-mCherry-CAAX in pcDNA3 vector. F-11 cells are a hybridoma between rat neuroblastoma and mouse DRG neurons (Francel et al., 1987). We used dual-color TIRF microscopy to record $p85^{iSH}$-PIF-YFP and Akt-PH-CFP fluorescence from the cell footprint. Fig. 4.8 B shows representative TIRF fluorescence images of F-11 transiently expressing PhyB-mCherry-CAAX, $p85^{iSH}$-PIF-YFP and Akt-PH-CFP before during and after 650 nm light illumination. Fig. 4.8 B-D shows measured normalized TIRF intensity of the entire cell footprint plotted over time (gray traces – each individual cell, bold green or blue traces – mean). The majority of cells exhibited reversible translocation of $p85^{iSH}$-PIF to the PM (Fig. 4.8 B, top). This was followed by generation of PIP_3 as seen from translocation of the Akt-PH to the PM (Fig. 4.8 B, bottom). This indicates that we were able to successfully activate PI3K with light in transiently transfected F-11 cells.

There was a variability of responses to light between cells. We identified three populations of cell responses to 650 nm light illumination (Fig. 4.8 E). Cells were assigned to a population called “reversible” if averaged normalized intensity measured for 2 min during 650 nm illumination was >0.04 higher than both before 650 nm and after 650 nm. Cells were assigned to a population called “non-reversible” if two criteria were true: 1) norm intensity during 650 nm illumination was >0.04 higher than before 650 nm and 2) norm intensity measured after 650 nm was >0.01 higher than during 650 nm. All other cells were assigned to a population called “no-response”.

In the majority of cells (46.2%), 650 nm illumination led to the reversible recruitment of $p85^{iSH}$-PIF or Akt-PH to the plasma membrane (Fig. 4.8 B). A second population of cells (30.8%) exhibited steady increase in $p85^{iSH}$-PIF or Akt-PH at the PM (Fig. 4.8 C). A third minor population of cells (23.1%) never responsed to 650 nm light illumination (Fig. 4.8 D). Several factors contribute to such a heterogeneity of cell populations. First, transient transfection resulted in ~60-80% cells positive for each fluorescently-

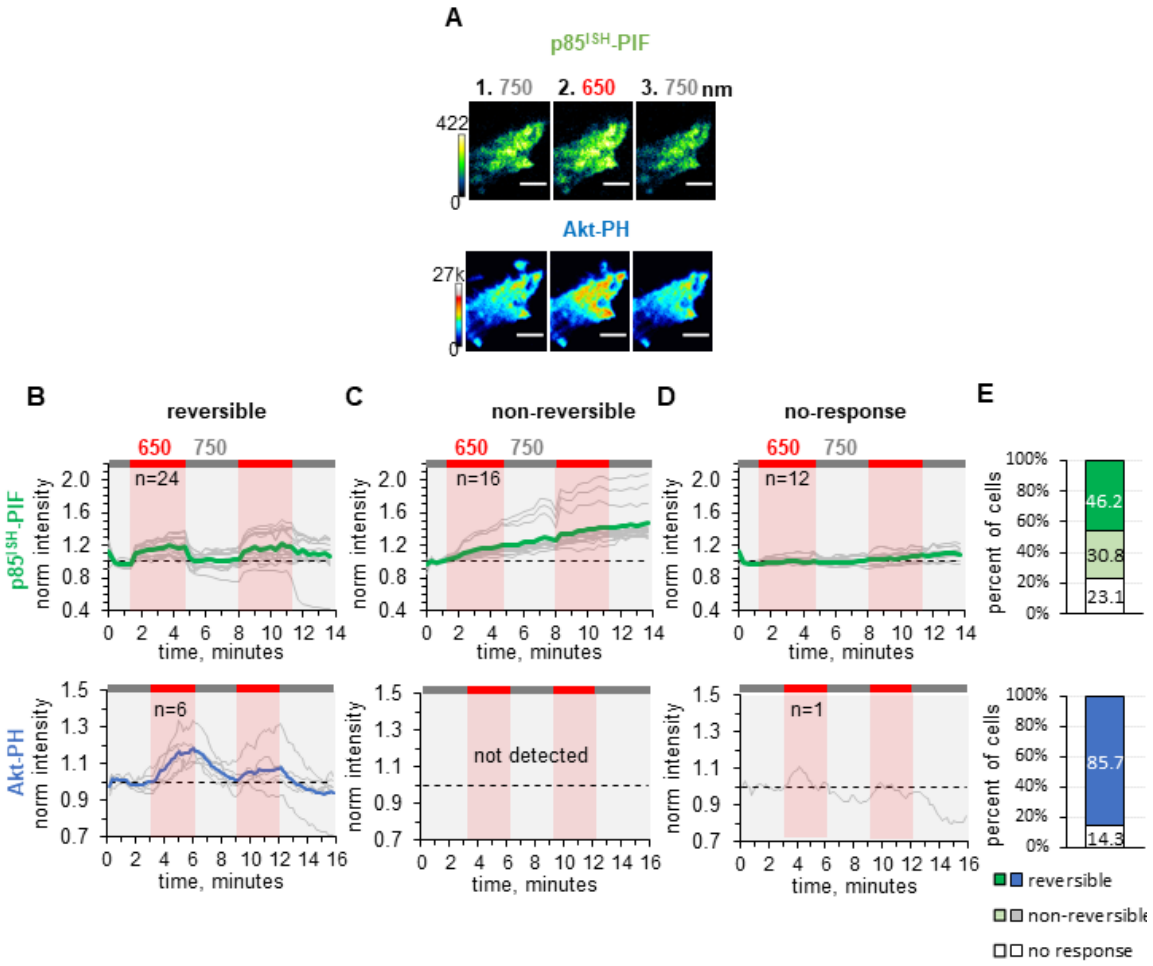

Fig. 4.8 Implementing opto-PI3K via transient transfection of F-11 cells.

A) Representative TIRF fluorescence images of F-11 cells transfected with PhyB-mCherry-CAAX, p85^{ISH}-PIF-YFP and Akt-PH-CFP before, during and after 650 nm illumination.

B-D) Collected traces from cells categorized by responses to 650 nm light illumination: reversible (B), non-reversible (C), no-response (D). Individual cell fluorescence in gray. Mean fluorescence in green for p85^{ISH}-PIF-YFP (top) and in blue for Akt-PH-CFP (bottom).

E) Percent of cells categorized by p85^{ISH}-PIF-YFP (top) and Akt-PH-CFP (bottom) responses to 650 nm light illumination: reversible (dark color), non-reversible (light color), no-response (white)

labeled component (visually identified under the low magnification). Second, it has been previously reported that an ideal ratio between membrane-tethered PhyB and PIF must occur within the cell in order to maximize PIF translocation (Levskaya et al., 2009). Considering this we will focus on comparison of the same populations from different experimental conditions.

4.2.3 TRPV1 retains p85^{iSH} at the PM

We sought to better understand consequences of PI3K activation in the presence of TRPV1 using opto-PI3K. TRPV1 has been shown to interact with PI3K and is involved in reciprocal regulation of NGF-induced PI3K activity (Stein et al., 2006, Stratiievska et al., 2018). We co-transfected F-11 cells with the opto-PI3K system components and full-length TRPV1 (Fig. 4.9). Surprisingly, in the majority of cells (75%, Fig. 4.9 C and E, top), p85^{iSH}-PIF translocation with 650 nm light was abolished; instead, p85^{iSH}-PIF fluorescence continued to rise regardless of the wavelength of illumination (Fig. 4.9 C and D, top). No cells were detected with reversible translocation of p85^{iSH}-PIF (Fig. 4.9 B and E, top) and only 25% of cells exhibited no response to light (Fig. 4.9 D and E, top). This indicated that TRPV1 interfered with reversibility of the opto-PI3K system by retaining p85^{iSH}-PIF at the plasma membrane.

Our observation that TRPV1 retained p85^{iSH}-PIF at the plasma membrane, taken together with our previous findings of potentiation of PI3K by TRPV1, allowed us to formulate an interesting hypothesis. We hypothesized that TRPV1 sustained the activity of opto-PI3K at the PM. This predicts that if p85^{iSH}-PIF was retained at the PM through interaction with TRPV1 independent of light, PI3K activity would be sustained after the 650 nm light was turned off.

In the majority of cells, we observed an increase in Akt-PH membrane localization in response to 650 nm light illumination. This indicates an increase in PIP_3 concentration after the exposure to 650 nm light, that was sustained at higher levels (Fig. 4.9 B and C, middle). In contrast to p85^{iSH}-PIF, Akt-PH levels eventually fell back to the basal levels in majority of cells with deactivating 750 nm light, although it took ~10 min which was much longer compared to control (~3min). PIP_3 concentration at the PM represents a balance of multiple mechanisms for phosphorylation (PI3K) and de-phosphorylation. Therefore, it is not surprising that PIP_3 levels eventually returned to the level observed under basal conditions. Taken together, we observed that TRPV1 retained opto-PI3K at the PM, but the activity of PI3K as seen from Akt-PH translocation, was eventually reversed to basal levels. These data suggest that Akt-PH translocation is a more sensitive read-out of PI3K activity than p85^{iSH}-PIF localization.

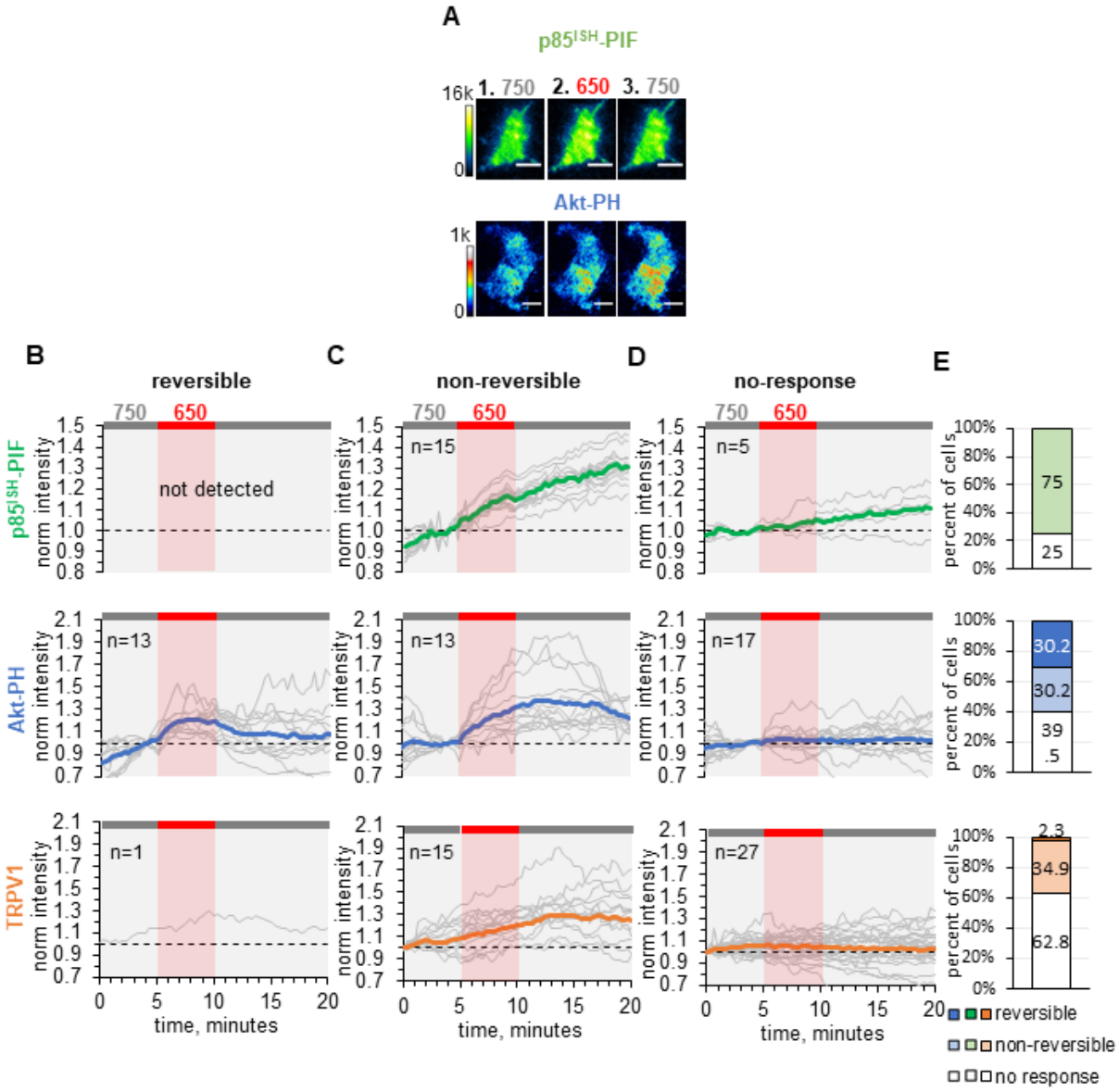

Fig. 4.9 TRPV1 retains PI3K at the PM of F-11 cells.

A) Representative TIRF fluorescence images of F-11 cells transfected with PhyB-mCherry-CAAX, p85^{ISH}-PIF-YFP, Akt-PH-CFP and TRPV1 before, during and after 650 nm illumination.

B-D) Collected traces from cells categorized by responses to 650 nm light illumination: reversible (B), non-reversible (C), no-response (D). Individual cell fluorescence in gray. Mean fluorescence in green for p85^{ISH}-PIF-YFP (top) and in blue for Akt-PH-CFP (middle) and in orange TRPV1 (bottom).

E) Percent of cells categorized by p85^{ISH}-PIF-YFP (top) and Akt-PH-CFP (middle) and TRPV1 (bottom) responses to 650 nm light illumination: reversible (dark color), non-reversible (light color), no-response (white)

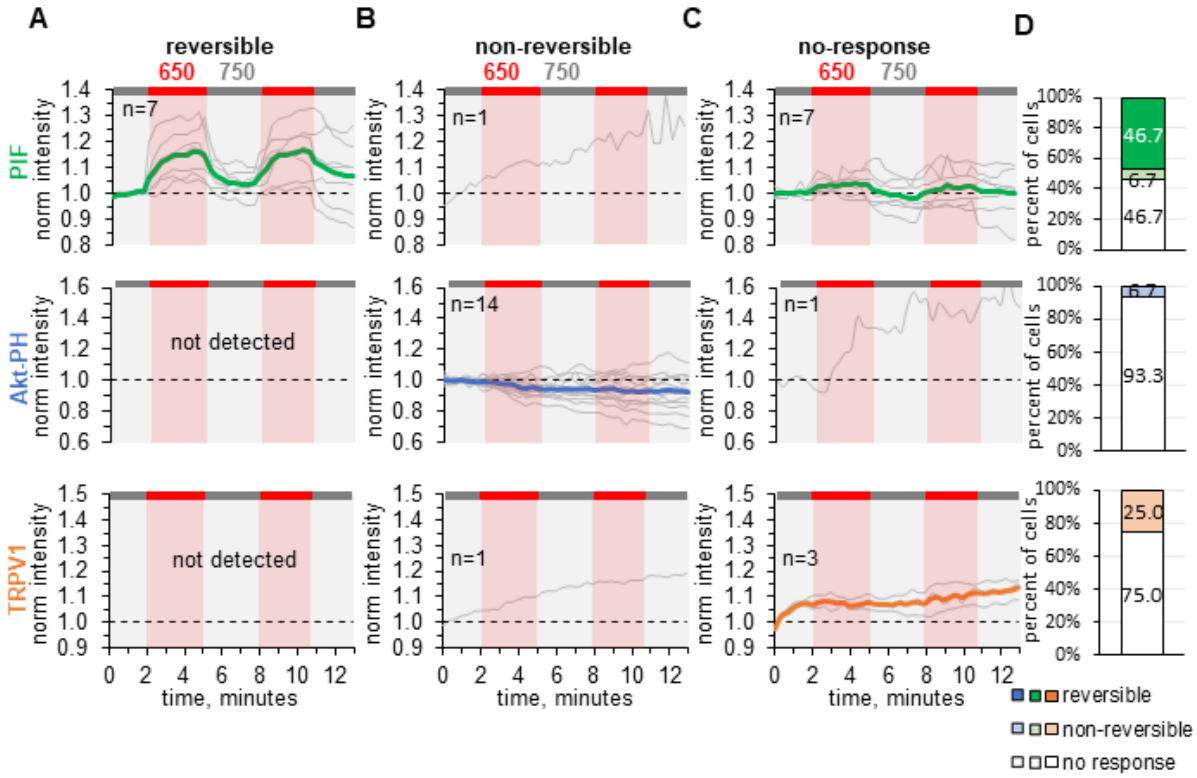

Fig. 4.10 TRPV1 does not retain PIF lacking p8ISH at the PM of F-11 cells.

Normalized TIRF fluorescence was recorded in F-11 cells transfected with PhyB-mCherry-CAAX, p85^{ISH}-PIF-YFP, Akt-PH-CFP and TRPV1 before, during and after 650 nm illumination.

A-C) Collected traces from cells categorized by responses to 650 nm light illumination: reversible (B), non-reversible (C), no-response (D). Individual cell fluorescence in gray. Mean fluorescence in green for p85^{ISH}-PIF-YFP (top) and in blue for Akt-PH-CFP (middle) and in orange TRPV1 (bottom).

D) Percent of cells categorized by p85^{ISH}-PIF-YFP (top) and Akt-PH-CFP (middle) and TRPV1 (bottom) responses to 650 nm light illumination: reversible (dark color), non-reversible (light color), no-response (white)

An alternative explanation for the effects of TRPV1 on retention of PI3K using opto-PI3K is the possibility of unspecific interaction between PIF and TRPV1. TRPV1 might interact with PIF independently of p85^{iSH}, which predicts that TRPV1 retains PIF without p85^{iSH}. To eliminate this possibility, we expressed full-length TRPV1 with PhyB-mCherry-CAAX and PIF-YFP which was not fused to p85^{iSH} domain of PI3K. Fig. 4.10 top panel shows that, PIF without p85^{iSH} was reversibly translocating in response to 650 nm in cells co-expressing full-length TRPV1. Furthermore, there was no Akt-PH translocation in response to 650 nm light illumination, suggesting that p85^{iSH} is required for activation of opto-PI3K. These findings eliminate the possibility of unspecific interaction between PIF and TRPV1.

Taken together, we show that TRPV1 retained p85^{iSH}-PIF at the plasma membrane through a specific TRPV1-PI3K interaction. It was previously reported that two SH2 domain regions of p85 subunit and the N-terminus of TRPV1 could be co-immunoprecipitated (Stein et al., 2006). Our data suggest a possibility that the minimum domain for TRPV1 and p85 interaction may be localized to the iSH domain of p85. Alternatively, the p110 subunit of PI3K may interact with TRPV1 directly, independent of p85. Currently, there is no evidence for or against a direct interaction between p110 and TRPV1. This possibility is very hard to address, because the p110 subunit of PI3K is unstable in solution when expressed recombinantly without the p85 subunit. Answering these questions will require further investigation using *in vitro* biochemical assays.

4.2.4 Activation of PI3K with light leads to trafficking of TRPV1 to the plasma membrane

PI3K activation is required for TRPV1 trafficking to the PM during inflammation (Bonnington and McNaughton, 2003, Stratiievska et al., 2018). We studied the effect of a light controlled PIP_3 generation on TRPV1 trafficking. We recorded TRPV1 fluorescence in F-11 cells and activated PI3K using opto-PI3K (Fig. 4.9 B-D, bottom). There was a large population of cells (34.9%, Fig. 4.9 C and E, bottom) that exhibited TRPV1 trafficking in response to 650 nm light. In addition, in control experiments when we co-transfected TRPV1 with PIF lacking p85^{iSH}, there was no trafficking of TRPV1 to the PM Fig. 4.10 bottom. These findings suggest that activation of PI3K with light was sufficient to stimulate TRPV1 trafficking to the plasma membrane and did not require other signaling cascades activated by the NGF receptor TrkA.

4.2.5 Soluble TRPV1-ARD fragment was sufficient to retain opto-PI3K

We have previously reported that a cytosolic portion of the TRPV1 protein corresponding to the ARD (TRPV1-ARD) was sufficient to potentiate NGF-induced PI3K activity (Stratiievska et al., 2018). We proposed two possible mechanisms for TRPV1 potentiation of PI3K Fig. 4.11. First, since TRPV1 is a transmembrane protein and PI3K is activated by recruitment to the PM, we hypothesized that TRPV1 potentiated PI3K by localizing it to the PM. The second possibility was that interaction between PI3K and the N-terminus of TRPV1 allosterically increased enzymatic activity of PI3K. We addressed the second

possibility in Chapter 3 (Stratiievska et al., 2018) Our results showing soluble portion of TRPV1-ARD supported both possibilities. Our findings showing TRPV1 retention of opto-PI3K at the PM are the first direct evidence for the first mechanism of potentiation through membrane localization.

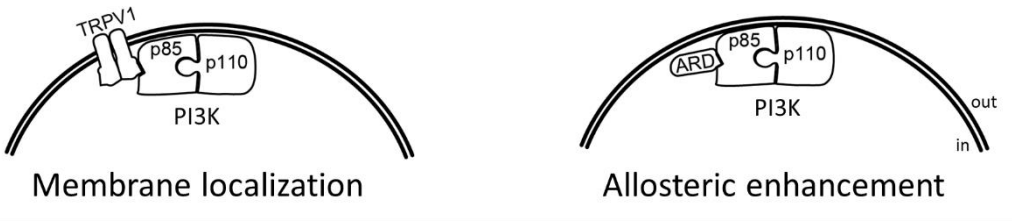

Fig. 4.11 Cartoon representation of two possible mechanisms of PI3K potentiation by TRPV1. Membrane localization suggests that TRPV1 retains PI3K at the PM through physical localization. Physical interaction with TRPV1-ARD may lead to allosteric enhancement of PI3K activity.

In order to directly test the second mechanism, TRPV1 potentiation of PI3K through allosteric enhancement, we used a more direct approach. We studied effects of soluble TRPV1-ARD on opto-PI3K activation with light. We hypothesized that opto-PI3K activation would be enhanced and/or prolonged in the presence of soluble TRPV1-ARD. We co-expressed soluble TRPV1-ARD fused to mCerulean1 and $p85^{iSH}$-PIF fused to YFP in NIH3t3 cells stably expressing PhyB-Cherry-CAAX. We recorded $p85^{iSH}$-PIF and TRPV1-ARD fluorescence simultaneously (Fig. 4.12, top and bottom respectively) every 20 seconds while illuminating the entire coverslip of cells with 750 nm or 650 nm light. Unlike full-length TRPV1, in a small population of cells (Fig. 4.12 D, top; ~4-fold smaller population compared to control, Fig. 4.8), there was an increase in $p85^{iSH}$-PIF fluorescence in response to 650 nm which was reversible with de-activating 750 nm light illumination (Fig. 4.12 A, top). But the majority of cells were either non-reversible or not responsive upon 650 nm light illumination (Fig. 4.12 D, top). These finding indicate, that the soluble TRPV1-ARD fragment increased membrane localization of the PI3K in the majority of cells. Unfortunately, these findings do not distinguish opto-PI3K membrane localization from activity. We aim to investigate opto-PI3K activation in presence of TRPV1-ARD in the near future.

Interestingly, TIRF fluorescence of the soluble TRPV1-ARD was increased with 650 nm light illumination in 40% of the cells (Fig. 4.12 D, bottom). There are two possible explanations for increased TRPV1-ARD membrane localization. First, since TRPV1-ARD interacts with PI3K, soluble TRPV1-ARD

may be brought to the membrane along with the PhyB-PIF complex in a light-induced manner. This predicts that there would be a sizable population of cells exhibiting reversible translocation of TRPV1-ARD upon 650 nm light illumination. We did not observe a population of cells which exhibited reversible translocation of TRPV1-ARD to the PM with light (Fig. 4.12 A, bottom). Therefore, a more likely second scenario suggests that, similarly to full-length TRPV1, opto-PI3K activation induced trafficking of the TRPV1-ARD to the plasma membrane.

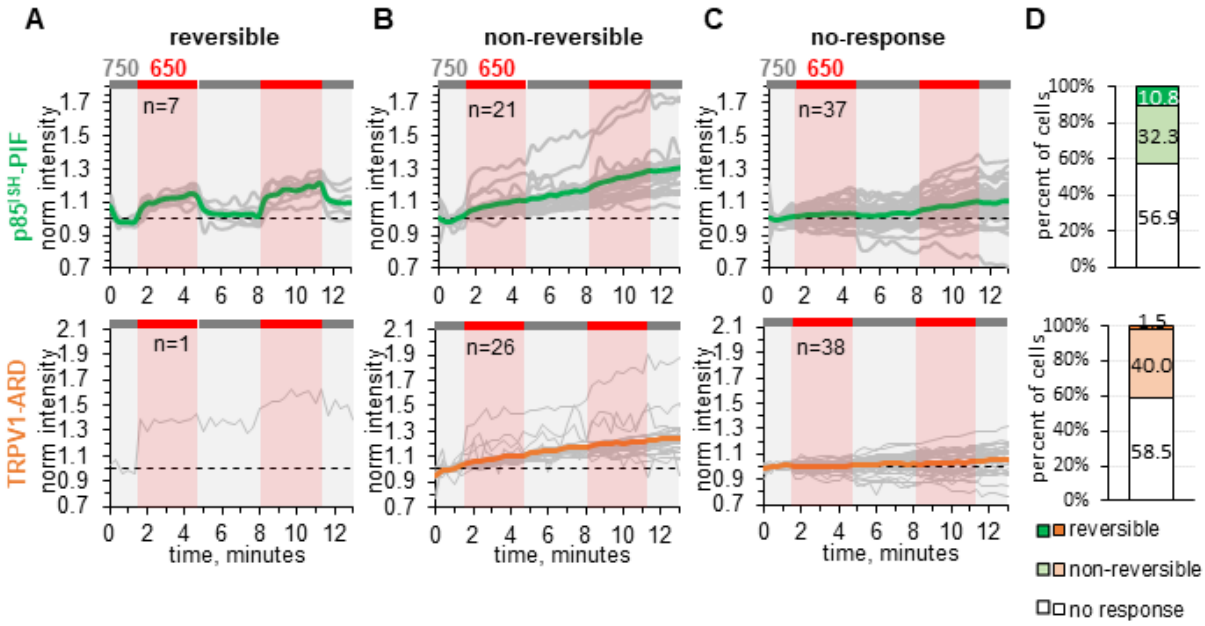

Fig. 4.12 Soluble TRPV1-ARD fragment was sufficient to retain opoto-PI3K

Normalized TIRF fluorescence was recorded in F-11 cells transfected with PhyB-mCherry-CAAX, p85ISH-PIF-YFP and TRPV1-ARD-mCerulean before, during and after 650 nm illumination.

A-C) Collected traces from cells categorized by responses to 650 nm light illumination: reversible (A), non-reversible (B), no-response (C). Individual cell fluorescence in gray. Mean fluorescence in green for p85ISH-PIF-YFP (top) and in orange for TRPV1-ARD (bottom).

D) Percent of cells categorized by p85ISH-PIF-YFP (top) and TRPV1-ARD (bottom) responses to 650 nm light illumination: reversible (dark color), non-reversible (light color), no-response (white)

4.2.6 TRPV2 channels retain PI3K at the PM

TRPV family channels contain a highly conserved Ankyrin repeats domain (ARD) and exhibit very similar structures, recently resolved by CryoEM (Fig. 1.5) (Gao et al., 2016, Shigematsu et al., 2010, Huynh et al., 2016a, Huynh et al., 2016b). We sought to investigate effects of other TRP channels containing ARD on PI3K activation with light. TRPV2 is the closest by similarity to TRPV1 (V'yacheslav Lehen'kyi, 2016). First, we co-expressed components of the opto-PI3K system with TRPV2 (rat) fused to YFP. We observed that in a large population (28%, Fig. 4.13 D, top) of cells with 650 nmillumination TRPV2 sustained Akt-PH levels after initial increase in PIP_3 levels (Fig. 4.13 B, top). A small population of cells exhibited reversible activation of PI3K upon 650 nmillumination, although it was ~10-fold smaller compared to control cells without TRPV2 (Fig. 4.8). This indicated that TRPV2 had similar effect on opto-PI3K activity to TRPV1.

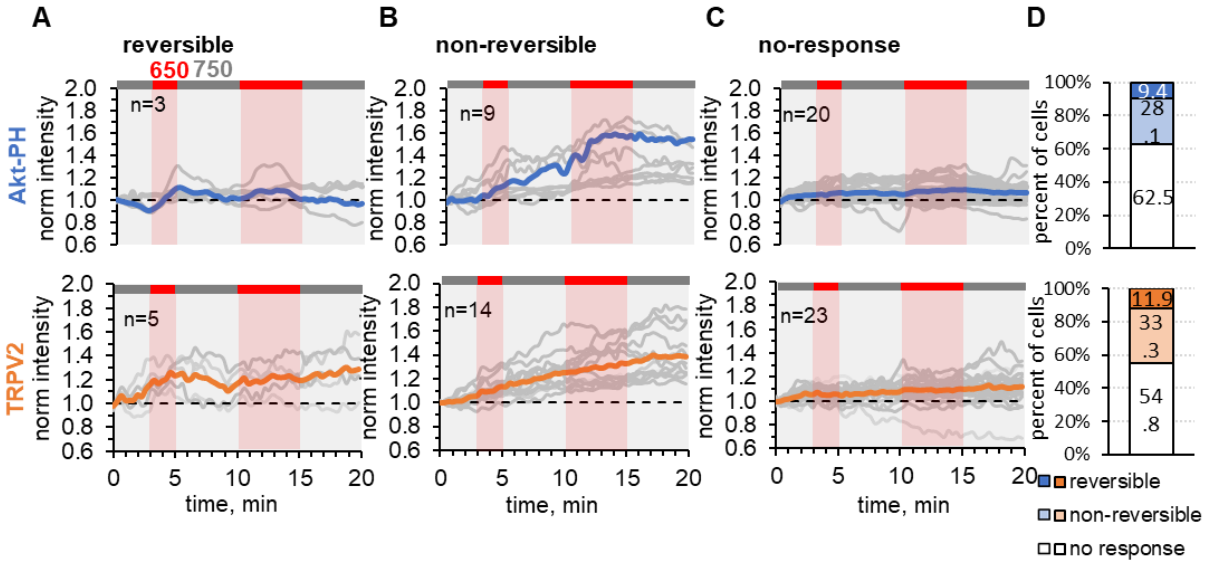

Fig. 4.13 TRPV2 retains PI3K at the PM of F-11 cells.

Normalized TIRF fluorescence was recorded in F-11 cells transfected with PhyB-mCherry-CAAX, $p85^{ISH}$-PIF-FLAG, Akt-PH-CFP and TRPV2-YFP before, during and after 650 nm illumination.

A-C) Collected traces from cells categorized by responses to 650 nm light illumination: reversible (A), non-reversible (B), no-response (C). Individual cell fluorescence in gray. Mean fluorescence in blue for Akt-PH-CFP (top) and in orange TRPV2 (bottom).

D) Percent of cells categorized by Akt-PH-CFP (top) and TRPV2 (bottom) responses to 650 nm light illumination: reversible (dark color), non-reversible (light color), no-response (white)

Along, with previously reported findings of potentiation of NGF-induced PI3K activity by TRPV2 (Stratiievska et al., 2018), this suggests a common mechanism for TRPV1 and TRPV2 for reciprocal regulation of PI3K.

In addition, a large number of cells exhibited increase in TRPV2 fluorescence in response to 650 nm light illumination (Fig. 4.13 A and B). These data suggests that, similarly to TRPV1, PI3K activation with light was sufficient to stimulate trafficking to the PM.

4.2.7 TRPV4 channels do not retain PI3K at the PM

In order to test if effects of retention of PI3K by TRPV1 would extend to another ARD-containing TRPV channel TRPV4, we co-expressed TRPV4 (human) fused to EGFP with components of opto-PI3K system. We observed that there was a significant population of cells exhibiting reversible translocation of both p85^{iSH}-PIF and Akt-PH to the PM (Fig. 4.14). In TRPV4-expressing cells there was a ~2-fold decrease

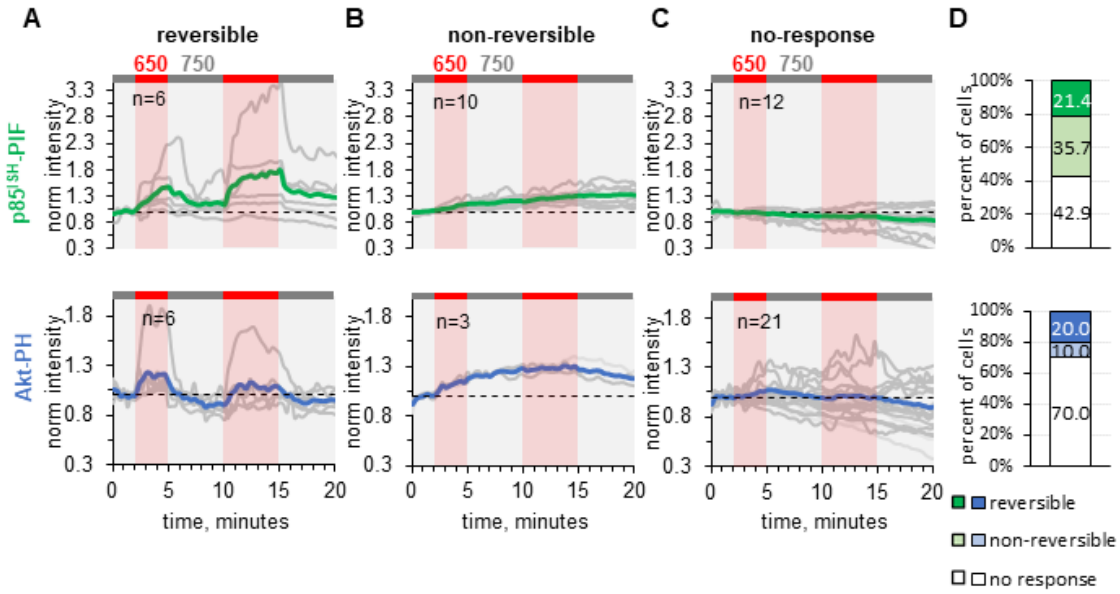

Fig. 4.14 TRPV4 does not retain PI3K at the PM of F-11 cells.

Normalized TIRF fluorescence was recorded in F-11 cells transfected with PhyB-mCherry-CAAX, p85^{ISH}-PIF-FLAG, Akt-PH-CFP and TRPV4-EGFP before, during and after 650 nm illumination.

A-C) Collected traces from cells categorized by responses to 650 nm light illumination: reversible (A), non-reversible (B), no-response (C). Individual cell fluorescence in gray. Mean fluorescence in green for p85^{ISH}-PIF-YFP (top) and in blue for Akt-PH-CFP (bottom).

D) Percent of cells categorized by p85^{ISH}-PIF-YFP (top) and Akt-PH-CFP (bottom) responses to 650 nm light illumination: reversible (dark color), non-reversible (light color), no-response (white)

in the reversible population. These findings indicate that TRPV4 expression did not lead to PI3K retention at the PM, at least not to the extent of full-length TRPV1. We previously reported that TRPV4 similarly to TRPV1 and TRPV2 potentiated NGF-induced PI3K activity. Our findings raise an interesting question: does

TRPV4 lead to potentiation of PI3K activity through a different mechanism, which does not involve PI3K retention and sustaining activity? Alternatively, this points to the potential differences between the interaction of TRPV1 and TRPV4 ARDs with PI3K. One possibility is that TRPV4 may exhibit a lower apparent affinity towards PI3K. Further studies to address these questions are needed.

4.2.8 TRPV6 channels do not retain PI3K at the PM

In order to test if effects of retention of PI3K by TRPV1 would extend to TRPV6, we co-expressed

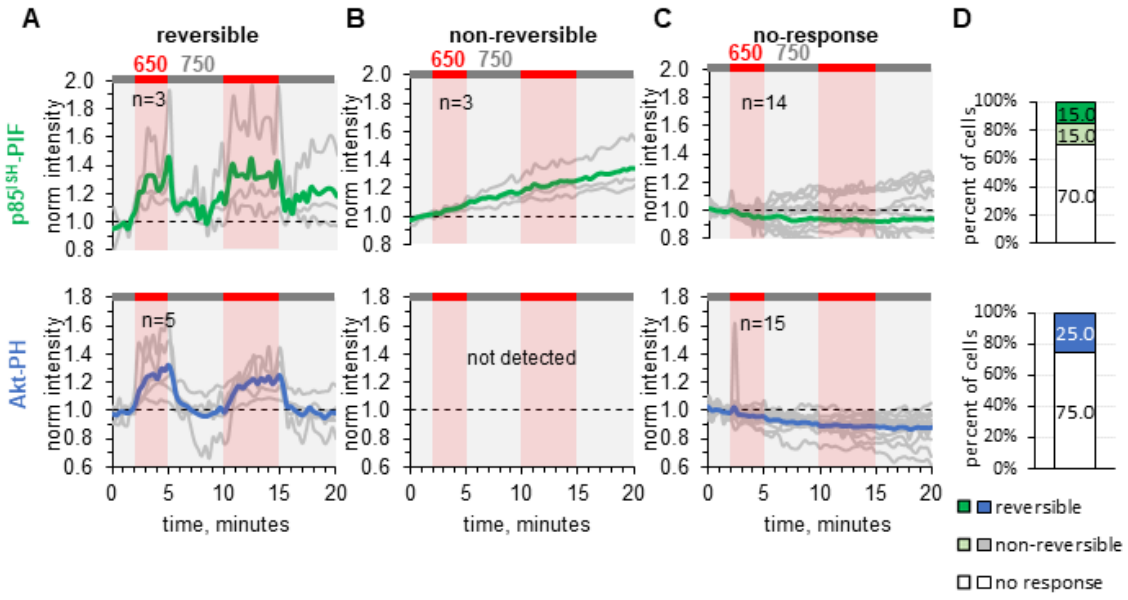

Fig. 4.15 TRPV6 do not retain PI3K at the PM of F-11 cells.

Normalized TIRF fluorescence was recorded in F-11 cells transfected with PhyB-mCherry-CAAX, p85^{iSH}-PIF-FLAG, Akt-PH-CFP and TRPV6-EGFP before, during and after 650 nm illumination.

A-C) Collected traces from cells categorized by responses to 650 nm light illumination: reversible (A), non-reversible (B), no-response (C). Individual cell fluorescence in gray. Mean fluorescence in green for p85^{iSH}-PIF-YFP (top) and in blue for Akt-PH-CFP (bottom).

D) Percent of cells categorized by p85^{iSH}-PIF-YFP (top) and Akt-PH-CFP (bottom) responses to 650 nm light illumination: reversible (dark color), non-reversible (light color), no-response (white)

TRPV6 (human) fused to EGFP with components of opto-PI3K system. In the majority of cells expressing TRPV6 we did not observe marked translocation of both p85^{iSH}-PIF and Akt-PH to the PM (70% and 75% respectively) (Fig. 4.15). A small population of cells exhibited reversible translocation of both p85^{iSH}-PIF

and Akt-PH (15% and 25% respectively, compared to 46.2 and 85.7% in control cells without TRPV6) (Fig. 4.15). These findings suggest that TRPV6 drastically decreased the reversibility of opto-PI3K, but unlike TRPV1, did not retain PI3K at the PM.

4.2.9 TRPA1 channels retain PI3K at the PM and inhibit PI3K

Next we investigated if effects of retention of PI3K would extend to another ARD-containing TRP channel TRPA1. The CryoEM structure of TRPA1 differs from those of TRPV family by an ARD orientation perpendicular to the PM as well as a number of ARD repeats (>16 of TRPA1 vs. 6 of TRPV1. Fig. 1.5).

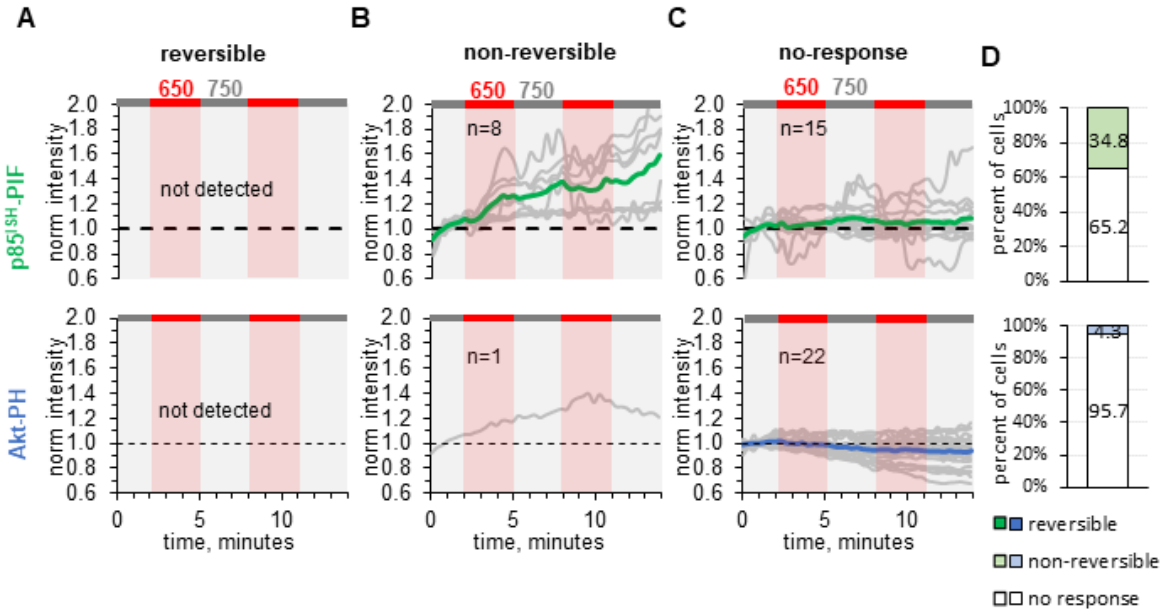

Fig. 4.16 TRPA1 retain at the PM and inhibit PI3K.

Normalized TIRF fluorescence was recorded in F-11 cells transfected with PhyB-mCherry-CAAX, p85ISH-PIF-FLAG, Akt-PH-CFP and TRPA1-EGFP before, during and after 650 nm illumination.

A-C) Collected traces from cells categorized by responses to 650 nm light illumination: reversible (A), non-reversible (B), no-response (C). Individual cell fluorescence in gray. Mean fluorescence in green for p85ISH-PIF-YFP (top) and in blue for Akt-PH-CFP (bottom).

D) Percent of cells categorized by p85ISH-PIF-YFP (top) and Akt-PH-CFP (bottom) responses to 650 nm light illumination: reversible (dark color), non-reversible (light color), no-response (white)

We co-expressed TRPA1 (zebrafish) fused to EGFP with components of the opto-PI3K system. We observed that TRPA1 retained PI3K at the PM but did not show profound sustaining of opto-PI3K activity at the PM (Fig. 4.16). This indicates that TRPA1 prevented opto-PI3K activation. One possibility is that the TRPA1-ARD interacts with PI3K but inhibits its activation. Further studies to address this possibility are

needed. This may have interesting physiological consequences, because TRPA1 and TRPV1 are co-expressed in a subset of sensory DRG neurons.

4.2.10 TRPM4 channels do not retain PI3K at the PM

It had been believed that all channels of TRPM family do not contain ARD. Unexpectedly, recent TRPM4 Cryo-EM structure revealed two ankyrin-like domains in the N-terminus, that were not predicted because of a poor sequence similarity with other ARDs (Winkler et al., 2017). We sought to investigate the effects of TRPM4 on opto-PI3K activity at the plasma membrane. Fig. 4.17 A top shows that in the majority of cells expressing TRPM4 (50%) there was clear reversible translocation of $p85^{iSH}$-PIF to the PM in response to 650 nm light. In addition, a substantial population of cells (30.6%) exhibited reversible translocation of Akt-PH to the PM in response to 650 nm light (Fig. 4.17 A, middle). These data suggest that TRPM4 does not retain PI3K at the PM and does not interfere with opto-PI3K activity. This is interesting because in Chapter 3, we observed that TRPM4 potentiated NGF-induced PI3K activity. Taken together, TRPM4 may affect NGF-induced PI3K activity in a different manner, without affecting PI3K translocation.

Interestingly, we observed a light-induced increase in TRPM4 fluorescence in a large population of cells (Fig. 4.17 D, bottom). This indicated that activation of opto-PI3K leads to trafficking of TRPM4 channels to the PM. This finding does not align with our observation from Chapter 3 that there was no NGF-induced TRPM4 trafficking to the PM. One possible explanation for this is that activation of opto-PI3K leads to substantially higher levels of PIP_3 that were sufficient to stimulate TRPM4 trafficking to the extent at which we were able to detect it. Further investigation using different strength of opto-PI3K activation is required to definitively address this phenomenon.

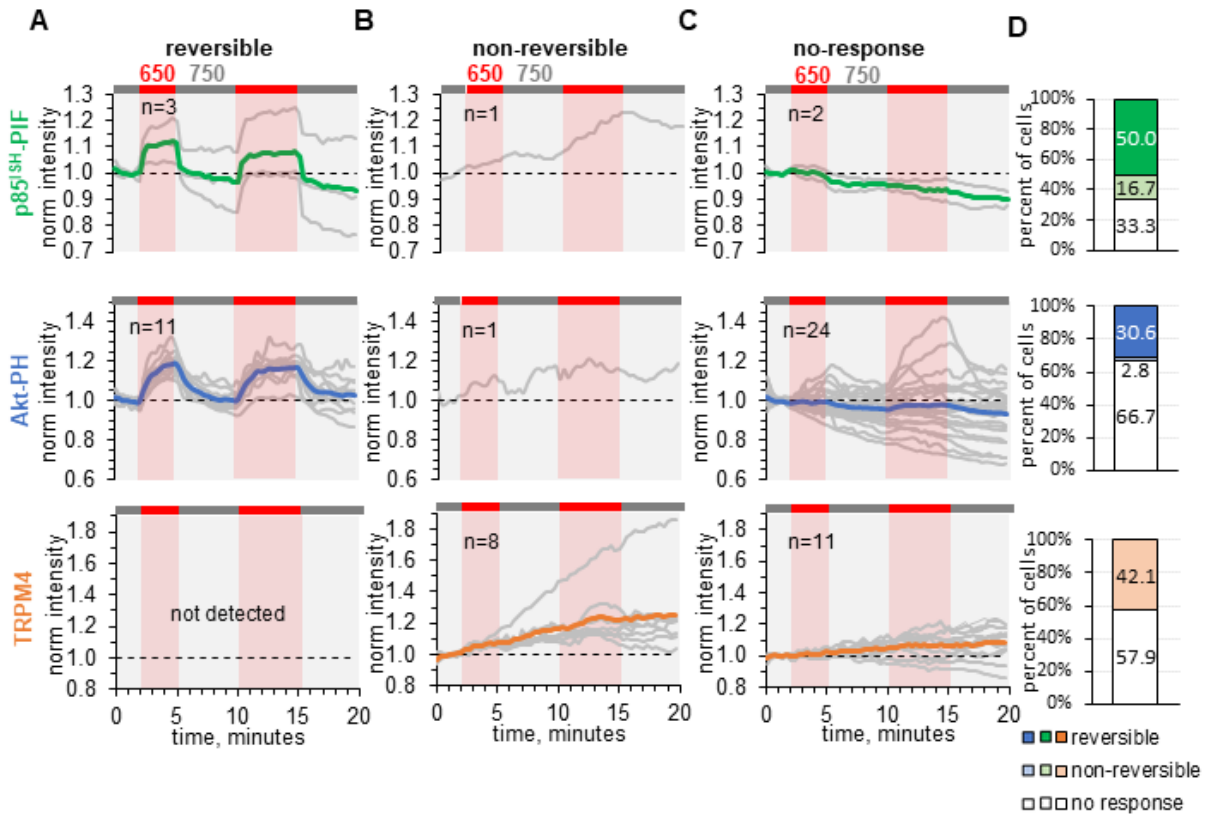

Fig. 4.17 TRPM4 channels do not retain PI3K at the PM of F-11 cells.

Normalized TIRF fluorescence was recorded in F-11 cells transfected with PhyB-mCherry-CAAX, p85ISH-PIF, Akt-PH and TRPM4 before, during and after 650 nm illumination.

A-C) Collected traces from cells categorized by responses to 650 nm light illumination: reversible (B), non-reversible (C), no-response (D). Individual cell fluorescence in gray. Mean fluorescence in green for p85ISH-PIF-YFP (top) and in blue for Akt-PH-CFP (middle) and in orange TRPM4 (bottom).

D) Percent of cells categorized by p85ISH-PIF-YFP (top) and Akt-PH-CFP (middle) and TRPM4 (bottom) responses to 650 nm light illumination: reversible (dark color), non-reversible (light color), no-response (white)

4.2.11 TRPM8 channels do not retain PI3K at the PM

We aimed to investigate the effects of a channel completely lacking the ARD on opto-PI3K activity. TRPM8 channels do not contain an ARD as seen from a recent Cryo-EM structure (Yin et al., 2017). Therefore, we co-expressed TPRM8 (mouse) fused to GFP with the components of opto-PI3K. As shown in Fig. 4.18 A, a large population of cells showed reversible translocation of both p85^{iSH}-PIF and AKt-PH in response to 650 nm light. In fact, the distribution between reversible, non-reversible and non-responsive populations in both p85^{iSH}-PIF and Akt-PH was similar to the control cells lacking any TRP channel. These findings indicate that expression of a TRP channel lacking the ARD does not retain PI3K at the membrane and does not interfere with PI3K activation.

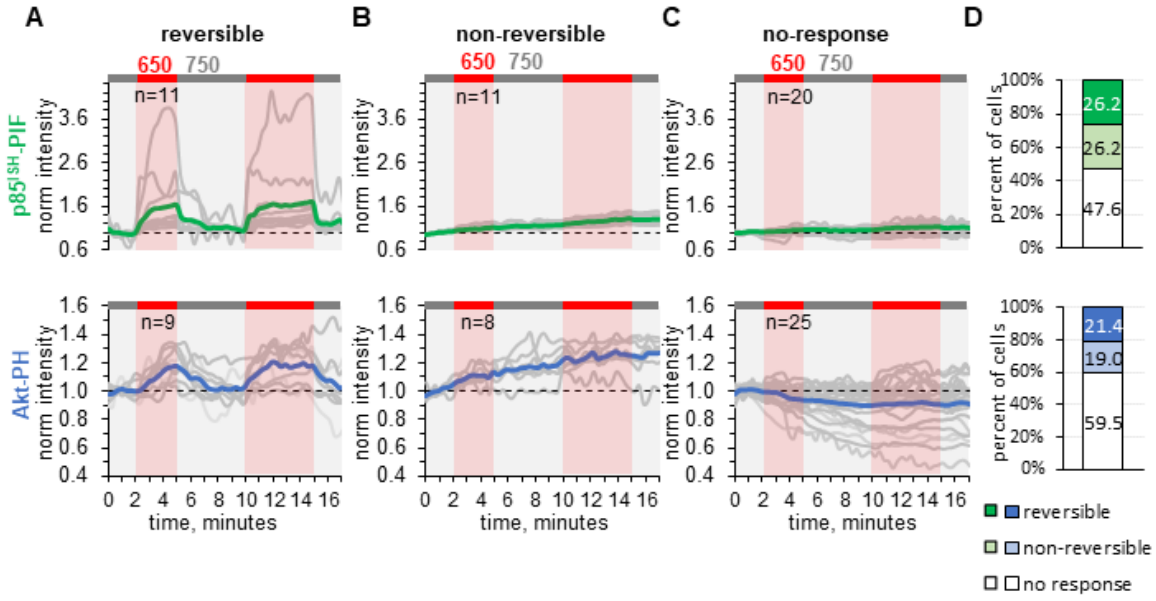

Fig. 4.18 TRPM8 channels do not retain PI3K at the PM

Normalized TIRF fluorescence was recorded in F-11 cells transfected with PhyB-mCherry-CAAX, p85ISH-PIF-FLAG, Akt-PH-CFP and TRPV6-EGFP before, during and after 650 nm illumination.

A-C) Collected traces from cells categorized by responses to 650 nm light illumination: reversible (A), non-reversible (B), no-response (C). Individual cell fluorescence in gray. Mean fluorescence in green for p85ISH-PIF-YFP (top) and in blue for Akt-PH-CFP (bottom).

D) Percent of cells categorized by p85ISH-PIF-YFP (top) and Akt-PH-CFP (bottom) responses to 650 nm light illumination: reversible (dark color), non-reversible (light color), no-response (white)

4.2.12 Calcium imaging in NIH cells shows 650 nm-induced potentiation of Ca^{2+} responses

Next, we asked if the opto-PI3K system can be used to mimic NGF-treatment to achieve sensitization of TRPV1 responses to capsaicin. We and others have previously demonstrated that TRPV1 responses to capsaicin are sensitized upon treatment with NGF by using calcium imaging of DRG neurons ((Zhu and Oxford, 2007, Bonnington and McNaughton, 2003) and Chapter 3). Furthermore, we have identified that in order to observe robust sensitization after NGF-treatment, cells needed to be repetitively exposed to capsaicin which leads to desensitization of TRPV1 responses (see Chapter 3). We aimed to apply similar protocol for TRPV1 desensitization with repetitive capsaicin application and activate opto-PI3K with light to mimic NGF-induced PI3K activation. In addition to PI3K, NGF activation of TrkA leads to activation of PLC and hydrolysis of PIP_2. This mechanism is thought to underlie Ca^{2+} -dependent desensitization of TRPV1 by decreasing the PIP_2 which is required for TRPV1 activation. Conversely, PIP_2 is a substrate used by PI3K to generate PIP_3. Therefore, simultaneous activation of PLC and PI3K may result in lower levels of PIP_3 at the PM. Using opto-PI3K approach allows for isolating the PI3K pathway from other downstream signaling pathways such as PLC.

In order to mimic NGF-induced PI3K activation from PLC, we activated opto-PI3K with light. We used NIH3T3 cells stably expressing all components for opto-PI3K system (PhyB-mCherry-CAAX, $p85^{iSH}$-PIF-YFP and Akt-PH-CFP) and transfected them with TRPV1. The cells were prepared as described above in section 3. Briefly, cells were transfected with TRPV1 24hrs prior to recording, loaded with Fluo4-AM for 30min and then with PCB and for additional 1 hr in the dark @37C. We utilized the same protocol used in calcium imaging of DRG neurons described in section 3 with modifications to accommodate for control of opto-PI3K activation (Fig. 4.21). Fig. 4.19 A shows control cells that were illuminated with 750 nm light for the duration of experiment. 650 nm light was never turned on. As quantified in Fig. 4.19 B, there was no significant difference between the amplitudes of the 4^{th}, 5^{th} and 6^{th} capsaicin responses (n=22, ns indicates lack of significance of Wilcoxon rank test $p>0.05$). Next, we illuminated the cells with 650 nm light between 5^{th} and 6^{th} capsaicin applications to mimic NGF-induced PI3K activation. Fig. 4.19 C shows an increase in capsaicin response after the cells were illuminated with 650 nm light. Only cells with desensitization of

TRPV1 responses were included in the analysis shown in Fig. 4.19 D (n=164, asterisks indicate significance levels of Wilcoxon rank test (*** - p< 0.001, ** - p<0.005, * - p<0.05)). The purple in Fig. 4.19 C trace represents a cell that exhibited potentiation at 6th application. These data suggest that in NIH3T3 cells activation of opto-PI3K produced TRPV1 sensitization. In conclusion, activation of PI3K with light was sufficient to mimic NGF-induced TRPV1 sensitization.

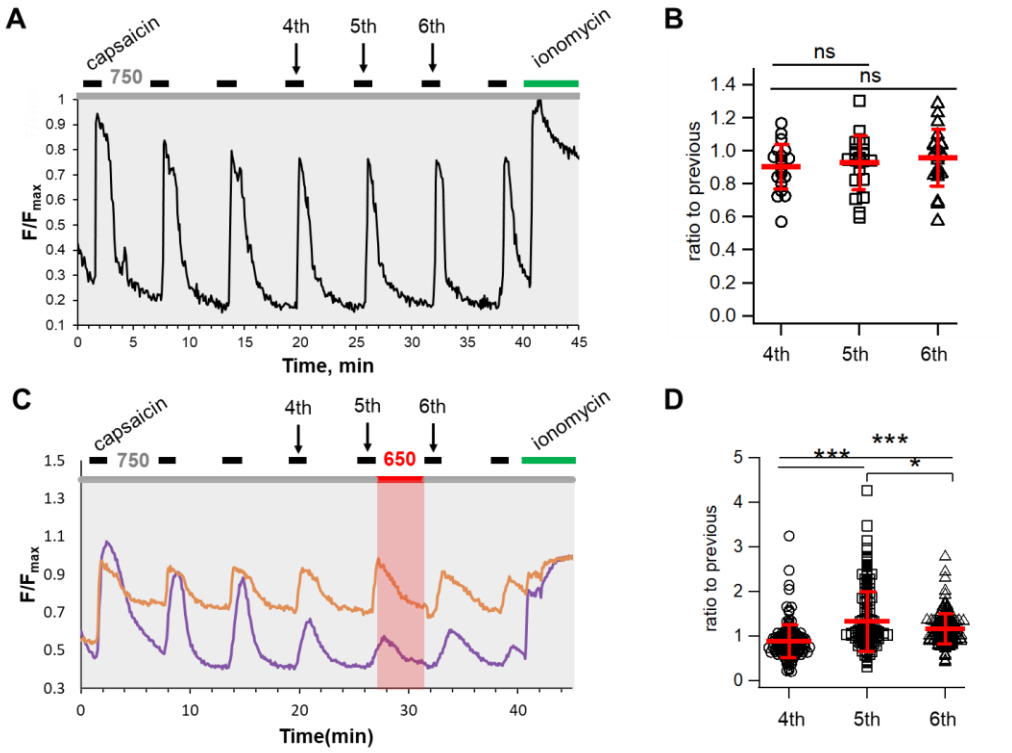

Fig. 4.19 Calcium imaging recording in NIH 3T3 cells stably expressing components of opto-PI3K system. Fluo4 fluorescence intensity normalized to Fmax. during ionomycin (10uM). Capsaicin (100nm) was applied repetitively with continuous 750nm illumination.

A) Fluo4 fluorescence of a representative control cell which was never illuminated with 650nm light in response to capsaicin.

B) Scatterplot showing capsaicin response amplitudes in response to 4th, 5th and 6th applications normalized to immediately preceding application (n=22, ns indicates lack of significance of Wilcoxon rank test p>0.05)

C) Fluo4 fluorescence of two representative cells illuminated with 650nm light between 5th and 6th applications of capsaicin. The purple trace represents a cell that exhibited potentiation at 6th application. The orange trace represents a cell that was potentiated at 5th application

*D) Scatterplot showing capsaicin response amplitudes in response to 4th, 5th and 6th applications normalized to immediately preceding application (n=164). Asterisks indicate significance levels of Wilcoxon rank test (*** - p< 0.001, ** - p<0.005, * - p<0.05)*

Interestingly, some cells exhibited potentiation at the 5th capsaicin application that also co-inided with the start of 650 nm ilumination. The orange trace in Fig. 4.19 C represents a cell that was potentiated at 5th application. This phenomenon may be due to potentiation by the newly synthesized PIP_3 of the TRPV1 channels that were previously desensitized.

4.3 Discussion

Here we established a troubleshooting strategy for the opto-PI3K system. It allowed us to implement opto-PI3K in transiently transfected neuronal F-11 cells. We observed robust and quickly reversible activation of PI3K with light using dual-color TIRF microscopy.

We show that, when co-expressed with opto-PI3K, full-length TRPV1 retains PI3K at the PM in response to the 650 nm light illumination. As shown in Fig. 4.20, initially under 750 nm illumination opto-PI3K is localized to cytoplasm and inactive. Upon the exposure to 650 nm light, opto-PI3K is activated by membrane localization because of the interaction between the PhyB and p85^{iSH}-PIF. Since TRPV1 is embedded into the membrane, opto-PI3K may interact with TRPV1 once activated with light. Upon the second illumination with 750 nm light, PhyB and p85^{iSH}-PIF interaction is eliminated but opto-PI3K is retained at the membrane by the interaction with the TRPV1. This leads to prolonged activity of opto-PI3K and sustained levels of PIP_3.

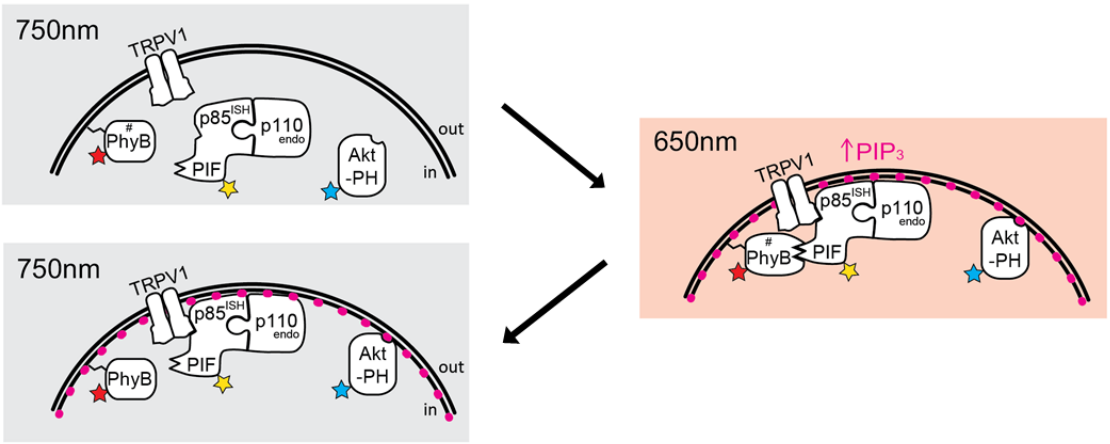

Fig. 4.20 Cartoon representation of our understanding for TRPV1 retention of PI3K at the PM. TRPV1 retains the PI3K dimer at the PM through physical interaction via ARD. This leads to increased and sustained PIP3 levels at the PM after opto-PI3K activation with light.

Earlier we demonstrated a reciprocal regulation between TRPV1 and PI3K upon application of NGF (Stratiievska et al., 2018), when TRPV1 increased PI3K activity and PI3K activation increased number of TRPV1 channels at the PM. Our findings of PI3K retention at the membrane by the TRPV1 indicate that reciprocal regulation of NGF-induced PI3K activity by TRPV1 involves PM localization of PI3K (Fig. 4.20). Prolonged activity of PI3K in presence of TRPV1 leads to an accumulation of higher levels of PIP_3. This supports the involvement of the second proposed mechanism for potentiation of PI3K by TRPV1 – membrane localization (Fig. 3.19).

Next, we show for the first time that a soluble TRPV1-ARD fragment leads to a prolonged membrane localization of PI3K. Taken together with our findings that soluble TRPV1-ARD was sufficient to potentiate NGF-induced PI3K activity, this provides the first direct evidence for an allosteric enhancement that contributes to PI3K potentiation by TRPV1. To summarize, we suggest a combination of two mechanisms for TRPV1 potentiation of PI3K – membrane localization and allosteric enhancement.

In addition, for the first time, we show that direct activation of PI3K with light leads to trafficking of TRPV1 to the PM. Two lines of evidence support this: calcium imaging of capsaicin-induced TRPV1 responses and direct measurements of TRPV1 fluorescence. To date it was shown that PI3K was necessary for TRPV1-induced TRPV1 sensitization, but no studies addressed if PI3K activation was sufficient. Our findings indicate that activation of PI3K is sufficient for TRPV1 trafficking during inflammation.

Finally, we tested multiple ARD-containing TRP channels and the non-ARD channel TRPM8 using opto-PI3K. We observed that TRPV2, TRPV4, TRPV6, TRPM4 and TRPM8 channels did not retain PI3K at the PM, at least not to the extent of TRPV1. We previously reported that TRPV2 and TRPV4 potentiated NGF-induced PI3K activity but to a lower extent (Stratiievska et al., 2018). Taken together, our findings suggest that other ARD-containing TRP channels may have less profound effect on PI3K. One possibility is that despite being highly conserved, ARDs of other TRP channels have lower affinity to PI3K or exhibit less pronounced allosteric enhancement of PI3K activity. These hypotheses require future evaluation by more direct methods such as *in vitro* kinase assay.

Interestingly, ARD-containing TRPA1 channels completely suppressed PI3K activation with light. We previously showed that although TRPA1 did not significantly potentiate NGF-induced PI3K activity, NGF

did induce TRPA1 trafficking to the PM. We hypothesize, that TRPA1 may exhibit differential effects on PI3K which result in an activation of PI3K sufficient for induced trafficking. Further investigation of the TRPA1 – PI3K interaction are required in order to establish effects of TRPA1 on PI3K activity.

The biggest limitation of our approach is the intrinsic heterogeneity of the transient transfection. This leads to different populations of cells with regard to the reversibility of opto-PI3K activation which have different balance between components of opto-PI3K. This makes it challenging to interpret changes in population distributions. This may be addressed by generation of stable cell lines.

4.4 Future directions

The next questions to be addressed are related to the biochemistry of the TRPV1-PI3K interaction site. What is the affinity of this interaction *in vitro*? For example, this could be measured by Surface Plasmon resonance (SPR) using purified recombinant proteins.

Experiments in Chapters 3 and 4 do not rule out the possibility of multiple interaction sites between PI3K subunits and TRPV1. Direct evidence exists for interaction between recombinant p85 SH2 domains and TRPV1. But, does TRPV1 have direct interaction site with p110 subunit of PI3K? This question may be addressed using a Hydrogen-Deuterium exchange technique or high-resolution cross-linking.

What are the effects of TRPV1-PI3K interaction on *in vitro* PI3K kinase activity? This may be addressed by classical *in vitro* kinase assays, but more elegant approach is the one applied by Falke lab (Ziemba et al., 2012). *In vitro* kinase assay which involves single molecule imaging for detection of both single molecule interactions with TRPV1 and PI3K activity at the same.

In the long-term, polypeptides may be designed to compete off the interaction between TRPV1 and PI3K. These may be useful as local agents applied to the site of inflammation to perturb the reciprocal regulation among TRPV1 and PI3K but preserve normal functioning of each protein.

4.5 Methods

4.5.1 Cell culture /transfection/ DNA constructs/ solutions

F-11 cells (a gift from M.C. Fishman, Massachusetts General Hospital, Boston, MA; (Francel et al., 1987)) were cultured at 37°C, 5% CO_2 in Ham's F-12 Nutrient Mixture (#11765-054; Gibco) supplemented with 20% fetal bovine serum (#26140-079; Gibco, Grand Island, NY), HAT supplement (100 µM sodium hypoxanthine, 400 nM aminopterin, 16 µM thymidine; #21060-017; Gibco), and penicillin/streptomycin (#17-602E, Lonza, Switzerland). F-11 cells tested negative for mycoplasma contamination using Universal Mycoplasma Detection Kit (# ATCC 30-1012K, ATCC, Manassas, VA). NIH/3T3 w/PhyB-Cherry-CAAX cells (a gift from Orion Weiner, UCSF, CA (Toettcher et al., 2011)) were cultured at 37°C, 5% CO_2 in DMEM (#11995-065; Gibco) supplemented with 10% bovine calf serum (#SH30073.03 ; Hyclone), L-Glutamine (#25030-081 and penicillin/streptomycin (#17-602E, Lonza, Switzerland).

Cells for imaging experiments were plated on Poly-Lysine (#P1274, Sigma, St. Louis, MO) coated 0.15 mm x 25 mm coverslips (#64-0715 (CS-25R15), Warner Instruments, Hamden, CT) in a 6-well plate. Cells were transfected with Lipofectamine 2000 (4ul/well, Invitrogen, Grand Island, NY) reagent using 1-3 ug of cDNA per well. Cells were taken in experiment 24 hrs post-transfection. During experiments, cells were perfused with HEPES-buffered saline (HBR, double deionized water and in mM: 140 NaCl, 4 KCl, 1 $MgCl_2$, 1.8 $CaCl_2$, 10 HEPES (free acid) and 5 glucose) As described previously by (Levskaya et al., 2009), cells were loaded with PCB in culture medium at (10 µM) for at least 1 hrprior experiment in the dark. To avoid photodamage, PCB was handled in the dark room with green safety flashlight.

TRPV1-cYFP (rat) (Ufret-Vincenty et al., 2015), TRPV1-ARD-ctagRFP (rat), TRPV2-cYFP (rat) (Mercado et al., 2010) DNA constructs were made in the pcDNA3 vector (Invitrogen), where "-n" or "-c" indicates that the fluorescent protein is on the N- or C-terminus, respectively. TRPV4-EGFP (human) in pEGFP was obtained from Tim D. Plant (Charite-Universitatsmedizine, Berlin) (Strotmann et al., 2003). hTRPV6-nYFP was obtained from Tibor Rohacs (Rutgers, The State University of New Jersey, Newark, NJ). TrkA (rat) in the pcCMV5 vector and $p75_{NTR}$ (rat) in the pcDNA3 vector were obtained from Mark Bothwell (University of Washington, Seattle). PH-Akt-cCerulean in the pcDNA3-k vector was made based

on the construct in the pHR vector from the Weiner Lab (Toettcher et al., 2011). The function of the ion channels tested was confirmed using Ca^{2+} imaging and/or patch clamp electrophysiology.

4.5.2 TIRF imaging for opto-PI3K

The total internal fluorescence (TIRF) imaging set up was as described previously (Stratiievska et al., 2018) with several modifications for the opto-PI3K system. We used an inverted microscope (NIKON Ti-E) equipped for total internal fluorescence (TIRF) imaging with a 60x objective (NA 1.49). Glass coverslips with adherent cells were placed in a custom-made chamber. The chamber volume (~1 ml) was exchanged using a gravity-driven perfusion system. Cells were acclimated to flow for at least 5 min prior to the start of an experiment. For activating / deactivating opto-PI3K with light we used HQ630/20 X (42490) and HQ760/40 X (226723) excitation filters inserted in the overhead condenser filter slider. The whole experimental chamber was illuminated with activating or deactivating light using the maximum intensity (12V) of the condenser lamp. Akt-PH fused to Cyan Fluorescent Protein (CFP) was imaged using excitation

Fig. 4.21 Microscope set up for TIRF imaging and opto-PI3K.

We used inverted TIRF microscope with several modifications for simultaneous IR illumination and imaging (Fig.9). For manipulation of opto-PI3K, overhead illumination (red arrows) is used from a white lamp light source which was turned on to maximum 12V at all times. A bandpass filter for 650nm or 750nm illumination is inserted into overhead lamp filter slider. Filter slider is manually moved to switch between 750nm or 650nm filter positions. The fluorescent proteins in the sample are excited using a laser light source from the bottom (green arrows).

from a 447 nm laser and a 480/40 emission filter. Yellow Fluorescent Protein (YFP) fusion proteins were imaged using the 488 nm line of an argon laser and a 525/50 emission filter.

Time-lapse images were obtained by taking consecutive CFP and YFP images every 20 seconds. Movies were then processed using ImageJ software (NIH) (Rasband, 1997-2016). Regions of interest (ROI) were drawn around the footprint of individual cells and the average ROI pixel intensity was measured. Measurements were analyzed using Excel 2013 (Microsoft Corporation), by subtracting the background ROI intensity from the intensity of each cell ROI. Traces were normalized by the average intensity during 1 min time period prior to activating light application.

Note, that PhyB loaded with PCB is extremely sensitive to light (ref to light sensitivity spectra), light of any wavelength between ~450-650 nmwill turn activate PhyB once PCB is added. This means, that experiments should never be carried out in the absence of 750 nmde-activating light, because even the light from the computer monitor is sufficient to activate PhyB-PIF interaction.

References:

AHMED, S., XIE, J., HORNE, D. & WILLIAMS, J. C. 2014. Photocleavable dimerizer for the rapid reversal of molecular trap antagonists. *J Biol Chem,* 289**,** 4546-52.

AIKAWA, R., NAWANO, M., GU, Y., KATAGIRI, H., ASANO, T., ZHU, W., NAGAI, R. & KOMURO, I. 2000. Insulin prevents cardiomyocytes from oxidative stress-induced apoptosis through activation of PI3 kinase/Akt. *Circulation,* 102**,** 2873-9.

ALESSANDRI-HABER, N., DINA, O. A., JOSEPH, E. K., REICHLING, D. & LEVINE, J. D. 2006. A transient receptor potential vanilloid 4-dependent mechanism of hyperalgesia is engaged by concerted action of inflammatory mediators. *J Neurosci,* 26**,** 3864-74.

ALESSI, D. R., JAMES, S. R., DOWNES, C. P., HOLMES, A. B., GAFFNEY, P. R., REESE, C. B. & COHEN, P. 1997. Characterization of a 3-phosphoinositide-dependent protein kinase which phosphorylates and activates protein kinase Balpha. *Curr Biol,* 7**,** 261-9.

ALEXANDER SPH, M. A., PETERS JA 2011. Ion Channels. *Br J Pharmacol,* 164**,** S137-74.

AMBROSE, E. J. 1961. The movements of fibrocytes. *Exp Cell Res,* Suppl 8**,** 54-73.

AUGER, K. R., CARPENTER, C. L., CANTLEY, L. C. & VARTICOVSKI, L. 1989. Phosphatidylinositol 3-kinase and its novel product, phosphatidylinositol 3-phosphate, are present in Saccharomyces cerevisiae. *J Biol Chem,* 264**,** 20181-4.

AXELROD, D. 1981. Cell-substrate contacts illuminated by total internal reflection fluorescence. *J Cell Biol.*

BAI, J. & PAGANO, R. E. 1997. Measurement of spontaneous transfer and transbilayer movement of BODIPY-labeled lipids in lipid vesicles. *Biochemistry,* 36**,** 8840-8.

BARDE, Y. A., EDGAR, D. & THOENEN, H. 1980. Sensory neurons in culture: changing requirements for survival factors during embryonic development. *Proc Natl Acad Sci U S A,* 77**,** 1199-203.

BAUTISTA, D. M., JORDT, S. E., NIKAI, T., TSURUDA, P. R., READ, A. J., POBLETE, J., YAMOAH, E. N., BASBAUM, A. I. & JULIUS, D. 2006. TRPA1 mediates the inflammatory actions of environmental irritants and proalgesic agents. *Cell,* 124**,** 1269-82.

BEVAN, S. & YEATS, J. 1991. Protons activate a cation conductance in a sub-population of rat dorsal root ganglion neurones. *J Physiol,* 433**,** 145-61.

BEVERS, E. M. & WILLIAMSON, P. L. 2010. Phospholipid scramblase: an update. *FEBS Lett,* 584**,** 2724-30.

BHAVE, G., HU, H.-J., GLAUNER, K. S., ZHU, W., WANG, H., BRASIER, D. J., OXFORD, G. S. & IV, R. W. G. 2003. Protein kinase C phosphorylation sensitizes but does not activate the capsaicin receptor transient receptor potential vanilloid 1 (TRPV1).

BHAVE, G., ZHU, W., WANG, H., BRASIER, D. J., OXFORD, G. S. & GEREAU, R. W. T. 2002. cAMP-dependent protein kinase regulates desensitization of the capsaicin receptor (VR1) by direct phosphorylation. *Neuron,* 35**,** 721-31.

BONNINGTON, J. K. & MCNAUGHTON, P. A. 2003. Signalling pathways involved in the sensitisation of mouse nociceptive neurones by nerve growth factor. *J Physiol,* 551**,** 433-46.

BUCKLES, T. C., ZIEMBA, B. P., MASSON, G. R., WILLIAMS, R. L. & FALKE, J. J. 2017. Single-Molecule Study Reveals How Receptor and Ras Synergistically Activate PI3Kα and PIP. *Biophys J,* 113**,** 2396-2405.

BURGERING, B. M. & COFFER, P. J. 1995. Protein kinase B (c-Akt) in phosphatidylinositol-3-OH kinase signal transduction. *Nature,* 376**,** 599-602.

BURKE, J. E. & WILLIAMS, R. L. 2015. Synergy in activating class I PI3Ks. *Trends Biochem Sci,* 40**,** 88-100.

BURNSTOCK, G. 1972. Purinergic nerves. *Pharmacol Rev,* 24**,** 509-81.

BURRISS GARRETT, R. J. & REDMAN, C. M. 1975. Localization of enzymes involved in polyphosphoinositids metabolism on the cytoplasmic surface of the human erythrocyte membrane. *Biochim Biophys Acta,* 382**,** 58-64.

CAMPRUBI-ROBLES, M., PLANELLS-CASES, R. & FERRER-MONTIEL, A. 2009. Differential contribution of SNARE-dependent exocytosis to inflammatory potentiation of TRPV1 in nociceptors. *Faseb j,* 23**,** 3722-33.

CANTLEY, L. C. 2002. The phosphoinositide 3-kinase pathway. *Science,* 296**,** 1655-7.

CAO, E., CORDERO-MORALES, J. F., LIU, B., QIN, F. & JULIUS, D. 2013a. TRPV1 channels are intrinsically heat sensitive and negatively regulated by phosphoinositide lipids. *Neuron,* 77**,** 667-79.

CAO, E., LIAO, M., CHENG, Y. & JULIUS, D. 2013b. TRPV1 structures in distinct conformations reveal activation mechanisms. *Nature,* 504**,** 113-8.

CARSON, J. D., VAN ALLER, G., LEHR, R., SINNAMON, R. H., KIRKPATRICK, R. B., AUGER, K. R., DHANAK, D., COPELAND, R. A., GONTAREK, R. R., TUMMINO, P. J. & LUO, L. 2008. Effects of oncogenic p110alpha subunit mutations on the lipid kinase activity of phosphoinositide 3-kinase. *Biochem J,* 409**,** 519-24.

CATERINA, M. J., LEFFLER, A., MALMBERG, A. B., MARTIN, W. J., TRAFTON, J., PETERSEN-ZEITZ, K. R., KOLTZENBURG, M., BASBAUM, A. I. & JULIUS, D. 2000a. Impaired nociception and pain sensation in mice lacking the capsaicin receptor. *Science,* 288**,** 306-13.

CATERINA, M. J., LEFFLER, A., MALMBERG, A. B., MARTIN, W. J., TRAFTON, J., PETERSEN-ZEITZ, K. R., KOLTZENBURG, M., BASBAUM, A. I. & JULIUS, D. 2000b. Impaired nociception and pain sensation in mice lacking the capsaicin receptor. *Science,* 288**,** 306-13.

CATERINA, M. J., ROSEN, T. A., TOMINAGA, M., BRAKE, A. J. & JULIUS, D. 1999. A capsaicin-receptor homologue with a high threshold for noxious heat. *Nature,* 398**,** 436-41.

CATERINA, M. J., SCHUMACHER, M. A., TOMINAGA, M., ROSEN, T. A., LEVINE, J. D. & JULIUS, D. 1997. The capsaicin receptor: a heat-activated ion channel in the pain pathway. *Nature,* 389**,** 816-24.

CENAC, N., ALTIER, C., MOTTA, J. P., D'ALDEBERT, E., GALEANO, S., ZAMPONI, G. W. & VERGNOLLE, N. 2010. Potentiation of TRPV4 signalling by histamine and serotonin: an important mechanism for visceral hypersensitivity. *Gut,* 59**,** 481-8.

CESARE, P. & MCNAUGHTON, P. 1996. A novel heat-activated current in nociceptive neurons and its sensitization by bradykinin. *Proc Natl Acad Sci U S A,* 93**,** 15435-9.

CHAO, M. V. 2003. Neurotrophins and their receptors: A convergence point for many signalling pathways. *Nature Reviews Neuroscience,* 4**,** 299-309.

CHEN, D., GIBSON, E. S. & KENNEDY, M. J. 2013. A light-triggered protein secretion system. *J Cell Biol,* 201**,** 631-40.

CHENG, H., JIANG, X. & HAN, X. 2007. Alterations in lipid homeostasis of mouse dorsal root ganglia induced by apolipoprotein E deficiency: a shotgun lipidomics study. *J Neurochem,* 101**,** 57-76.

CHEUNG, L. W., WALKIEWICZ, K. W., BESONG, T. M., GUO, H., HAWKE, D. H., AROLD, S. T. & MILLS, G. B. 2015. Regulation of the PI3K pathway through a p85alpha monomer-homodimer equilibrium. *Elife,* 4**,** e06866.

CHUANG, H. H., PRESCOTT, E. D., KONG, H., SHIELDS, S., JORDT, S. E., BASBAUM, A. I., CHAO, M. V. & JULIUS, D. 2001. Bradykinin and nerve growth factor release the capsaicin receptor from PtdIns(4,5)P2-mediated inhibition. *Nature,* 411**,** 957-62.

CLACKSON, T., YANG, W., ROZAMUS, L. W., HATADA, M., AMARA, J. F., ROLLINS, C. T., STEVENSON, L. F., MAGARI, S. R., WOOD, S. A., COURAGE, N. L., LU, X., CERASOLI, F., JR., GILMAN, M. & HOLT, D. A. 1998. Redesigning an FKBP-ligand interface to generate chemical dimerizers with novel specificity. *Proc Natl Acad Sci U S A,* 95**,** 10437-42.

CLAPHAM, D. E. 1995. Calcium signaling. *Cell,* 80**,** 259-68.

CLAUSEN, M. V., HILBERS, F. & POULSEN, H. 2017. The Structure and Function of the Na,K-ATPase Isoforms in Health and Disease. *Front Physiol,* 8.

COLLINS, M. D. & GORDON, S. E. 2013a. Giant liposome preparation for imaging and patch-clamp electrophysiology. *J Vis Exp*.

COLLINS, M. D. & GORDON, S. E. 2013b. Short-chain phosphoinositide partitioning into plasma membrane models. *Biophys J,* 105**,** 2485-94.

CUNNINGHAM, M. E., STEPHENS, R. M., KAPLAN, D. R. & GREENE, L. A. 1997. Autophosphorylation of activation loop tyrosines regulates signaling by the TRK nerve growth factor receptor. *J Biol Chem,* 272**,** 10957-67.

D, D. & NICOL, J. A. C. 1955. Luminescence in Hydromedusae.

DAHIM, M., MIZUNO, N. K., LI, X. M., MOMSEN, W. E., MOMSEN, M. M. & BROCKMAN, H. L. 2002. Physical and photophysical characterization of a BODIPY phosphatidylcholine as a membrane probe. *Biophys J,* 83**,** 1511-24.

DAVIS, J. B., GRAY, J., GUNTHORPE, M. J., HATCHER, J. P., DAVEY, P. T., OVEREND, P., HARRIES, M. H., LATCHAM, J., CLAPHAM, C., ATKINSON, K., HUGHES, S. A., RANCE, K., GRAU, E., HARPER, A. J., PUGH, P. L., ROGERS, D. C., BINGHAM, S., RANDALL, A. & SHEARDOWN, S. A. 2000. Vanilloid receptor-1 is essential for inflammatory thermal hyperalgesia. *Nature,* 405**,** 183-7.

DENG, Z., PAKNEJAD, N., MAKSAEV, G., SALA-RABANAL, M., NICHOLS, C. G., HITE, R. K. & YUAN, P. 2018. Cryo-EM and X-ray structures of TRPV4 reveal insight into ion permeation and gating mechanisms. *Nat Struct Mol Biol,* 25**,** 252-260.

DEVAUX, P. F. 1992. Protein involvement in transmembrane lipid asymmetry. *Annu Rev Biophys Biomol Struct,* 21**,** 417-39.

DICKENSON, A. H. & SULLIVAN, A. F. 1987. Subcutaneous formalin-induced activity of dorsal horn neurones in the rat: differential response to an intrathecal opiate administered pre or post formalin. *Pain,* 30**,** 349-60.

DIKIC, I., BATZER, A. G., BLAIKIE, P., OBERMEIER, A., ULLRICH, A., SCHLESSINGER, J. & MARGOLIS, B. 1995. Shc binding to nerve growth factor receptor is mediated by the phosphotyrosine interaction domain. *J Biol Chem,* 270**,** 15125-9.

DOCHERTY, R. J., YEATS, J. C., BEVAN, S. & BODDEKE, H. W. 1996. Inhibition of calcineurin inhibits the desensitization of capsaicin-evoked currents in cultured dorsal root ganglion neurones from adult rats. *Pflugers Arch,* 431**,** 828-37.

DONNERER, J., SCHULIGOI, R. & STEIN, C. 1992. Increased content and transport of substance P and calcitonin gene-related peptide in sensory nerves innervating inflamed tissue: evidence for a regulatory function of nerve growth factor in vivo. *Neuroscience,* 49**,** 693-8.

DOWNES, P. & MICHELL, R. H. 1982. Phosphatidylinositol 4-phosphate and phosphatidylinositol 4,5-bisphosphate: lipids in search of a function. *Cell Calcium,* 3**,** 467-502.

DU, X., HAO, H., GIGOUT, S., HUANG, D., YANG, Y., LI, L., WANG, C., SUNDT, D., JAFFE, D. B., ZHANG, H. & GAMPER, N. 2014. Control of somatic membrane potential in nociceptive neurons and its implications for peripheral nociceptive transmission. *Pain.*

EHLERS, M. D., KAPLAN, D. R., PRICE, D. L. & KOLIATSOS, V. E. 1995. NGF-stimulated retrograde transport of trkA in the mammalian nervous system. *J Cell Biol,* 130**,** 149-56.

EMBL-EBI, I. 2019. Proteins matched: Ankyrin repeat (IPR002110) filtered by species.

ERLER, I., HIRNET, D., WISSENBACH, U., FLOCKERZI, V. & NIEMEYER, B. A. 2004. Ca2+-selective transient receptor potential V channel architecture and function require a specific ankyrin repeat. *J Biol Chem,* 279**,** 34456-63.

ESCOBEDO, J. A., NAVANKASATTUSAS, S., KAVANAUGH, W. M., MILFAY, D., FRIED, V. A. & WILLIAMS, L. T. 1991. cDNA cloning of a novel 85 kd protein that has SH2 domains and regulates binding of PI3-kinase to the PDGF beta-receptor. *Cell,* 65**,** 75-82.

FENG, S., LAKETA, V., STEIN, F., RUTKOWSKA, A., MACNAMARA, A., DEPNER, S., KLINGMULLER, U., SAEZ-RODRIGUEZ, J. & SCHULTZ, C. 2014. A rapidly reversible chemical dimerizer system to study lipid signaling in living cells. *Angew Chem Int Ed Engl,* 53**,** 6720-3.

FERRANDIZ-HUERTAS, C., MATHIVANAN, S., WOLF, C. J., DEVESA, I. & FERRER-MONTIEL, A. 2014. Trafficking of ThermoTRP Channels. *Membranes (Basel).*

FRANCEL, P. C., MILLER, R. J. & DAWSON, G. 1987. Modulation of bradykinin-induced inositol trisphosphate release in a novel neuroblastoma x dorsal root ganglion sensory neuron cell line (F-11). *J Neurochem,* 48**,** 1632-9.

FRECH, M., ANDJELKOVIC, M., INGLEY, E., REDDY, K. K., FALCK, J. R. & HEMMINGS, B. A. 1997. High affinity binding of inositol phosphates and phosphoinositides to the pleckstrin homology domain of RAC/protein kinase B and their influence on kinase activity. *J Biol Chem,* 272**,** 8474-81.

GABELLI, S. B., ECHEVERRIA, I., ALEXANDER, M., DUONG-LY, K. C., CHAVES-MOREIRA, D., BROWER, E. T., VOGELSTEIN, B. & AMZEL, L. M. 2014. Activation of PI3Kα by physiological effectors and by oncogenic mutations: structural and dynamic effects. *Biophys Rev,* 6**,** 89-95.

GAO, Y., CAO, E., JULIUS, D. & CHENG, Y. 2016. TRPV1 structures in nanodiscs reveal mechanisms of ligand and lipid action. *Nature,* 534**,** 347-351.

GASCARD, P., SULPICE, J. C., TRAN, D., SAUVAGE, M., CLARET, M., ZACHOWSKI, A., DEVAUX, P. F. & GIRAUD, F. 1993. Trans-bilayer distribution of phosphatidylinositol 4,5-bisphosphate and its role in the changes of lipid asymmetry in the human erythrocyte membrane. *Biochem Soc Trans,* 21**,** 253-7.

GASCARD, P., TRAN, D., SAUVAGE, M., SULPICE, J. C., FUKAMI, K., TAKENAWA, T., CLARET, M. & GIRAUD, F. 1991. Asymmetric distribution of phosphoinositides and phosphatidic acid in the human erythrocyte membrane. *Biochim Biophys Acta,* 1069**,** 27-36.

GAUDET, R. 2008. A primer on ankyrin repeat function in TRP channels and beyond. *Mol Biosyst,* 4**,** 372-9.

GEERING, B., CUTILLAS, P. R., NOCK, G., GHARBI, S. I. & VANHAESEBROECK, B. 2007. Class IA phosphoinositide 3-kinases are obligate p85-p110 heterodimers. *Proc Natl Acad Sci U S A,* 104**,** 7809-14.

GONZALEZ, I. F., MERCADO, J. L., UFRET-VINCENTY, C. A. & GORDON, S. E. 2012. Bradykinin Sensitization of TRPV1 Channels. *Biophysical Journal,* 102**,** 341a.

GORDON-SHAAG, A., ZAGOTTA, W. N. & GORDON, S. E. 2008. Mechanism of Ca(2+)-dependent desensitization in TRP channels. *Channels (Austin),* 2**,** 125-9.

GOSWAMI, C. 2012. TRPV1-tubulin complex: involvement of membrane tubulin in the regulation of chemotherapy-induced peripheral neuropathy. *J Neurochem,* 123**,** 1-13.

GOSWAMI, C., HUCHO, T. B. & HUCHO, F. 2007. Identification and characterisation of novel tubulin-binding motifs located within the C-terminus of TRPV1. *J Neurochem,* 101**,** 250-62.

GRIMES, M. L., ZHOU, J., BEATTIE, E. C., YUEN, E. C., HALL, D. E., VALLETTA, J. S., TOPP, K. S., LAVAIL, J. H., BUNNETT, N. W. & MOBLEY, W. C. 1996. Endocytosis of activated TrkA: evidence that nerve growth factor induces formation of signaling endosomes. *J Neurosci,* 16**,** 7950-64.

GU, Q., KWONG, K. & LEE, L. Y. 2003. Ca2+ transient evoked by chemical stimulation is enhanced by PGE2 in vagal sensory neurons: role of cAMP/PKA signaling pathway. *J Neurophysiol,* 89**,** 1985-93.

HAMILL, O. P., MARTY, A., NEHER, E., SAKMANN, B. & SIGWORTH, F. J. 1981. Improved patch-clamp techniques for high-resolution current recording from cells and cell-free membrane patches. *Pflugers Arch,* 391**,** 85-100.

HAMILTON, S. G., WADE, A. & MCMAHON, S. B. 1999. The effects of inflammation and inflammatory mediators on nociceptive behaviour induced by ATP analogues in the rat. *Br J Pharmacol.*

HASAN, R., LEESON-PAYNE, A. T. S., JAGGAR, J. H. & ZHANG, X. 2017. Calmodulin is responsible for Ca2+-dependent regulation of TRPA1 Channels. *Sci Rep.*

HAUGH, J. M., CODAZZI, F., TERUEL, M. & MEYER, T. 2000. Spatial sensing in fibroblasts mediated by 3' phosphoinositides. *J Cell Biol,* 151**,** 1269-80.

HAWKINS, P. T., ANDERSON, K. E., DAVIDSON, K. & STEPHENS, L. R. 2006. Signalling through Class I PI3Ks in mammalian cells. *Biochem Soc Trans,* 34**,** 647-62.

HAWKINS, P. T. & STEPHENS, L. R. 2016. Emerging evidence of signalling roles for PI(3,4)P2 in Class I and II PI3K-regulated pathways. *Biochem Soc Trans,* 44**,** 307-14.

HILES, I. D., OTSU, M., VOLINIA, S., FRY, M. J., GOUT, I., DHAND, R., PANAYOTOU, G., RUIZ-LARREA, F., THOMPSON, A., TOTTY, N. F. & ET AL. 1992. Phosphatidylinositol 3-kinase: structure and expression of the 110 kd catalytic subunit. *Cell,* 70**,** 419-29.

HODGKIN, A. L. & HUXLEY, A. F. 1952a. A quantitative description of membrane current and its application to conduction and excitation in nerve. *J Physiol,* 117**,** 500-44.

HODGKIN, A. L. & HUXLEY, A. F. 1952b. The components of membrane conductance in the giant axon of Loligo. *J Physiol,* 116**,** 473-96.

HODGKIN, A. L. & HUXLEY, A. F. 1952c. The dual effect of membrane potential on sodium conductance in the giant axon of Loligo. *J Physiol,* 116**,** 497-506.

HODGKIN, A. L., HUXLEY, A. F. & KATZ, B. 1952. Measurement of current-voltage relations in the membrane of the giant axon of Loligo. *J Physiol,* 116**,** 424-48.

HUANG, S. & CZECH, M. P. 2007. The GLUT4 glucose transporter. *Cell Metab,* 5**,** 237-52.

HUGHES, R. M., BOLGER, S., TAPADIA, H. & TUCKER, C. L. 2012. Light-mediated control of DNA transcription in yeast. *Methods,* 58**,** 385-91.

HUYNH, K. W., COHEN, M. R., JIANG, J., SAMANTA, A., LODOWSKI, D. T., ZHOU, Z. H. & MOISEENKOVA-BELL, V. Y. 2016a. Structure of the full-length TRPV2 channel by cryo-EM. *Nat Commun,* 7**,** 11130.

HUYNH, K. W., COHEN, M. R., JIANG, J., SAMANTA, A., LODOWSKI, D. T., ZHOU, Z. H. & MOISEENKOVA-BELL, V. Y. 2016b. Structure of the full-length TRPV2 channel by cryo-EM. *Nature Communications, Published online: 29 March 2016;* | *doi:10.1038/ncomms11130*.

IDEVALL-HAGREN, O., DICKSON, E. J., HILLE, B., TOOMRE, D. K. & DE CAMILLI, P. 2012. Optogenetic control of phosphoinositide metabolism. *Proc Natl Acad Sci U S A,* 109**,** E2316-23.

INOUYE, S., NOGUCHI, M., SAKAKI, Y., TAKAGI, Y., MIYATA, T., IWANAGA, S. & TSUJI, F. I. 1985. Cloning and sequence analysis of cDNA for the luminescent protein aequorin. *Proc Natl Acad Sci U S A,* 82**,** 3154-8.

INSALL, R. H. & WEINER, O. D. 2001. PIP3, PIP2, and Cell Movement—Similar Messages, Different Meanings? *Dev Cell,* 1**,** 743.

IWATA, Y., KATANOSAKA, Y., ARAI, Y., KOMAMURA, K., MIYATAKE, K. & SHIGEKAWA, M. 2003. A novel mechanism of myocyte degeneration involving the Ca2+-permeable growth factor–regulated channel.

IWATA, Y., KATANOSAKA, Y., ARAI, Y., SHIGEKAWA, M. & WAKABAYASHI, S. 2009. Dominant-negative inhibition of Ca2+ influx via TRPV2 ameliorates muscular dystrophy in animal models. *Hum Mol Genet,* 18**,** 824-34.

JAMES, S. R., DOWNES, C. P., GIGG, R., GROVE, S. J., HOLMES, A. B. & ALESSI, D. R. 1996. Specific binding of the Akt-1 protein kinase to phosphatidylinositol 3,4,5-trisphosphate without subsequent activation. *Biochem J,* 315**,** 709-13.

JESKE, N. A., DIOGENES, A., RUPAREL, N. B., FEHRENBACHER, J. C., HENRY, M., AKOPIAN, A. N. & HARGREAVES, K. M. 2008. A-kinase anchoring protein mediates TRPV1 thermal hyperalgesia through PKA phosphorylation of TRPV1. *Pain,* 138**,** 604-16.

JI, R.-R., XU, Z.-Z. & GAO, Y.-J. 2014. Emerging targets in neuroinflammation-driven chronic pain. *Nature Reviews Drug Discovery,* 13**,** 533-548.

JI, R. R., SAMAD, T. A., JIN, S. X., SCHMOLL, R. & WOOLF, C. J. 2002. p38 MAPK activation by NGF in primary sensory neurons after inflammation increases TRPV1 levels and maintains heat hyperalgesia. *Neuron,* 36**,** 57-68.

JIE, P., HONG, Z., TIAN, Y., LI, Y., LIN, L., ZHOU, L., DU, Y. & CHEN, L. 2015. Activation of transient receptor potential vanilloid 4 induces apoptosis in hippocampus through downregulating PI3K/Akt and upregulating p38 MAPK signaling pathways. *Cell Death Dis,* 6**,** e1775.

JOHANNES, C. B., LE, T. K., ZHOU, X., JOHNSTON, J. A. & DWORKIN, R. H. 2010. The prevalence of chronic pain in United States adults: results of an Internet-based survey. *J Pain,* 11**,** 1230-9.

JOYAL, J. L., BURKS, D. J., PONS, S., MATTER, W. F., VLAHOS, C. J., WHITE, M. F. & SACKS, D. B. 1997. Calmodulin activates phosphatidylinositol 3-kinase. *J Biol Chem,* 272**,** 28183-6.

JUNG, J., HWANG, S. W., KWAK, J., LEE, S. Y., KANG, C. J., KIM, W. B., KIM, D. & OH, U. 1999. Capsaicin binds to the intracellular domain of the capsaicin-activated ion channel. *J Neurosci,* 19**,** 529-38.

KANZAKI, M., ZHANG*, Y.-Q., MASHIMA*, H., LI*, L., SHIBATA*, H. & KOJIMA, I. 1999. Translocation of a calcium-permeable cation channel induced by insulin-like growth factor-I. *Nature Cell Biology,* 1**,** 165-170.

KARASHIMA, Y., TALAVERA, K., EVERAERTS, W., JANSSENS, A., KWAN, K. Y., VENNEKENS, R., NILIUS, B. & VOETS, T. 2009. TRPA1 acts as a cold sensor in vitro and in vivo. *Proc Natl Acad Sci U S A,* 106**,** 1273-8.

KATANOSAKA, Y., IWASAKI, K., UJIHARA, Y., TAKATSU, S., NISHITSUJI, K., KANAGAWA, M., SUDO, A., TODA, T., KATANOSAKA, K., MOHRI, S. & NARUSE, K. 2014. TRPV2 is critical for the maintenance of cardiac structure and function in mice. *Nature Communications, Published online: 29 May 2014;* | *doi:10.1038/ncomms4932*.

KEH, S. M., FACER, P., SIMPSON, K. D., SANDHU, G., SALEH, H. A. & ANAND, P. 2008. Increased nerve fiber expression of sensory sodium channels Nav1.7, Nav1.8, And Nav1.9 in rhinitis. *Laryngoscope,* 118**,** 573-9.

KENNEDY, M. J., HUGHES, R. M., PETEYA, L. A., SCHWARTZ, J. W., EHLERS, M. D. & TUCKER, C. L. 2010. Rapid blue-light-mediated induction of protein interactions in living cells. *Nat Methods,* 7**,** 973-5.

KLEIN, R. M., UFRET-VINCENTY, C. A., HUA, L. & GORDON, S. E. 2008. Determinants of molecular specificity in phosphoinositide regulation. Phosphatidylinositol (4,5)-bisphosphate (PI(4,5)P2) is the endogenous lipid regulating TRPV1. *J Biol Chem,* 283**,** 26208-16.

KOHN, A. D., KOVACINA, K. S. & ROTH, R. A. 1995. Insulin stimulates the kinase activity of RAC-PK, a pleckstrin homology domain containing ser/thr kinase. *Embo j,* 14**,** 4288-95.

KOZIK, A., MOORE, R. B., POTEMPA, J., IMAMURA, T., RAPALA-KOZIK, M. & TRAVIS, J. 1998. A novel mechanism for bradykinin production at inflammatory sites. Diverse effects of a mixture of neutrophil elastase and mast cell tryptase versus tissue and plasma kallikreins on native and oxidized kininogens. *J Biol Chem,* 273**,** 33224-9.

KRAUSS, U., LEE, J., BENKOVIC, S. J. & JAEGER, K. E. 2010. LOVely enzymes - towards engineering light-controllable biocatalysts. *Microb Biotechnol,* 3**,** 15-23.

KWAN, K. Y., ALLCHORNE, A. J., VOLLRATH, M. A., CHRISTENSEN, A. P., ZHANG, D. S., WOOLF, C. J. & COREY, D. P. 2006. TRPA1 contributes to cold, mechanical, and chemical nociception but is not essential for hair-cell transduction. *Neuron,* 50**,** 277-89.

LANDER, E. S., LINTON, L. M., BIRREN, B., NUSBAUM, C., ZODY, M. C., BALDWIN, J., DEVON, K., DEWAR, K., DOYLE, M., FITZHUGH, W., FUNKE, R., GAGE, D., HARRIS, K., HEAFORD, A., HOWLAND, J., KANN, L., LEHOCZKY, J., LEVINE, R., MCEWAN, P., MCKERNAN, K., MELDRIM, J., MESIROV, J. P., MIRANDA, C., MORRIS, W., NAYLOR, J., RAYMOND, C., ROSETTI, M., SANTOS, R., SHERIDAN, A., SOUGNEZ, C., STANGE-THOMANN, Y., STOJANOVIC, N., SUBRAMANIAN, A., WYMAN, D., ROGERS, J., SULSTON, J., AINSCOUGH, R., BECK, S., BENTLEY, D., BURTON, J., CLEE, C., CARTER, N., COULSON, A., DEADMAN, R., DELOUKAS, P., DUNHAM, A., DUNHAM, I., DURBIN, R., FRENCH, L., GRAFHAM, D., GREGORY, S., HUBBARD, T., HUMPHRAY, S., HUNT, A., JONES, M., LLOYD, C., MCMURRAY, A., MATTHEWS, L., MERCER, S., MILNE, S., MULLIKIN, J. C., MUNGALL, A., PLUMB, R., ROSS, M., SHOWNKEEN, R., SIMS, S., WATERSTON, R. H., WILSON, R. K., HILLIER, L. W., MCPHERSON, J. D., MARRA, M. A., MARDIS, E. R., FULTON, L. A., CHINWALLA, A. T., PEPIN, K. H., GISH, W. R., CHISSOE, S. L., WENDL, M. C., DELEHAUNTY, K. D., MINER, T. L., DELEHAUNTY, A.,

KRAMER, J. B., COOK, L. L., FULTON, R. S., JOHNSON, D. L., MINX, P. J., CLIFTON, S. W., HAWKINS, T., BRANSCOMB, E., PREDKI, P., RICHARDSON, P., WENNING, S., SLEZAK, T., DOGGETT, N., CHENG, J. F., OLSEN, A., LUCAS, S., ELKIN, C., UBERBACHER, E., FRAZIER, M., et al. 2001. Initial sequencing and analysis of the human genome. *Nature,* 409**,** 860-921.

LARDNER, A. 2001. The effects of extracellular pH on immune function. *J Leukoc Biol,* 69**,** 522-30.

LATORRE, R., BRAUCHI, S., ORTA, G., ZAELZER, C. & VARGAS, G. 2007. ThermoTRP channels as modular proteins with allosteric gating. *Cell Calcium,* 42**,** 427-38.

LAU, S. Y., PROCKO, E. & GAUDET, R. 2012. Distinct properties of Ca2+-calmodulin binding to N- and C-terminal regulatory regions of the TRPV1 channel. *J Gen Physiol,* 140**,** 541-55.

LEE, K. F., LI, E., HUBER, L. J., LANDIS, S. C., SHARPE, A. H., CHAO, M. V. & JAENISCH, R. 1992. Targeted mutation of the gene encoding the low affinity NGF receptor p75 leads to deficits in the peripheral sensory nervous system. *Cell,* 69**,** 737-49.

LEMMON, M. 2008. Membrane recognition by phospholipid-binding domains. *Nat Rev Mol Cell Biol,* 9**,** 99-111.

LEMMON, M. A. & SCHLESSINGER, J. 2010. Cell signaling by receptor-tyrosine kinases. *Cell,* 141**,** 1117-34.

LEVSKAYA, A., WEINER, O. D., LIM, W. A. & VOIGT, C. A. 2009. Spatiotemporal control of cell signalling using a light-switchable protein interaction. *Nature,* 461**,** 997-1001.

LI, X. Y. & TOYODA, H. 2015. Role of leak potassium channels in pain signaling. *Brain Res Bull,* 119**,** 73-9.

LIAO, M., CAO, E., JULIUS, D. & CHENG, Y. 2013. Structure of the TRPV1 ion channel determined by electron cryo-microscopy. *Nature,* 504**,** 107-12.

LISHKO, P. V., PROCKO, E., JIN, X., PHELPS, C. B. & GAUDET, R. 2007. The ankyrin repeats of TRPV1 bind multiple ligands and modulate channel sensitivity. *Neuron,* 54**,** 905-18.

LORIN, C., VOGELI, I. & NIGGLI, E. 2015. Dystrophic cardiomyopathy: role of TRPV2 channels in stretch-induced cell damage. *Cardiovasc Res,* 106**,** 153-62.

LUBMAN, O. Y., KOROLEV, S. V. & KOPAN, R. 2004. Anchoring notch genetics and biochemistry; structural analysis of the ankyrin domain sheds light on existing data. *Mol Cell,* 13**,** 619-26.

LUKACS, V., RIVES, J. M., SUN, X., ZAKHARIAN, E. & ROHACS, T. 2013. Promiscuous activation of transient receptor potential vanilloid 1 (TRPV1) channels by negatively charged intracellular lipids: the key role of endogenous phosphoinositides in maintaining channel activity. *J Biol Chem,* 288**,** 35003-13.

LUKACS, V., THYAGARAJAN, B., VARNAI, P., BALLA, A., BALLA, T. & ROHACS, T. 2007. Dual regulation of TRPV1 by phosphoinositides. *J Neurosci,* 27**,** 7070-80.

MACK, K. & FISCHER, M. J. M. 2017. Disrupting sensitization of TRPV4. *Neuroscience,* 352**,** 1-8.

MALEK, M., KIELKOWSKA, A., CHESSA, T., ANDERSON, K. E., BARNEDA, D., PIR, P., NAKANISHI, H., EGUCHI, S., KOIZUMI, A., SASAKI, J., JUVIN, V., KISELEV, V. Y., NIEWCZAS, I., GRAY, A., VALAYER, A., SPENSBERGER, D., IMBERT, M., FELISBINO, S., HABUCHI, T., BEINKE, S., COSULICH, S., LE NOVERE, N., SASAKI, T., CLARK, J., HAWKINS, P. T. & STEPHENS, L. R. 2017. PTEN Regulates PI(3,4)P2 Signaling Downstream of Class I PI3K. *Mol Cell,* 68**,** 566-580.e10.

MATHIVANAN, S., DEVESA, I., CHANGEUX, J. P. & FERRER-MONTIEL, A. 2016. Bradykinin Induces TRPV1 Exocytotic Recruitment in Peptidergic Nociceptors. *Front Pharmacol,* 7.

MATTHEYSES, A. L. & AXELROD, D. 2006. Direct measurement of the evanescent field profile produced by objective-based total internal reflection fluorescence. *J Biomed Opt,* 11**,** 014006.

MATTHEYSES, A. L., SIMON, S. M. & RAPPOPORT, J. Z. 2010. Imaging with total internal reflection fluorescence microscopy for the cell biologist. *J Cell Sci,* 123**,** 3621-8.

MCMAHON, S. B., BENNETT, D. L., PRIESTLEY, J. V. & SHELTON, D. L. 1995. The biological effects of endogenous nerve growth factor on adult sensory neurons revealed by a trkA-IgG fusion molecule. *Nat Med,* 1**,** 774-80.

MEENTS, J. E., FISCHER, M. J. M. & MCNAUGHTON, P. A. 2017. Sensitization of TRPA1 by Protein Kinase A. *PLoS One.*

MERCADO, J., GORDON-SHAAG, A., ZAGOTTA, W. N. & GORDON, S. E. 2010. Ca2+-dependent Desensitization of TRPV2 Channels is Mediated by Hydrolysis of Phosphatidylinositol 4,5-Bisphosphate. *J Neurosci,* 30**,** 13338-47.

MESSLINGER, K. 1997. [What is a nociceptor?]. *Anaesthesist,* 46**,** 142-53.

MICHAELY, P., TOMCHICK, D. R., MACHIUS, M. & ANDERSON, R. G. 2002. Crystal structure of a 12 ANK repeat stack from human ankyrinR. *Embo j,* 21**,** 6387-96.

MILED, N., YAN, Y., HON, W. C., PERISIC, O., ZVELEBIL, M., INBAR, Y., SCHNEIDMAN-DUHOVNY, D., WOLFSON, H. J., BACKER, J. M. & WILLIAMS, R. L. 2007. Mechanism of two classes of cancer mutations in the phosphoinositide 3-kinase catalytic subunit. *Science,* 317**,** 239-42.

MILLER, M. S., SCHMIDT-KITTLER, O., BOLDUC, D. M., BROWER, E. T., CHAVES-MOREIRA, D., ALLAIRE, M., KINZLER, K. W., JENNINGS, I. G., THOMPSON, P. E., COLE, P. A., AMZEL, L. M., VOGELSTEIN, B. & GABELLI, S. B. 2014. Structural basis of nSH2 regulation and lipid binding in PI3Kα. *Oncotarget,* 5**,** 5198-208.

MOHAPATRA, D. P. & NAU, C. 2003. Desensitization of capsaicin-activated currents in the vanilloid receptor TRPV1 is decreased by the cyclic AMP-dependent protein kinase pathway. *J Biol Chem,* 278**,** 50080-90.

MOHAPATRA, D. P. & NAU, C. 2005. Regulation of Ca2+-dependent desensitization in the vanilloid receptor TRPV1 by calcineurin and cAMP-dependent protein kinase. *J Biol Chem,* 280**,** 13424-32.

MORENILLA-PALAO, C., PLANELLS-CASES, R., GARCIA-SANZ, N. & FERRER-MONTIEL, A. 2004. Regulated exocytosis contributes to protein kinase C potentiation of vanilloid receptor activity. *J Biol Chem,* 279**,** 25665-72.

MOSAVI, L. K., CAMMETT, T. J., DESROSIERS, D. C. & PENG, Z. Y. 2004. The ankyrin repeat as molecular architecture for protein recognition. *Protein Sci,* 13**,** 1435-48.

NAKAI, J., OHKURA, M. & IMOTO, K. 2001. A high signal-to-noise Ca(2+) probe composed of a single green fluorescent protein. *Nat Biotechnol,* 19**,** 137-41.

NASUHOGLU, C., FENG, S., MAO, J., YAMAMOTO, M., YIN, H. L., EARNEST, S., BARYLKO, B., ALBANESI, J. P. & HILGEMANN, D. W. 2002. Nonradioactive analysis of phosphatidylinositides and other anionic phospholipids by anion-exchange high-performance liquid chromatography with suppressed conductivity detection. *Anal Biochem,* 301**,** 243-54.

NOVAKOVA-TOUSOVA, K., VYKLICKY, L., SUSANKOVA, K., BENEDIKT, J., SAMAD, A., TEISINGER, J. & VLACHOVA, V. 2007. Functional changes in the vanilloid receptor subtype 1 channel during and after acute desensitization. *Neuroscience,* 149**,** 144-54.

NUMAZAKI, M., TOMINAGA, T., TAKEUCHI, K., MURAYAMA, N., TOYOOKA, H. & TOMINAGA, M. 2003. Structural determinant of TRPV1 desensitization interacts with calmodulin. *Proc Natl Acad Sci U S A.*

OBATA, K., KATSURA, H., MIZUSHIMA, T., YAMANAKA, H., KOBAYASHI, K., DAI, Y., FUKUOKA, T., TOKUNAGA, A., TOMINAGA, M. & NOGUCHI, K. 2005. TRPA1 induced in sensory neurons contributes to cold hyperalgesia after inflammation and nerve injury. *J Clin Invest,* 115**,** 2393-401.

OZATO-SAKURAI, N., FUJITA, A. & FUJIMOTO, T. 2011. The distribution of phosphatidylinositol 4,5-bisphosphate in acinar cells of rat pancreas revealed with the freeze-fracture replica labeling method. *PLoS One,* 6**,** e23567.

PARK, U., VASTANI, N., GUAN, Y., RAJA, S. N., KOLTZENBURG, M. & CATERINA, M. J. 2011. TRP vanilloid 2 knock-out mice are susceptible to perinatal lethality but display normal thermal and mechanical nociception. *J Neurosci,* 31**,** 11425-36.

PATEL, T. D., JACKMAN, A., RICE, F. L., KUCERA, J. & SNIDER, W. D. 2000. Development of sensory neurons in the absence of NGF/TrkA signaling in vivo. *Neuron,* 25**,** 345-57.

PAULSEN, C. E., ARMACHE, J. P., GAO, Y., CHENG, Y. & JULIUS, D. 2015. Structure of the TRPA1 ion channel suggests regulatory mechanisms. *Nature,* 520**,** 511-7.

PEITZSCH, R. M., EISENBERG, M., SHARP, K. A. & MCLAUGHLIN, S. 1995. Calculations of the electrostatic potential adjacent to model phospholipid bilayers. *Biophys J,* 68**,** 729-38.

PERÁLVAREZ-MARÍN, A., DOÑATE-MACIAN, P. & GAUDET, R. 2013. What do we know about the Transient Receptor Potential Vanilloid 2 (TRPV2) ion channel? *FEBS J,* 280**,** 5471-87.

PETTY, B. G., CORNBLATH, D. R., ADORNATO, B. T., CHAUDHRY, V., FLEXNER, C., WACHSMAN, M., SINICROPI, D., BURTON, L. E. & PEROUTKA, S. J. 1994. The effect of systemically administered recombinant human nerve growth factor in healthy human subjects. *Ann Neurol,* 36**,** 244-6.

PHELPS, C. B., WANG, R. R., CHOO, S. S. & GAUDET, R. 2010. Differential Regulation of TRPV1, TRPV3, and TRPV4 Sensitivity through a Conserved Binding Site on the Ankyrin Repeat Domain*. *J Biol Chem.*

PRANKERD, T. A. J. 1965. Transport and Diffusion in Red Blood Cells. *Proc R Soc Med,* 58**,** 157.

PRESCOTT, E. D. & JULIUS, D. 2003. A modular PIP2 binding site as a determinant of capsaicin receptor sensitivity. *Science,* 300**,** 1284-8.

PUTYRSKI, M. & SCHULTZ, C. 2012. Protein translocation as a tool: The current rapamycin story. *FEBS Lett,* 586**,** 2097-105.

RAFFIONI, S. & BRADSHAW, R. A. 1992. Activation of phosphatidylinositol 3-kinase by epidermal growth factor, basic fibroblast growth factor, and nerve growth factor in PC12 pheochromocytoma cells. *Proc Natl Acad Sci U S A,* 89**,** 9121-5.

RAHAMAN, S. O., GROVE, L. M., PARUCHURI, S., SOUTHERN, B. D., ABRAHAM, S., NIESE, K. A., SCHERAGA, R. G., GHOSH, S., THODETI, C. K., ZHANG, D. X., MORAN, M. M., SCHILLING, W. P., TSCHUMPERLIN, D. J. & OLMAN, M. A. 2014. TRPV4 mediates myofibroblast differentiation and pulmonary fibrosis in mice. *J Clin Invest.*

RAMASWAMY, S., NAKAMURA, N., VAZQUEZ, F., BATT, D. B., PERERA, S., ROBERTS, T. M. & SELLERS, W. R. 1999. Regulation of G1 progression by the PTEN tumor suppressor protein is linked to inhibition of the phosphatidylinositol 3-kinase/Akt pathway. *Proc Natl Acad Sci U S A,* 96**,** 2110-5.

RASBAND, W. S. 1997-2016. ImageJ. U. S. National Institutes of Health, Bethesda, Maryland, USA.

REICHHART, N., KECKEIS, S., FRIED, F., FELS, G. & STRAUSS, O. 2015. Regulation of surface expression of TRPV2 channels in the retinal pigment epithelium. *Graefes Arch Clin Exp Ophthalmol,* 253**,** 865-74.

REN, K. & DUBNER, R. 1999. Inflammatory Models of Pain and Hyperalgesia. *Ilar j,* 40**,** 111-118.

RIVERA, V. M., CLACKSON, T., NATESAN, S., POLLOCK, R., AMARA, J. F., KEENAN, T., MAGARI, S. R., PHILLIPS, T., COURAGE, N. L., CERASOLI, F., HOLT, D. A. & GILMAN, M. 2019. A humanized system for pharmacologic control of gene expression. *Nature Medicine,* 2**,** 1028-1032.

ROSENBAUM, T., GORDON-SHAAG, A., MUNARI, M. & GORDON, S. E. 2004. Ca2+/Calmodulin Modulates TRPV1 Activation by Capsaicin. *J Gen Physiol.*

SAKMANN, B. & NEHER, E. 1984. Patch clamp techniques for studying ionic channels in excitable membranes. *Annu Rev Physiol,* 46**,** 455-72.

SANDERSON, M. J., SMITH, I., PARKER, I. & BOOTMAN, M. D. 2014. Fluorescence Microscopy. *Cold Spring Harb Protoc,* 2014**,** pdb top071795.

SAOTOME, K., SINGH, A. K., YELSHANSKAYA, M. V. & SOBOLEVSKY, A. I. 2016. Crystal structure of the epithelial calcium channel TRPV6. *Nature,* 534**,** 506-11.

SARBASSOV, D. D., GUERTIN, D. A., ALI, S. M. & SABATINI, D. M. 2005. Phosphorylation and regulation of Akt/PKB by the rictor-mTOR complex. *Science,* 307**,** 1098-101.

SCHNEIDER, C. A., RASBAND, W. S. & ELICEIRI, K. W. 2012. NIH Image to ImageJ: 25 years of image analysis. *Nat Methods,* 9**,** 671-5.

SEDGWICK, S. G. & SMERDON, S. J. 1999. The ankyrin repeat: a diversity of interactions on a common structural framework. *Trends Biochem Sci,* 24**,** 311-6.

SHARMA, S., GOSWAMI, R., MERTH, M., COHEN, J., LEI, K. Y., ZHANG, D. X. & RAHAMAN, S. O. 2017. TRPV4 ion channel is a novel regulator of dermal myofibroblast differentiation. *Am J Physiol Cell Physiol,* 312**,** C562-c572.

SHIGEMATSU, H., SOKABE, T., DANEV, R., TOMINAGA, M. & NAGAYAMA, K. 2010. A 3.5-nm Structure of Rat TRPV4 Cation Channel Revealed by Zernike Phase-contrast Cryoelectron Microscopy*. *J Biol Chem.*

SHIMIZU-SATO, S., HUQ, E., TEPPERMAN, J. M. & QUAIL, P. H. 2002. A light-switchable gene promoter system. *Nat Biotechnol,* 20**,** 1041-4.

SHU, X. & MENDELL, L. M. 1999. Nerve growth factor acutely sensitizes the response of adult rat sensory neurons to capsaicin. *Neurosci Lett,* 274**,** 159-62.

SKOU, J. C. 1957. The influence of some cations on an adenosine triphosphatase from peripheral nerves. *Biochim Biophys Acta,* 23**,** 394-401.

SONGYANG, Z., SHOELSON, S. E., CHAUDHURI, M., GISH, G., PAWSON, T., HASER, W. G., KING, F., ROBERTS, T., RATNOFSKY, S., LECHLEIDER, R. J. & ET AL. 1993. SH2 domains recognize specific phosphopeptide sequences. *Cell,* 72**,** 767-78.

STEIN, A. T., UFRET-VINCENTY, C. A., HUA, L., SANTANA, L. F. & GORDON, S. E. 2006. Phosphoinositide 3-kinase binds to TRPV1 and mediates NGF-stimulated TRPV1 trafficking to the plasma membrane. *J Gen Physiol,* 128**,** 509-22.

STOKOE, D., STEPHENS, L. R., COPELAND, T., GAFFNEY, P. R., REESE, C. B., PAINTER, G. F., HOLMES, A. B., MCCORMICK, F. & HAWKINS, P. T. 1997. Dual role of phosphatidylinositol-3,4,5-trisphosphate in the activation of protein kinase B. *Science,* 277**,** 567-70.

STRATIIEVSKA, A., NELSON, S., SENNING, E. N., LAUTZ, J. D., SMITH, S. E. & GORDON, S. E. 2018. Reciprocal regulation among TRPV1 channels and phosphoinositide 3-kinase in response to nerve growth factor. *Elife,* 7.

STROTMANN, R., SCHULTZ, G. & PLANT, T. D. 2003. Ca2+-dependent potentiation of the nonselective cation channel TRPV4 is mediated by a C-terminal calmodulin binding site. *J Biol Chem,* 278**,** 26541-9.

SU, Y. S. & LAGARIAS, J. C. 2007. Light-independent phytochrome signaling mediated by dominant GAF domain tyrosine mutants of Arabidopsis phytochromes in transgenic plants. *Plant Cell,* 19**,** 2124-39.

SUH, B. C. & HILLE, B. 2008. PIP2 is a necessary cofactor for ion channel function: How and why? *Annu Rev Biophys,* 37**,** 175-95.

SUH, Y. G. & OH, U. 2005. Activation and activators of TRPV1 and their pharmaceutical implication. *Curr Pharm Des,* 11**,** 2687-98.

SUN, R., YAN, J. & WILLIS, W. D. 2007. Activation of protein kinase B/Akt in the periphery contributes to pain behavior induced by capsaicin in rats. *Neuroscience,* 144**,** 286-94.

TAKAHASHI, N., HAMADA-NAKAHARA, S., ITOH, Y., TAKEMURA, K., SHIMADA, A., UEDA, Y., KITAMATA, M., MATSUOKA, R., HANAWA-SUETSUGU, K., SENJU, Y., MORI, M. X., KIYONAKA, S., KOHDA, D., KITAO, A., MORI, Y. & SUETSUGU, S. 2014. TRPV4 channel activity is modulated by direct interaction of the ankyrin domain to PI(4,5)P(2). *Nat Commun,* 5**,** 4994.

TANAKA, Y., NIWA, S., DONG, M., FARKHONDEH, A., WANG, L., ZHOU, R. & HIROKAWA, N. 2016. The Molecular Motor KIF1A Transports the TrkA Neurotrophin Receptor and Is Essential for Sensory Neuron Survival and Function. *Neuron,* 90**,** 1215-29.

TANG, Q., GUO, W., ZHENG, L., WU, J. X., LIU, M., ZHOU, X., ZHANG, X. & CHEN, L. 2018. Structure of the receptor-activated human TRPC6 and TRPC3 ion channels. *Cell Res,* 28**,** 746-755.

THAKOR, D. K., LIN, A., MATSUKA, Y., MEYER, E. M., RUANGSRI, S., NISHIMURA, I. & SPIGELMAN, I. 2009. Increased peripheral nerve excitability and local NaV1.8 mRNA up-regulation in painful neuropathy. *Mol Pain.*

TISSOT, M., STRZALKO, S., THURET, A. & GIROUD, J. P. 1989. Prostanoid release by macrophages at a distance from an inflammatory site. *Br J Exp Pathol,* 70**,** 525-31.

TOETTCHER, J. E., GONG, D., LIM, W. A. & WEINER, O. D. 2011. Light-based feedback for controlling intracellular signaling dynamics. *Nat Methods,* 8**,** 837-9.

TREBINO, C. E., STOCK, J. L., GIBBONS, C. P., NAIMAN, B. M., WACHTMANN, T. S., UMLAND, J. P., PANDHER, K., LAPOINTE, J. M., SAHA, S., ROACH, M. L., CARTER, D., THOMAS, N. A., DURTSCHI, B. A., MCNEISH, J. D., HAMBOR, J. E., JAKOBSSON, P. J., CARTY, T. J., PEREZ, J. R. & AUDOLY, L. P. 2003. Impaired inflammatory and pain responses in mice lacking an inducible prostaglandin E synthase. *Proc Natl Acad Sci U S A.*

TSIEN, R. Y. 1980. New calcium indicators and buffers with high selectivity against magnesium and protons: design, synthesis, and properties of prototype structures. *Biochemistry,* 19**,** 2396-404.

TSUI-PIERCHALA, B. A. & GINTY, D. D. 1999. Characterization of an NGF-P-TrkA retrograde-signaling complex and age-dependent regulation of TrkA phosphorylation in sympathetic neurons. *J Neurosci,* 19**,** 8207-18.

UFRET-VINCENTY, C. A., KLEIN, R. M., COLLINS, M. D., ROSASCO, M. G., MARTINEZ, G. Q. & GORDON, S. E. 2015. Mechanism for phosphoinositide selectivity and activation of TRPV1 ion channels. *J Gen Physiol.*

UFRET-VINCENTY, C. A., KLEIN, R. M., HUA, L., ANGUEYRA, J. & GORDON, S. E. 2011. Localization of the PIP2 sensor of TRPV1 ion channels. *J Biol Chem,* 286**,** 9688-98.

UINGS, I. J. & FARROW, S. N. 2000. Cell receptors and cell signalling. *Mol Pathol.*

V'YACHESLAV LEHEN'KYI, N. P. 2016. TRPV2 (transient receptor potential cation channel, subfamily V, member 2). SOURCE (Princeton)TRPV2.

VANHAESEBROECK, B., GUILLERMET-GUIBERT, J., GRAUPERA, M. & BILANGES, B. 2010. The emerging mechanisms of isoform-specific PI3K signalling. *Nat Rev Mol Cell Biol,* 11**,** 329-41.

VARNAI, P., BONDEVA, T., TAMAS, P., TOTH, B., BUDAY, L., HUNYADY, L. & BALLA, T. 2005. Selective cellular effects of overexpressed pleckstrin-homology domains that recognize PtdIns(3,4,5)P3 suggest their interaction with protein binding partners. *J Cell Sci,* 118**,** 4879-88.

VETTER, M. L., MARTIN-ZANCA, D., PARADA, L. F., BISHOP, J. M. & KAPLAN, D. R. 1991. Nerve growth factor rapidly stimulates tyrosine phosphorylation of phospholipase C-gamma 1 by a kinase activity associated with the product of the trk protooncogene. *Proc Natl Acad Sci U S A,* 88**,** 5650-4.

VOSS, S., KLEWER, L. & WU, Y. W. 2015. Chemically induced dimerization: reversible and spatiotemporal control of protein function in cells. *Curr Opin Chem Biol,* 28**,** 194-201.

WANG, S., DAI, Y., FUKUOKA, T., YAMANAKA, H., KOBAYASHI, K., OBATA, K., CUI, X., TOMINAGA, M. & NOGUCHI, K. 2008. Phospholipase C and protein kinase A mediate bradykinin sensitization of TRPA1: a molecular mechanism of inflammatory pain. *Brain,* 131**,** 1241-51.

WATANABE, H., VRIENS, J., PRENEN, J., DROOGMANS, G., VOETS, T. & NILIUS, B. 2003. Anandamide and arachidonic acid use epoxyeicosatrienoic acids to activate TRPV4 channels. *Nature,* 424**,** 434-8.

WENK, M. R., LUCAST, L., DI PAOLO, G., ROMANELLI, A. J., SUCHY, S. F., NUSSBAUM, R. L., CLINE, G. W., SHULMAN, G. I., MCMURRAY, W. & DE CAMILLI, P. 2003. Phosphoinositide profiling in complex lipid mixtures using electrospray ionization mass spectrometry. *Nat Biotechnol,* 21**,** 813-7.

WICKENDEN, A. D. 2014. Overview of Electrophysiological Techniques. *Curr Protoc Pharmacol,* 64**,** 11.1.1-17.

WILLIS, W. J. & COGGESHALL, R. 1978. *Sensory Mechanisms of the Spinal Cord* | *W. D. Willis* | *Springer*, Kluwer, New York.

WILLIS WJ, C. R. 1978. *Sensory Mechanisms of the Spinal Cord* | *W. D. Willis* | *Springer*, Kluwer, New York.

WINKLER, P. A., HUANG, Y., SUN, W., DU, J. & LÜ, W. 2017. Electron cryo-microscopy structure of a human TRPM4 channel. *Nature*.

XU, C., WATRAS, J. & LOEW, L. M. 2003. Kinetic analysis of receptor-activated phosphoinositide turnover. *J Cell Biol,* 161**,** 779-91.

XU, J. T., TU, H. Y., XIN, W. J., LIU, X. G., ZHANG, G. H. & ZHAI, C. H. 2007. Activation of phosphatidylinositol 3-kinase and protein kinase B/Akt in dorsal root ganglia and spinal cord contributes to the neuropathic pain induced by spinal nerve ligation in rats. *Exp Neurol,* 206**,** 269-79.

XU, Q., FITZSIMMONS, B., STEINAUER, J., O'NEILL, A., NEWTON, A. C., HUA, X. Y. & YAKSH, T. L. 2011. Spinal phosphinositide 3-kinase-Akt-mammalian target of rapamycin signaling cascades in inflammation-induced hyperalgesia. *J Neurosci,* 31**,** 2113-24.

YAO, J., LIU, B. & QIN, F. 2011. Modular thermal sensors in temperature-gated transient receptor potential (TRP) channels. *Proc Natl Acad Sci U S A,* 108**,** 11109-14.

YAO, J. & QIN, F. 2009. Interaction with phosphoinositides confers adaptation onto the TRPV1 pain receptor. *PLoS Biol,* 7**,** e46.

YIN, Y., WU, M., ZUBCEVIC, L., BORSCHEL, W. F., LANDER, G. C. & LEE, S.-Y. 2017. Structure of the cold- and menthol-sensing ion channel TRPM8.

ZHANG, X., HUANG, J. & MCNAUGHTON, P. A. 2005. NGF rapidly increases membrane expression of TRPV1 heat-gated ion channels. *EMBO J.*

ZHENG, J. & ZAGOTTA, W. N. 2003. Patch-clamp fluorometry recording of conformational rearrangements of ion channels. *Sci STKE,* 2003**,** Pl7.

ZHU, C., KANG, W., XU, F., CHENG, X., ZHANG, Z., JIA, L., JI, L., GUO, X., XIONG, H., SIMBRUNER, G., BLOMGREN, K. & WANG, X. 2009. Erythropoietin Improved Neurologic Outcomes in Newborns With Hypoxic-Ischemic Encephalopathy.

ZHU, W. & OXFORD, G. S. 2007. Phosphoinositide-3-kinase and mitogen activated protein kinase signaling pathways mediate acute NGF sensitization of TRPV1. *Mol Cell Neurosci,* 34**,** 689-700.

ZHUANG, Z. Y., XU, H., CLAPHAM, D. E. & JI, R. R. 2004. Phosphatidylinositol 3-kinase activates ERK in primary sensory neurons and mediates inflammatory heat hyperalgesia through TRPV1 sensitization. *J Neurosci,* 24**,** 8300-9.

ZIEMBA, B. P., KNIGHT, J. D. & FALKE, J. J. 2012. Assembly of Membrane-Bound Protein Complexes: Detection and Analysis by Single Molecule Diffusion. *Biochemistry,* 51**,** 1638-47.

ZUBCEVIC, L., HERZIK, M. A., JR., CHUNG, B. C., LIU, Z., LANDER, G. C. & LEE, S. Y. 2016a. Cryo-electron microscopy structure of the TRPV2 ion channel. *Nat Struct Mol Biol,* 23**,** 180-6.

ZUBCEVIC, L., JR, M. A. H., CHUNG, B. C., LIU, Z., LANDER, G. C. & LEE, S.-Y. 2016b. Cryo-electron microscopy structure of the TRPV2 ion channel. *Nature Structural & Molecular Biology,* 23**,** 180-186.

Vita

Anastasiia Stratiievska grew up in Kyiv, Ukraine. In 2010 she obtained a BS in Biophysics from Taras Shevchenko National University of Kyiv, Dept. of Biology, Kyiv, Ukraine. In 2008 – 2009 she worked as an Engineer I in the electron microscopy facility at the National Academy of Sciences of Ukraine M.G. Kholodny Institute of Botany, Kyiv, Ukraine. In addition, 2008 through 2012 she worked as an Engineer I, in the laboratory of Elena Lukyanetz at the National Academy of Sciences of Ukraine A.A. Bogomoletz Institute of Physiology, Dept. of General Physiology of Nervous System, Kyiv, Ukraine. Her work there in 2012 led to a completion of MS in Molecular Physiology and Biophysics at the Moscow Institute of Physics and Technology (State University, Kyiv affiliate), Dept. of Molecular and Biological Physics, Kyiv, Ukraine. Later in 2012 she moved to Seattle and started as a volunteer in the Lab of Sharona E. Gordon at the University of Washington, Seattle, WA. Sharona and coleagues became a new family, far from home in Kyiv. In 2015 she entered the Physiology and Biophysics PhD program. While working on her thesis, she with great joy provided training in imaging and cell culture techniques to undergraduate students Sara Nelson, Ruian Yang, Alex Pazevic and a visiting scientist from Brasil Lígia Araujo Naves. Neurobiology 2015 course at MBL, Marine Biological Laboratory, Woods Hole, MA was transformative for her as a scientist. Her graduate work resulted in two publications (and one more in preparation at the time of graduation). When not in the lab, Anastasiia enjoyed family time indoors and outdoors in the Pacific Northwest with her briliant husband Oleksandr and her son Demian.